OUKA
The University of Osaka
Institutional Knowledge Archive

Title	Studies on Novel Non-Natural Polypeptide “Arylopeptide”; Synthesis, Design of Higher-Order Structure, and Properties
Author(s)	石堂, 祐規
Citation	大阪大学, 2020, 博士論文
Version Type	VoR
URL	https://doi.org/10.18910/76399
rights	
Note	

The University of Osaka Institutional Knowledge Archive : OUKA

https://ir.library.osaka-u.ac.jp/

The University of Osaka

Studies on Novel Non-Natural Polypeptide “Arylopeptide”; Synthesis, Design of Higher-Order Structure, and Properties

A Doctoral Thesis

by

Yuki Ishido

Submitted to

The Graduate School of Science,

Osaka University

February, 2020

Acknowledgements

This thesis presents the research that the author performed at Graduate School of Science, Osaka University from 2015 to 2020 under the direction of Professor Kiyotaka Onitsuka.

First of all, the author expresses his deepest gratitude to Professor Kiyotaka Onitsuka for his continuous guidance, helpful suggestions, and kind encouragement. The author is grateful in Associate Professor Taka-aki Okamura for his suggestions from new perspective and positive encouragements. The author also appreciates Assistant Professor Naoya Kanbayashi for his millions of valuable advises, suggestive discussion and lectures of experimental procedures. The author could not have accomplished to construct this thesis without their guidance and advises.

The author thanks Dr. Yasuto Todokoro and Dr. Naoya Inazumi for NMR spectroscopic measurements. The author also thanks Dr. Akihito Ito for mass spectrometry.

The author's great thanks Professor Takahiro Sato for CD spectroscopy. The author also thanks Professor Takeharu Haino and Ms. Naoka Fujii (Hiroshima University) for AFM measurement and all the lab members for their lively discussion. The author is also grateful in Mr. Daisuke Yoshidome (Schrödinger corporation) for molecular mechanics calculation.

The author wishes to appreciate all the members of Onitsuka laboratory, whom the author shared precious days with. Especially, the author is indebted to Mr. Yuki Kataoka, which is my colleague for their helpful advises, encouragement and blessed time! The author thanks same project members; Ms. Marina Saegusa, Mr. Yusaku Ando, and Ms. Miho Nishio for their great efforts and unflagging enthusiasm. The author also thanks Dr. Koichiro Takii, Mr. Satoshi Yamashita, Ms. Yumi Nakamori, Mr. Toshihisa Kaga, Ms. Marina Okada, Ms. Kyoko Tsubouchi, Ms. Mami Ishikawa, Ms. Yuki Fukuda, Ms. Chinami Tsukude, Mr. Yoshio Matsukiyo, Mr. Yusuke Tomita, Ms. Manami Narukawa, Mr. Tomohiro Miyawaki, Ms. Ayumi Okada, Ms. Risa Miyagawa, Mr. Kazuki Yamazaki, Ms. Hinako Miyoshi, Mr. Ryoga Yamamoto and Ms Misaki Yamada for happy days.

The author greatly appreciates to financial supports from JSPS Research Fellowships for Young Scientist and Tonen General Sekiyu Research/Development Encouragement Foundation.

Finally, the author would like to show his cordial acknowledgement to his father Mr. Takashi Ishido; his mother, Mrs. Kayoko Ishido; his brother, Mr. Kohei Tokunaga; his sisters, Ms. Eri Ishido and Mrs. Nami; grandfather, Mr. Norihisa Ishido; grandmothers, Mrs. Mariko Ishido and Mrs. Yoshiko Miyata; true friends, Mr. Tokio Matsunaga, Mr. Yuhei Otsuka, Mr. Yoshiki Fujita, Mr. Yuki Hiraishi, Mr. Shoichi Taniguchi, Mr. Shogo Nakano, Mr. Akito Takiguchi, Dr. Daisuke Shimoyama, for their understanding, continuous support and warm encouragement.

February, 2020

Yuki Ishido
Department of Macromolecular Science
Graduate School of Science
Osaka University

Contents

Chapter 1

General Introduction

1-1: Background

Proteins are the most attractive biopolymers for researchers and commercial interests alike owing to their tendency to form higher-order structures which consist of sophisticated peptide chains with very diverse physical and chemical properties (Figure 1-1).[1,2] In paticular, the amide group on the main backbone of peptide chain can significantly limit the flexibility of polypeptide through planar restrictions, resulting in a structure defined mainly by dihedral angles (ϕ, ψ). The range that the dihedral angle adopts is known as the Ramachandran plot. Additionally, polypeptides comprised of L-amino acids, including D- and nonnatural amino acids, have entirely controlled asymmetric carbon in the main chain, which set the area limits of the Ramachandran plot. Also, the hydrogen bonds between the amide groups maintain the higher-order structure and, thus, the dynamics of these well-defined structures. Added together, these constraints in the flexibility of the polypeptide result in well-defined folded structures that are generally comprised of various combinations of about 20 core amino acids. These secondary and higher-order structures are also supported by the molecular effect exerted by their presence and the surrounding environment. One prime example of this effect in action can be observed during the elongation of the α-helix, which results in the lowered motility of the entire molecule, thus preventing the collapse of the helical conformation.

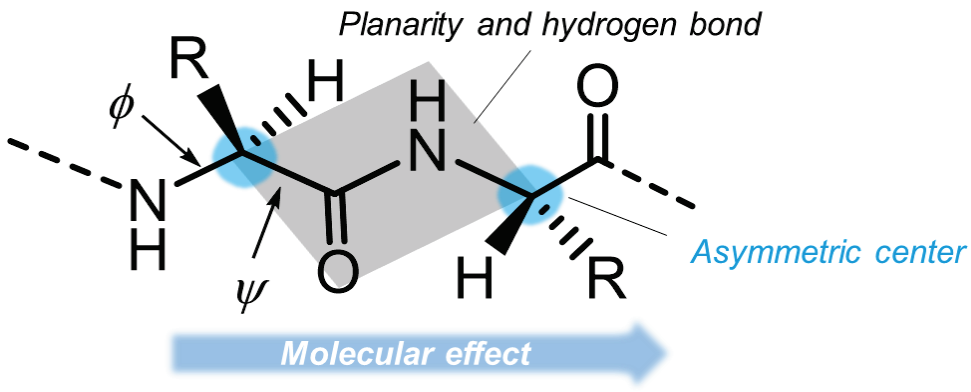

Figure 1-1. Chemical structure of peptide and factors of forming a well-defined structure.

Owing to their potential usefulness, polypeptides are often the bases for the molecular design of novel functional polymers. To develop new macromolecules, molecular designs are incorporated into the peptide backbones, while the polypeptide's distinct characteristics, such as its rigidity, are maintained. Given this,

aromatic rings have become promising candidates for the synthesis of useful polymers with well-defined structures, because the aromatic ring behaves like a rigid entity within the peptide chain, thus resulting in no loss in the original definition of the polypeptide chain. Additionally, more precise molecular design that feature *ortho*-, *meta*-, and *para*-arylene rings is available. Figure 1-2 presents the structural requirements for the creation of these types of the novel polypeptide-based polymers. In this chapter, previous studies related to these polymers, their synthesis, and the influence exerted by their distinct structural features are described.

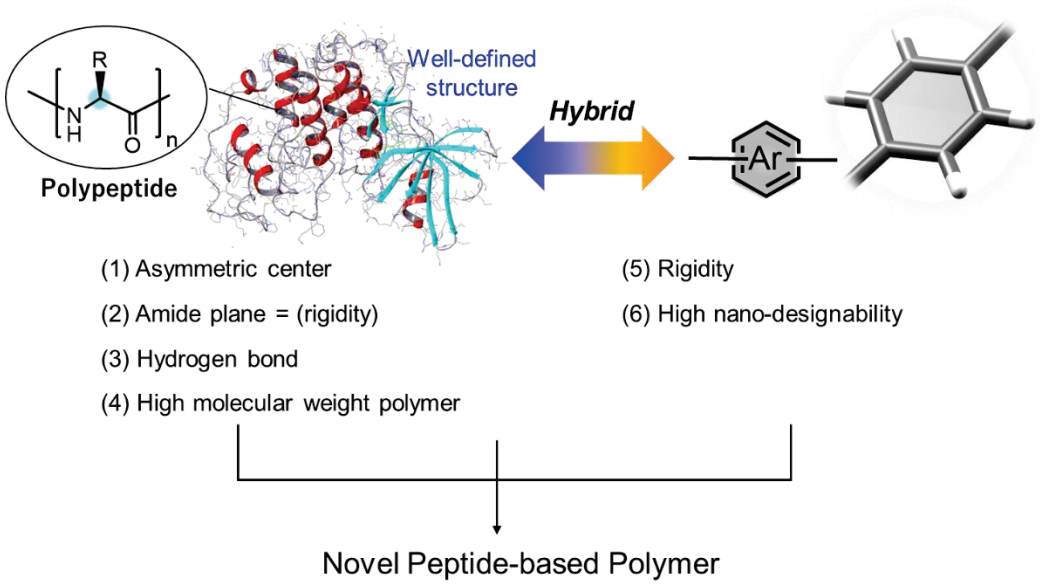

Figure 1-2. The requirements for a polypeptide-based polymer and incorporating aromatic property into peptide.

1-2: Foldamer

Since this molecule is known to form very well-defined structure, foldamer has become one of the most extensively studied molecules that feature a bottom-up design of primary and secondary structures.[3] The term "foldamer" is defined by Samuel Gellman in 1998 to describe discrete artificial molecules that adopt very specific and stable conformations.[4] In the early days of the foldamer research, the synthesis of polypeptide using nonnatural amino acids as the building blocks was conducted by Gellman and Seebach et al., (Figure 1-3).[5,6,7] Here, aliphatic nonnatural peptides underwent intramolecular hydrogen bonding like α-peptides to give helical structures according to each building block.

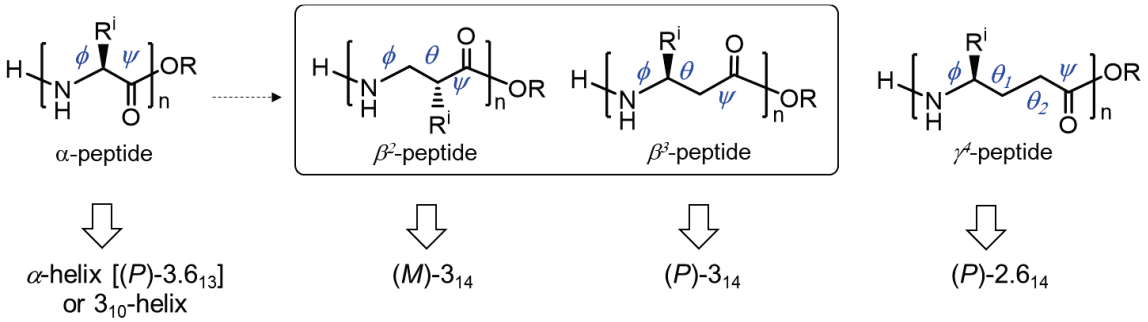

Figure 1-3. Peptide foldamers consisting of homolongated α-amino acids generated by insertion of one (→ β^2 and β^3-peptide) or two (→ γ^4-peptide) CH_2 groups.

While various types of aliphatic foldamers are still fervently being developed,[8] many aromatic amide foldamers have been debuted in recent years, which are both functional and easy to design.[9] In particular case, Huc et al.[3b,10] have succeeded in developing aromatic amide foldamers that were capable of adopting a wide variety of folding structures *via* precisely established intramolecular hydrogen bonds (Figure 1-4). Here the rotation and orientation of the aromatic ring were fixed by the hydrogen bonding between the N atom of quinoline and the NH of the amide, thereby forming a helical structure. As a result, aromatic rings significantly reduced the flexibility of the molecule, and the remaining latitudes were regulated by hydrogen bonds (Figure 1-4a). In addition to generating helical structures, Huc was able to synthesize soluble *β*-sheetlike aromatic foldarmers (Figure 1-4b),[11] despite the fact that sheetlike architectures often tended to become insoluble aggregate. As this example shows, one of the advantages of aromatic foldamer is that steric repulsion and solubility can be freely adjusted because substituents can be introduced into the aromatic ring. This sheet structure was designed to have a face-to-face orientation through the occurrence of steric repulsion between the xylene units. Many foldamers have been synthesized using a condensation reaction, including the helix–sheet–helix domains designed by Huc et al., through the combination of helix and sheet sequences (Figure 1-5).[12] These domains represent significant steps forward in the use of well-defined aromatic amide foldamers for applications as selective molecular encapsulation,[13] antibacterial properties,[14] protein inhibitors,[15] and electron transfer materials.[16] As described above, the chemical structures of aromatic amide facilitate functional, higher-level molecular designs that simply cannot be realized by their aliphatic counterparts.

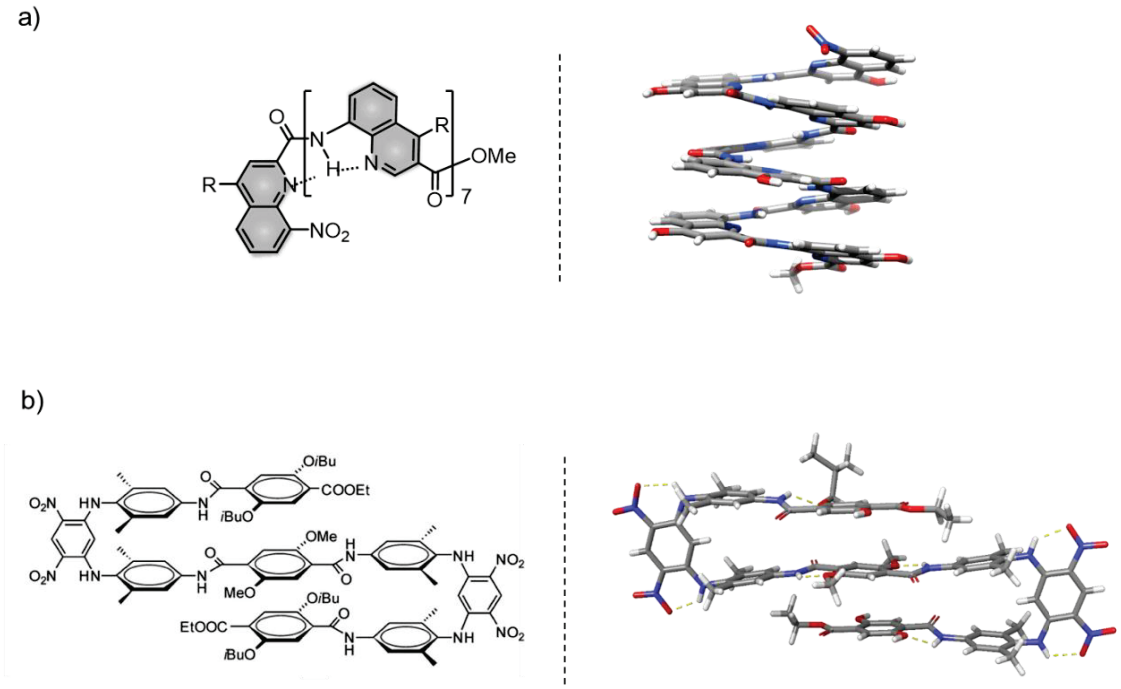

Figure 1-4. Arylene amide foldamers. (a) Helical structure. (b) Sheet-structure.

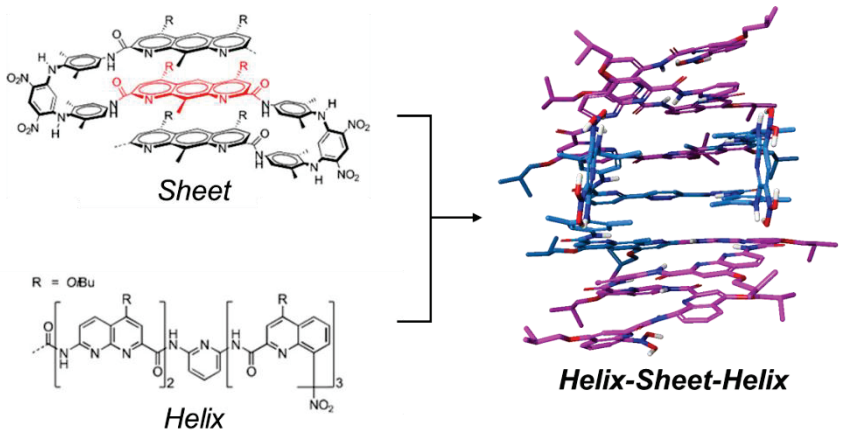

Figure 1-5. Helix-sheet-helix motif foldamer.

1-3: Rigidity and Macromolecular Effect of Polymer

Just as the α-helix can be stably present as the helical length increases, structural control utilizing this effect is also known for artificial polymers. Starting with the synthesis of poly(phenylmethyl methacrylate) by Okamoto et al.,[17] various helical polymers have been reported.[18] Unlike polypeptides and aromatic amide foldamers, which mainly fix helical structures by intramolecular hydrogen bonding, many artificial helical polymers utilize macromolecular effect based on cooperativity to fix the helical conformation. In a polymer, small energy difference of local structure is accumulated continuously by the multitude of monomer units which, in turn, amplifies these small energy differences and leads to a specific global structure. The most representative examples of such systems are polyacetylene[18a,18c] and polyisocyanate[19] which are helical polymers with achiral main chains and side chain that contain optically active substituents. Since the 1980s, Green[20] established the sergeants-and-soldiers effect and the majority-rule for induction of one-handed helical structures by the introduction of chiral side chains. These macromolecular effects enable the induction of a one-handed helical structure by some enantio-enriched difference on the side chain, even the slight difference between hydrogen and deuterium give distinct one-handed helical structure (Figure 1-6).[19] This macromolecular effect can converge some conformations into a regulated architecture even for a molecule that is not rigid enough to form a well-defined structure.

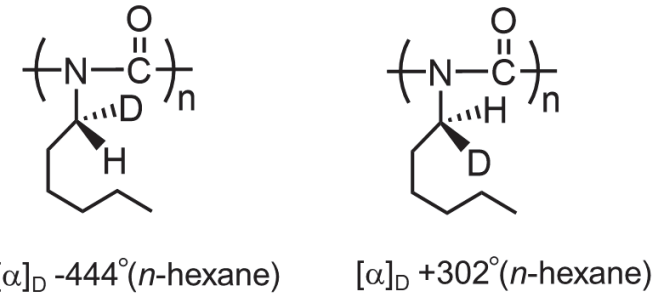

Figure 1-6. Chemical structures of poly(isocyanate)s and optical rotations at the sodium D line.

Remarkably, the dynamic helical polymers can undergo a switch of the helical chirality by external stimuli, such as temperature,[21] light,[22] metal ion,[23] and pH.[24] A difference of solvents also can cause a different folding structure.[25] Suginome et al.[26] investigated the solvent dependence of the helical structure of polyquinoxaline and found that even similar chemical property of cyclohexane and *n*-hexane gave a different screw-sense of helical structure. Recently, the origin of this solvent effect was revealed by neutron diffraction and molecular mechanics calculations.[27] A right-handed helix of polyquinoxaline is formed when the side chain extends and spreads, while a left-handed helix is formed when the side chain is located along the main chain. In this way, the macromolecular effect can generate drastic differences from slight differences that are insignificant for small molecules. The

macromolecular effect requires a sufficient high molecular weight to exhibit its effect. High molecular weight polypeptide is essential to design the peptide-based polymer utilizing a macromolecule effect.

1-4: Introduction of Asymmetric Carbon on the Main Chain

Biopolymers, such as protein, DNA and polysaccharide, always have asymmetric carbon on the main chain. To synthesize a polymer with an asymmetric carbon in the main chain, a naturally abundant compound is often used as a building block is often used. For example, the polymerization of α-amino acid *N*-carboxyanhydrides (NCA) uses various modified α-amino acids as the building blocks. This method produces high-molecular-weight polymers with a relatively narrow molecular weight distribution.[18h,28] However, since this method can only utilize α-amino acids as the starting materials, it is impossible to synthesize extremely diverse polymers. Asymmetric polymerization is an effective method to synthesize polymers having asymmetric carbon in the main chain. In recent years, various asymmetric reactions with metal catalysts have been developed. Nevertheless, there are not many reports of asymmetric polymerization using metal catalysts. As presented below, the polymerization process must be preferentially reactive so as to obtain a high-molecular-weight polymer and no side products. Moreover, perfect selectivity of the asymmetric carbon in the backbones is a necessary albeit rather difficult goal to accomplish. To this end, only a few asymmetric polymerizations with an asymmetric center in the main chain have been reported. Nozaki et al.[29] have reported the polyketones with an asymmetric carbon (> 95% ee) in the main chain using a palladium complex consisting of a chiral phosphine-phosphite ligand as the catalyst (Figure 1-7).The resulting polyketones do not form a well-defined structure due to a lack of other structural control factors. Despite the fact that polymer synthesis in which an asymmetric carbon is introduced into the main chain of each monomer unit is an underdeveloped field of research, many still believe that asymmetric carbons are key to the development of useful polymers, because this design feature is often found in crucial biopolymers, such as proteins, DNA, and polysaccharides.

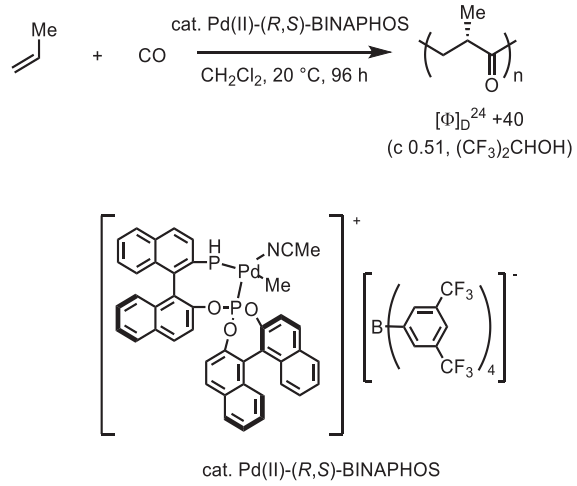

Figure 1-7. Nozaki's work.

1-5: Objective of This Thesis

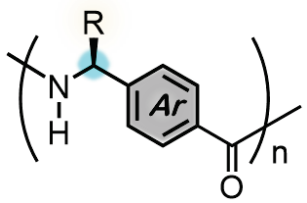

Figure 1-8. Chemical structure of arylopeptide.

T The main objective of this thesis is to create a novel peptide-based aromatic polymer that maintains the fundamental properties of the parent polypeptide while incorporating molecular design features, such as aromatic moiety, asymmetric centers, hydrogen bond, and planarity in amide group and aromatic ring into the concept for novel peptide-based polymer. Here, the author proposes a novel polymer design called "**Arylopeptide**" (Figure 1-8).[30] The design is very simple to carry out and satisfied all the requirements for synthesis that are highlighted in Figure 1-2.

Previously, our laboratory has reported an asymmetric allylic substitution reaction using a planar-chiral cyclopentadienyl–ruthenium complex, and has recently developed a method for asymmetric polymerization based on the allylic substitution reaction (Figure 1-9a, first step). The resulting optically active polymer had strictly controlled asymmetric centers in the main chain, and since various achiral monomers could be used, including an aromatic ring, the flexibility of the main chain was ensured. In addition to the flexibility of the main chain, the Kanbayashi et al. have reported the quantitative introduction of various substituents through the thiol–ene reaction, focusing on the terminal olefin of polymer (Figure 1-9a, second step).

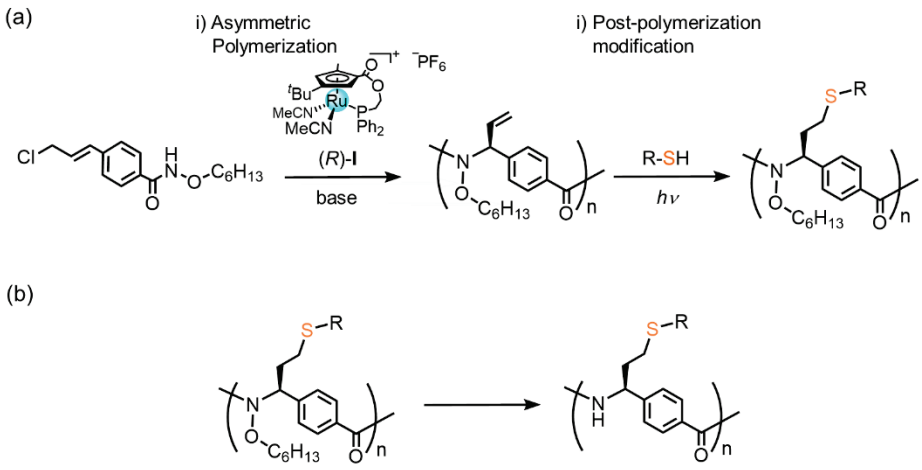

Figure 1-9. Previous work in our laboratory.

Therefore, conversion of the N–O bonds to N–H results in a polymer that possesses arylopeptide backbone (Figure 1-9b). This synthetic method of combining asymmetric polymerization and post-polymerization modifications is a practical tool for the successful synthesis of arylopeptides. Although this synthetic method limits the diversity of the side chain (R) to $–CHCH_2CH_2S–$ substituents, a sufficiently influential side chain effect is exerted on the polypeptide as shown in the following chapters.

This thesis is mainly composed of Chapters 2–5 (Figure 1-10). Chapter 2 focuses on the synthetic method of arylopeptide structural analysis. Chapters 3–5 describes the development and application of various arylopeptide analogs.

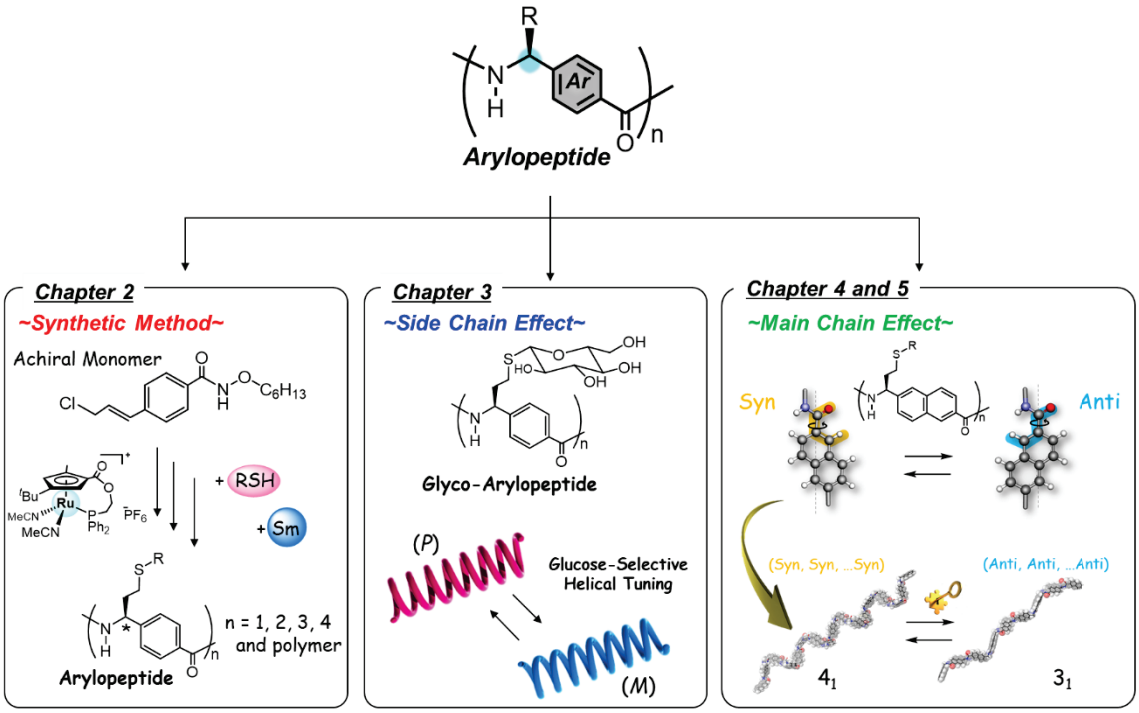

Figure 1-10. Outline of this thesis.

Chapter 2 presents the synthetic methodology for arylopeptide (Figure 1-11). To synthesize peptide backbone, the author develops the amino-acid-free peptide synthesis method via asymmetric polymerization and post-polymerizations. This method provides arylopeptides from the achiral monomer. The structure of synthesized arylopeptides are analyzed by a multi-method such as oligomers synthesis (n = 1, 2, 3, 4), theoretical analysis, and computational study.

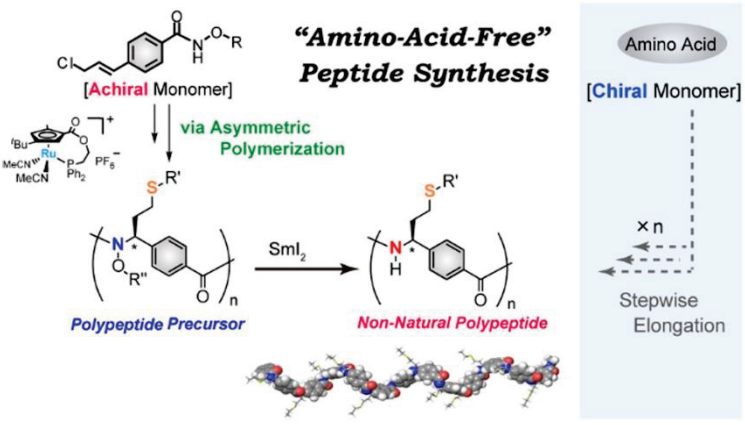

Figure 1-11. Synthetic method of arylopeptide using "*Amino-Acid-Free*" Peptide Synthesis

In Chapter 3, the side chain effect for the helical structure is shown. In particular, the structure and properties of glycopeptides are thoroughly examined. Arylopeptides distinguish the type of saccharide, producing distinct well-defined structures (Figure 1-12). This study indicates that even the properties of the arylopeptides, which are entirely artificial polypeptide molecules, are controlled by the type of saccharides similar to nature ivolving in the elaborated relationship between peptide backbone and glycoconjugate including chiral information and hydration.

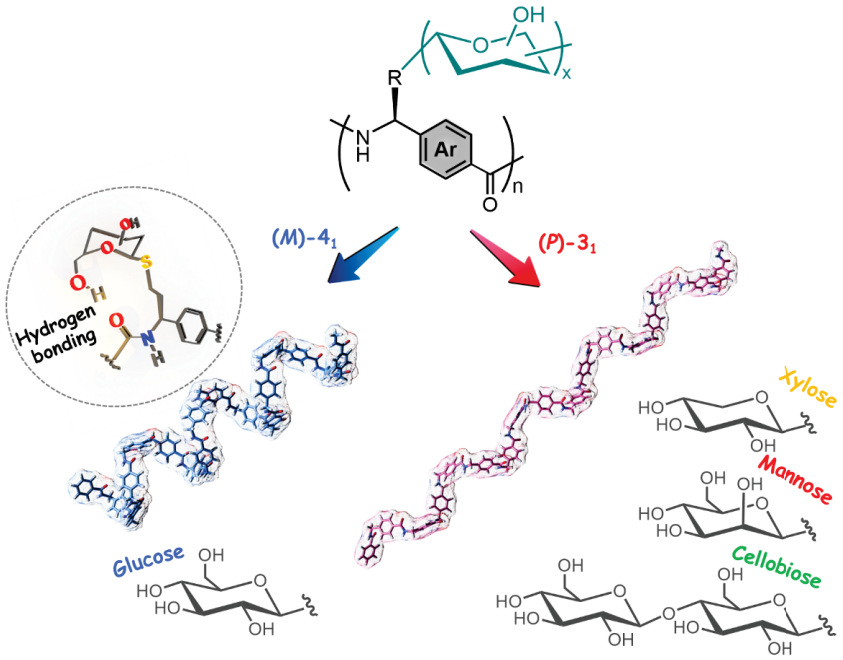

Figure 1-12. Glucose-selective Helical Tuning Information of Arylopeptide

Chapter 4 presents synthesis of arylopeptides bearing 2,6-naphthylene unit and side chain-driven dual system of helical conformations. 2,6-Naphthalene rings as axially unsymmetrical spacers, and the spacer has two

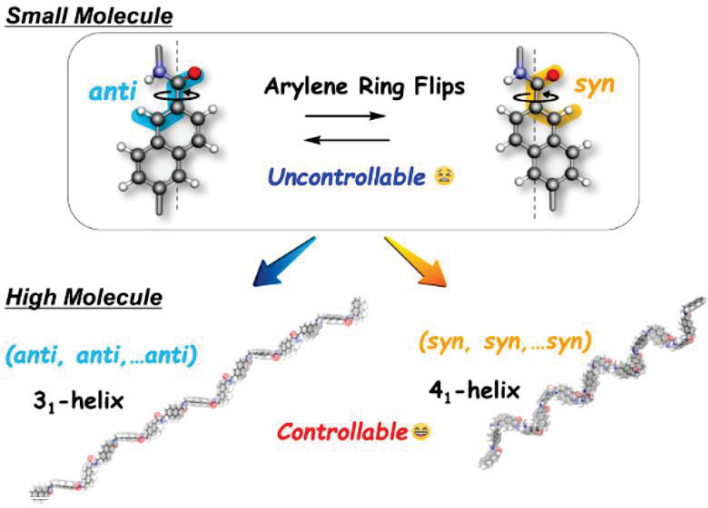

Figure 1-13. Side-chain Driven Dual Structural System of Helical Arylopeptide.

geometrical isomers, *anti* and *syn*, to create dual structural properties. The minuscule energy difference between the two geometrical isomers can be amplified by incorporating the 2,6-naphthylene units into the polypeptide backbone, which creates a thermodynamic driving force for the formation of two specific global structures (i.e., 3_1-helix or 4_1-helix) biased toward one side geometrical isomer depending on the side chain (Figure 1-13).

In Chapter 5, the relationship between backbone, side chain, and well-defined global conformation of arylopeptide was investigated. The helical structure of arylopeptide shows static or dynamic helical properties depending on backbones. The combination of side chains and solvent plays an important role in the folding selectivity of arylopeptide (Figure 1-14). The principle determining folding selectivity is revealed, and the molecular switch including helix-to-helix transition is developed.

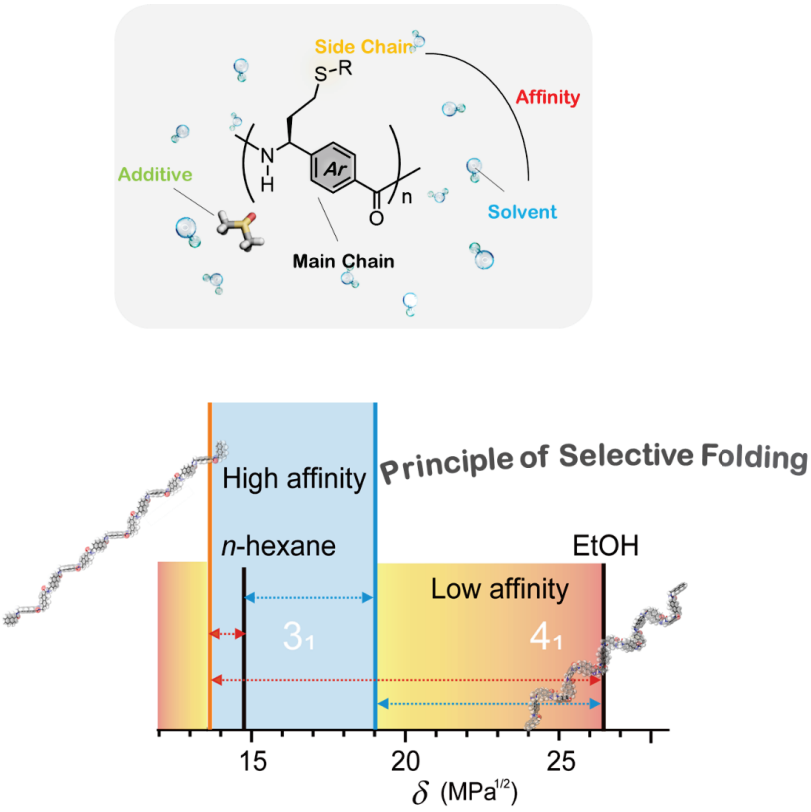

Figure 1-14. Outline of Chapter 5.

Reference

(1) Branden, C. I.; Tooze, J. *Introduction to protein structure*; Garland Publishing: New York, 1991.

(2) (a) Ramakrishnan, C.; Ramachandran, G. N. *Biophys. J.* **1965**, *5*, 909. (b) Schulz, G. E.; Schirmer, R. H. *Principles of protein structure*; Springer-Verlag: Now York, 1979.

(3) (a) Hill, D. J.; Mio, M. J.; Prince, R. B.; Hughes, T. S.; Moore, J. S. *Chem. Rev.* **2001**, *101*, 3893. (b) Huc, I. *Eur. J. Org. Chem.* **2004**, *2004*, 17. (c) Hecht, S.; Huc, I. *Foldamers: Structure, Properties, and Applications*;

Wiley-VCH: Weinheim, 2007. (d) Guichard, G.; Huc, I. *Chem. Commun.* **2011**, *47*, 5933.

(4) Gellman, S. H. *Acc. Chem. Res.* **1998**, *31*, 173.

(5) Cheng, R. P.; Gellman, S. H.; DeGrado, W. F. *Chem. Rev.* **2001**, *101*, 3219.

(6) (a) Dado, G. P.; Gellman, S. H. *J. Am. Chem. Soc.* **1994**, *116*, 1054. (b) Appella, D. H.; Christianson, L. A.; Karle, I. L.; Powell, D. R.; Gellman, S. H. *J. Am. Chem. Soc.* **1996**, *118*, 13071. (c) Seebach, D.; Overhand, M.; Kühnle, F. N.; Martinoni, B.; Oberer, L.; Hommel, U.; Widmer, H. *Helv. Chim. Acta* **1996**, *79*, 913.

(7) Hanessian, S.; Luo, X.; Schaum, R.; Michnick, S. *J. Am. Chem. Soc.* **1998**, *120*, 8569.

(8) (a) Zuckermann, R. N. *Curr. Opin. Struct. Biol.* **1993**, *3*, 580. (b) Armand, P.; Kirshenbaum, K.; Falicov, A.; Dunbrack, R. L.; Dill, K. A.; Zuckermann, R. N.; Cohen, F. E. *Fold. Des.* **1997**, *2*, 369. (c) Shin, S. B. Y.; Yoo, B.; Todaro, L. J.; Kirshenbaum, K. *J. Am. Chem. Soc.* **2007**, *129*, 3218. (d) Yoo, B.; Kirshenbaum, K. *Curr. Opin. Chem. Biol.* **2008**, *12*, 714. (e) Zuckermann, R. N. *Pept. Sci.* **2011**, *96*, 545. (f) Huang, M. L.; Ehre, D.; Jiang, Q.; Hu, C.; Kirshenbaum, K.; Ward, M. D. *Proc. Natl. Acad. Sci. U.S.A.* **2012**, *109*, 19922.

(9) Zhang, D.-W.; Zhao, X.; Hou, J.-L.; Li, Z.-T. *Chem. Rev.* **2012**, *112*, 5271.

(10) (a) Dolain, C.; Grélard, A.; Laguerre, M.; Jiang, H.; Maurizot, V.; Huc, I. *Chem. Eur. J.* **2005**, *11*, 6135. (b) Dolain, C.; Jiang, H.; Léger, J.-M.; Guionneau, P.; Huc, I. *J. Am. Chem. Soc.* **2005**, *127*, 12943. (c) Sanchez-Garcia, D.; Kauffmann, B.; Kawanami, T.; Ihara, H.; Takafuji, M.; Delville, M.H.; Huc, I. *J. Am. Chem. Soc.* **2009**, *131*, 8642. (d) Ferrand, Y.; Kendhale, A. M.; Garric, J.; Kauffmann, B.; Huc, I. *Angew. Chem., Int. Ed.* **2010**, *49*, 1778. (e) Dawson, S.; Hu, X.; Claerhout, S.; Huc, I. In *Methods in enzymology*; Elsevier, 2016; Vol. 580. (f) De, S.; Chi, B.; Granier, T.; Qi, T.; Maurizot, V.; Huc, I. *Nat. Chem.* **2018**, *10*, 51.

(11) Sebaoun, L.; Maurizot, V.; Granier, T.; Kauffmann, B.; Huc, I. *J. Am. Chem. Soc.* **2014**, *136*, 2168.

(12) Lamouroux, A.; Sebaoun, L.; Wicher, B.; Kauffmann, B.; Ferrand, Y.; Maurizot, V.; Huc, I. *J. Am. Chem. Soc.* **2017**, *139*, 14668.

(13) Saha, S.; Kauffmann, B.; Ferrand, Y.; Huc, I. *Angew. Chem., Int. Ed.* **2018**, *57*, 13542.

(14) Gillies, E. R.; Deiss, F.; Staedel, C.; Schmitter, J.-M.; Huc, I. *Angew. Chem., Int. Ed.* **2007**, *46*, 4081.

(15) Corvaglia, V.; Carbajo, D.; Prabhakaran, P.; Ziach, K.; Mandal, P. K.; Santos, V. D.; Legeay, C.; Vogel, R.; Parissi, V.; Pourquier, P.; Huc, I. *Nucleic Acids Research* **2019**, *47*, 5511.

(16) Li, X.; Markandeya, N.; Jonusauskas, G.; McClenaghan, N. D.; Maurizot, V.; Denisov, S. A.; Huc, I. *J. Am. Chem. Soc.* **2016**, *138*, 13568.

(17) Nakano, T.; Okamoto, Y. *Chem. Rev.* **2001**, *101*, 4013.

(18) (a) Ciardelli, F.; Lanzillo, S.; Pieroni, O. *Macromolecules* **1974**, *7*, 174. (b) Vogl, O.; Jaycox, G. D. *Chemtech* **1986**, *16*, 698. (c) Moore, J. S.; Gorman, C. B.; Grubbs, R. H. *J. Am. Chem. Soc.* **1991**, *113*, 1704. (d) Nolte, R. J. *Chem. Soc. Rev.* **1994**, *23*, 11. (e) Green, M. M.; Peterson, N. C.; Sato, T.; Teramoto, A.; Cook, R.; Lifson, S. *Science* **1995**, *268*, 1860. (f) Cornelissen, J. J. L. M.; Rowan, A. E.; Nolte, R. J. M.; Sommerdijk, N. A. J. M. *Chem. Rev.* **2001**, *101*, 4039. (g) Maeda, K.; Yashima, E. *J. Synth. Org. Chem. Jpn.* **2002**, *60*, 878. (h) Cheng, J.; Deming, T. J. *Top. Curr. Chem.* **2012**, *310*, 1.

(19) (a) Green, M. M.; Peterson, N. C.; Sato, T.; Teramoto, A.; Cook, R.; Lifson, S. *Science* **1995**, *268*, 1860. (b) Green, M. M.; Park, J.-W.; Sato, T.; Teramoto, A.; Lifson, S.; Selinger, R. L. B.; Selinger, J. V. *Angew. Chem., Int. Ed.* **1999**, *38*, 3138.

(20) (a) Green, M. M.; Reidy, M. P.; Johnson, R. D.; Darling, G.; O'Leary, D. J.; Willson, G. *J. Am. Chem. Soc.*

1989, *111*, 6452. (b) Green, M. M.; Garetz, B. A.; Munoz, B.; Chang, H.; Hoke, S.; Cooks, R. G. *J. Am. Chem. Soc.* **1995**, *117*, 4181.

(21) (a) Bouman, M. M.; Meijer, E. W. *Adv. Mater.* **1995**, *7*, 385. (b) Watanabe, J.; Okamoto, S.; Satoh, K.; Sakajiri, K.; Furuya, H.; Abe, A. *Macromolecules* **1996**, *29*, 7084. (c) Maeda, K.; Okamoto, Y. *Macromolecules* **1998**, *31*, 5164. (d) Cheon, K. S.; Selinger, J. V.; Green, M. M. *Angew. Chem., Int. Ed.* **2000**, *39*, 1482. (e) Fujiki, M. *J. Am. Chem. Soc.* **2000**, *122*, 3336. (f) Tang, K.; Green, M. M.; Cheon, K. S.; Selinger, J. V.; Garetz, B. A. *J. Am. Chem. Soc.* **2003**, *125*, 7313. (g) Ohira, A.; Kunitake, M.; Fujiki, M.; Naito, M.; Saxena, A. *Chem. Mater.* **2004**, *16*, 3919.

(22) (a) Maxein, G.; Zentel, R. *Macromolecules* **1995**, *28*, 8438. (b) Mayer, S.; Maxein, G.; Zentel, R. *Macromolecules* **1998**, *31*, 8522. (c) Li, J.; Schuster, G. B.; Cheon, K. S.; Green, M. M.; Selinger, J. V. *J. Am. Chem. Soc.* **2000**, *122*, 2603. (d) Pijper, D.; Feringa, B. L. *Angew. Chem., Int. Ed.* **2007**, *46*, 3693. (e) Pijper, D.; Jongejan, M. G. M.; Meetsmia, A.; Feringa, B. L. *J. Am. Chem. Soc.* **2008**, *130*, 4541.

(23) (a) Otsuka, I.; Sakai, R.; Satoh, T.; Kakuchi, R.; Kaga, H.; Kakuchi, T. *J. Polym. Sci., Part A: Polym. Chem.* **2005**, *43*, 5855. (b) Otsuka, I.; Sakai, R.; Kakuchi, R.; Satoh, T.; Kakuchi, T. *Eur. Polym. J.* **2008**, *44*, 2971. (c) Freire, F.; Seco, J. M.; Quinoa, E.; Riguera, R. *Angew. Chem., Int. Ed.* **2011**, *50*, 11692.

(24) (a) Okamoto, Y.; Nakano, T.; Ono, E.; Hatada, K. *Chem. Lett.* **1991**, 525. (b) Sanda, F.; Terada, K.; Masuda, T. *Macromolecules* **2005**, *38*, 8149.

(25) (a) Green, M. M.; Khatri, C.; Peterson, N. C. *J. Am. Chem. Soc.* **1993**, *115*, 4941. (b) Bidan, G.; Guillerez, S.; Sorokin, V. *Adv. Mater.* **1996**, *8*, 157. (c) Langeveld-Voss, B. M. W.; Christiaans, M. P. T.; Janssen, R. A. J.; Meijer, E. W. *Macromolecules* **1998**, *31*, 6702. (d) Goto, H.; Yashima, E.; Okamoto, Y. *Chirality* **2000**, *12*, 396. (e) Fujiki, M.; Koe, J. R.; Motonaga, M.; Nakashima, H.; Terao, K.; Teramoto, A. *J. Am. Chem. Soc.* **2001**, *123*, 6253. (f) Nakako, H.; Nomura, R.; Masuda, T. *Macromolecules* **2001**, *34*, 1496. (g) Cheuk, K. K. L.; Lam, J. W. Y.; Chen, J. W.; Lai, L. M.; Tang, B. Z. *Macromolecules* **2003**, *36*, 5947. (h) Cheuk, K. K. L.; Lam, J. W. Y.; Lai, L. M.; Dong, Y. P.; Tang, B. Z. *Macromolecules* **2003**, *36*, 9752. (i) Maeda, K.; Morino, K.; Yashima, E. *J. Polym. Sci., Part A: Polym. Chem.* **2003**, *41*, 3625. (j) Morino, K.; Maeda, K.; Yashima, E. *Macromolecules* **2003**, *36*, 1480. (k) Maeda, K.; Kamiya, N.; Yashima, E. *Chem. Eur. J.* **2004**, *10*, 4000. (l) Zhao, H. C.; Sanda, F.; Masuda, T. *Polymer* **2005**, *46*, 2841. (m) Yamazaki, K.; Yokoyama, A.; Yokozawa, T. *Macromolecules* **2006**, *39*, 2432. (n) Hasegawa, T.; Furusho, Y.; Katagiri, H.; Yashima, E. *Angew. Chem., Int. Ed.* **2007**, *46*, 5885. (o) Fukushima, T.; Tsuchihara, K. *Macromol. Rapid Commun.* **2009**, *30*, 1334.

(26) Nagata, Y.; Nishikawa, T.; Suginome, M. *J. Am. Chem. Soc* **2014**, *136*, 15901.

(27) Nagata, Y.; Nishikawa, T.; Suginome, M.; Sato, S.; Sugiyama, M.; Porcar, L.; Martel, A.; Inoue, R.; Sato, N. *J. Am. Chem. Soc.* **2018**, *140*, 2722.

(28) (a) Deming, T. J. *Polym. Chem.* **2000**, *38*, 3011. (b) Kramer, J. R.; Deming, T. J. *J. Am. Chem. Soc.* **2014**, *136*, 5547. (c) Deming, T. J. *Chem. Rev.* **2015**, *116*, 786.

(29) Nozaki, K.; Sato, N.; Tonomura, Y.; Yasutomi, M.; Takaya, H.; Hiyama, T.; Matsubara, T.; Koga, N. *J. Am. Chem. Soc.* **1997**, *119*, 12779.

(30) (a) Hjelmgaard, T.; Faure, S.; Staerk, D.; Taillefumier, C.; Nielsen, J. *Eur. J. Org. Chem.* **2011**, *2011*, 4121. (b) Hjelmgaard, T.; Nielsen, J. *Eur. J. Org. Chem.* **2013**, *2013*, 3574.

Chapter 2

Synthesis of Arylopeptide via Asymmetric Polymerization and Post-Polymerization Modifications and Structural Analysis

2-1: Introduction

Proteins are typical optically active polymers with the ability to adopt well-defined folding of the polypeptide chain. They exhibit biological functions such as catalysis, energy transduction, and molecular recognition. These excellent functions are inseparably linked to the higher-order structure arising from the sophisticated secondary structures. Therefore, synthesis of new structural building blocks that contain the programmed design required for folding are important. In the past two decades, nonnatural oligopeptides[1] containing various spacers, such as aliphatic[2] or aromatic[3] groups, have been designed and synthesized to develop functional materials and to understand the relationship between the primary structure, folding, and function in natural proteins. The amide bond group is a rigid structure with planarity, and acts as hydrogen bond acceptor and donor. The resulting oligopeptides can fold into a well-defined unique folded structure according to the designed backbone, which shows interesting functional properties.[4] The diversity of the backbones can lead to new motifs and functions.

Most nonnatural polypeptides have been synthesized by a condensation reaction of nonnatural chiral amino acids, which can realize polypeptides with perfectly defined lengths and sequences. However, the spacer group between amino acids is less amenable to design because synthesis of novel nonnatural amino acids requires the enantiomerically pure synthesis. Additionally, the synthesis of high-molecular-weight polymers is also difficult because racemization must be strictly prevented during all chain elongation steps, and purification is difficult due to the solubility of the product. Nonnatural polypeptides were synthesized by the ring-opening polymerization of chiral lactams,[5] which is a popular approach for the synthesis of the high-molecular-weight polypeptide. However, this technique also greatly limits the monomer structure that can be used.

As the author mentioned in Chapter 1, the main object of this thesis is to synthesize the novel type of nonnatural polypeptide called “arylopeptide,” which contains an aromatic ring in the main chain. Aromatic rings in the main chain provide moderate rigidity to the polymer chain and also enable high designability compared with the aliphatic polypeptide. However, the synthetic method is extremely difficult because the corresponding amino acids do not exist in nature, and organic synthesis of such an amino acid with perfectly enantio-selectivity is also difficult. Thus, a completely new synthetic pathway of generating arylopeptide is required.

Previously, our laboratory achieved the asymmetric polymerization[6] of achiral monomers based on asymmetric allylic substitution catalyzed by planar–chiral cyclopentadienylruthenium complexes (I)[7] to afford

poly-*N*-alkoxyamide (Scheme 2-1a, **poly-1**). The presence of asymmetric carbons in the main chain of the resulting polymer was precisely controlled, various arylene spacer could introduce since **poly-2** was synthesized by polycondensation. Furthermore, recently the authors have revealed that **poly-1** could easily modify via its side chains, using the thiol–ene reaction as a post-polymerization method to enable the quantitative introduction of a wide range of substituents (**poly-2**). The author focus on the chemical structure of **poly-2**. **Poly-2** is an optically active polymer having asymmetric carbons in the main chain and various side chains, and it can be regarded as a precursor of polypeptide after conversion of N–O to N–H bond.

Herein, we present the synthesis of arylopeptide using our asymmetric polymerization, followed by reductive cleavage of the N–O bonds. The simplest aromatic ring, *p*-phenylene, was used as a spacer. The synthesis of polypeptides with aromatic rings in the main chain is first achieved. This method is called "amino-acid-free peptide synthesis," which does not require precise stepwise elongation of enantiomerically pure amino acids. In addition, the arylopeptide formed well-defined helical structures because the asymmetric centers in the monomer unit and rigid amide plane are strictly realized like natural polypeptides.

Scheme 2-1. Synthetic approach to aryropeptide

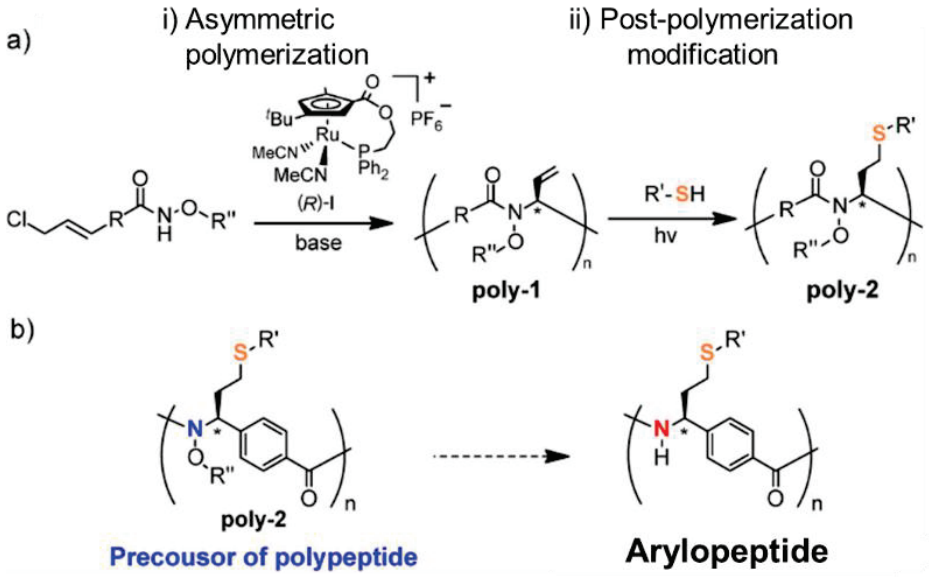

2-2: Results and Discussion

Synthesis and Characterization of Arylopeptide

Samarium(II) iodide tetrahydrofuran complex (SmI_2–THF) is known as a mild reductive reagent and the reductive cleavage of N–O bonds of low-molecular weight organic compounds has been reported.[8] To apply to post-polymerization, no side reactions are allowed from the viewpoint of purification. In addition, it is necessary to prevent racemization because this reaction is applied to chiral polymer. To investigate the applicability of the reductive reaction using SmI_2–THF as a post-polymerization, the synthesis of **3** as a model reaction was conducted using SmI_2–THF (Figure 2-1b). The expected amide compound was selectively obtained in a quantitative (>99%) yield, with neither racemization nor side reactions. Therefore, the reaction system was applied to **poly-2**.[9] In this study, **poly-2a** (R′ = $C_{12}H_{25}$, M_w = 51 000, M_w/M_n = 2.5, n = 110) was used as a start material, which was prepared according to the reported procedure using (*R*)-**I** as a catalyst.[6a,9] The treatment of **poly-2a** with SmI_2 in THF ([N–O of **poly-2a**]/[SmI_2] = 1/4.6) also resulted in the quantitative conversion of *N*-alkoxyamide moieties into amide groups even for polymer (Scheme 2-2). This is the first example in which the SmI_2 complex was applied in post-polymerization. **Poly-3a** was isolated in 83% yield by removing samarium(III) compound (it is easily removed by *n*-hexane). The ^{1}H NMR spectrum of **poly-3a** in $CDCl_3$ at 25 °C is

Scheme 2-2. Reductive cleavage of N–O bond of poly-2

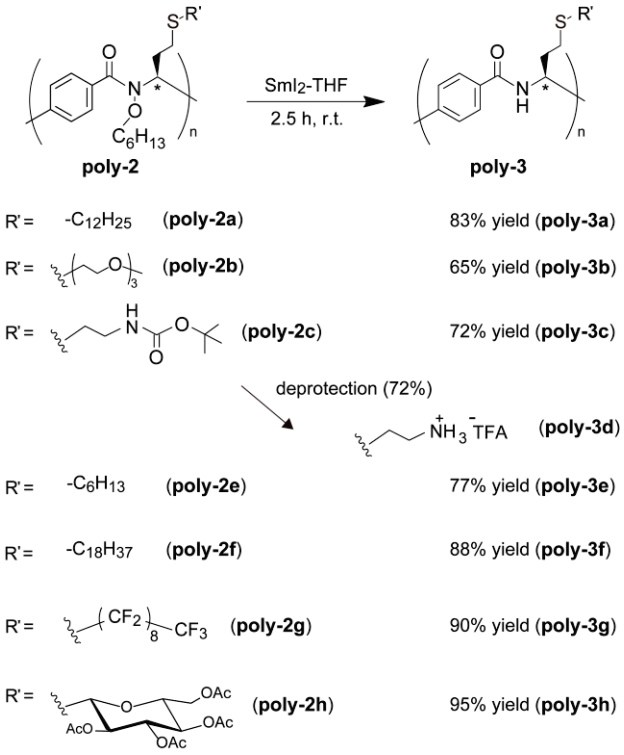

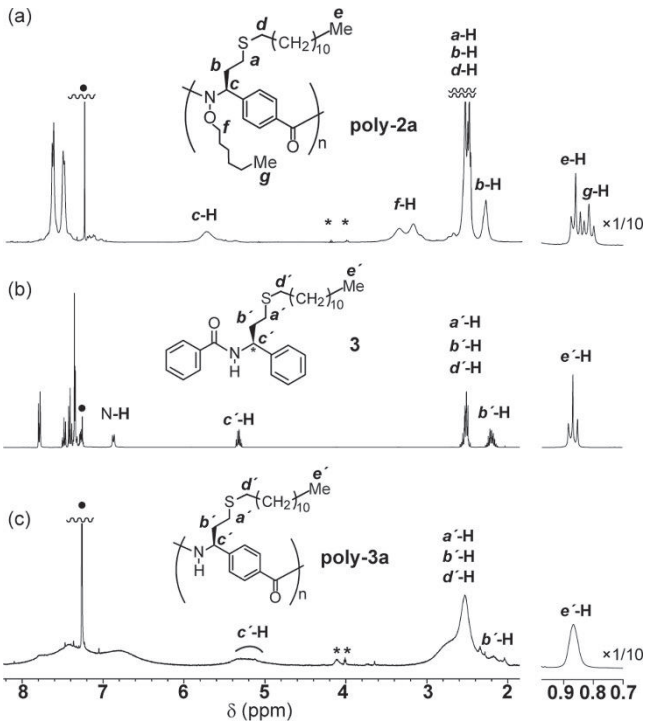

Figure 2-1. ^{1}H NMR (500 MHz, in $CDCl_3$ at 298 K) spectra of (a) **poly-2a**, (b) model compound **3**, and (c) **poly-3a**. The asterisks (*) denote impurity.

shown in Figure 2-1, in comparison with the model compound **3**. The reductive reaction was confirmed by the disappearance of the proton signals (*c*-H, *f*-H, and *g*-H) (Figure 2-1a) and the appearance of a new broad signal (*c*′-H) in **poly-3a** (Figure 2-1c), which is similar to the spectrum of **3** (Figure 2-1b). Any signal originated from undesired side reactions were not observed. The ^{1}H NMR signals of **poly-3a** were broader than those of **poly-2a** presumably because of intermolecular aggregation of the polymer at the concentration of NMR measurement ([**poly-3a**] = 134 mM). Indeed, after the addition of 2,2,2-trifluoroethanol (TFE)-d_3 as a hydrogen-bond competitor to a $CDCl_3$ solution of **poly-3a**, the signals became sharper (Figure 2-2b).

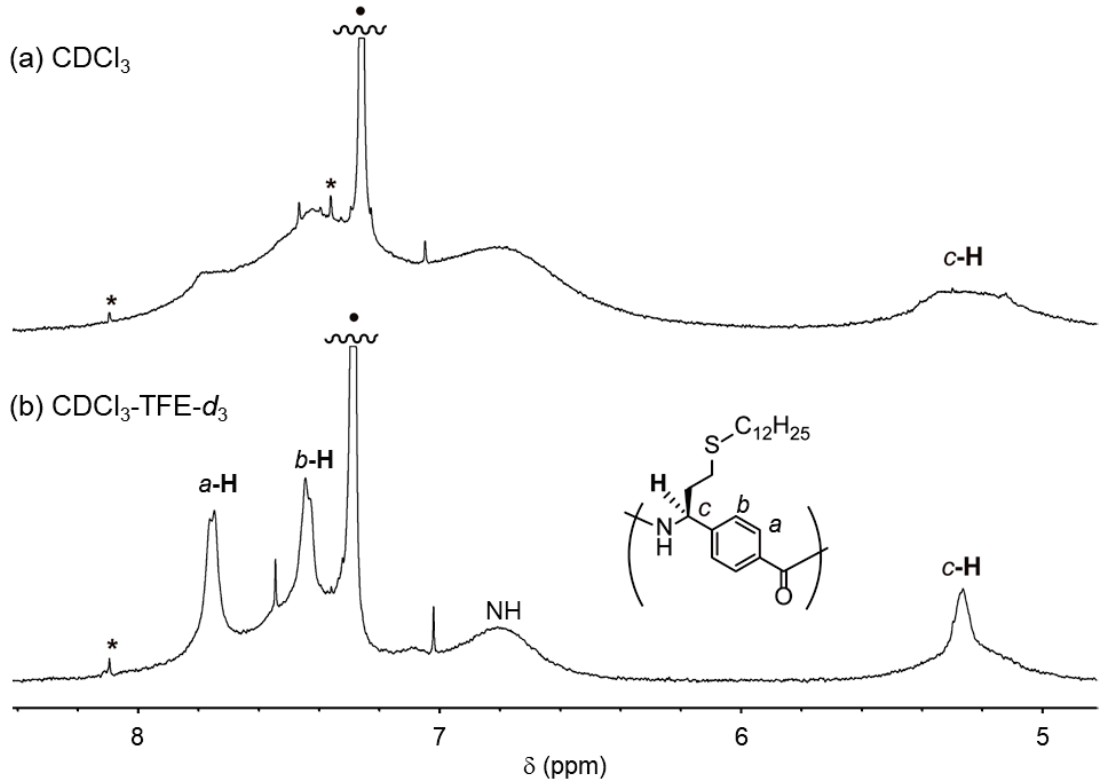

Figure 2-2. ^{1}H NMR (500 MHz, at 25 ºC) spectra of **poly-3a** in (a) $CDCl_3$, and (b) the mixture of $CDCl_3$/TFE-d_3 = 2:1 (v/v). Concentration: [**poly-3a**] = 134 mM. The asterisks (*) denote impurity, and the filled circles (•) denote the signal due to $CHCl_3$.

Although the N–H signal was not clearly observed in the ^{1}H NMR spectrum of **poly-3a**, the NH stretching band was detected at 3319 cm^{-1} in the IR spectrum of **poly-3a** (Figure 2-3). The M_w and M_w/M_n values of **poly-3a** were determined to be 3.9×10^4 and 2.6 by size-exclusion chromatography (SEC) with calibration using polystyrene standards (Figure 2-4). This reaction maintained the polymer backbone, and any undesired side reactions were not observed. The scope of this reaction for **poly-2** with different side chains (**poly-2b**, **c**, **e–h**) were also examined (Scheme 2-2). The reaction of all polymers proceeded with almost quantitative conversions, and the products **poly-3b**, **c**, **e-h** were isolated in good yields. For instance, since samarium has a high oxygen-affinity, the presence of multiple oxygen atoms is expected to afford a negative impact to reductive reaction, but the reaction proceeded successfully even when the side chain was an oligo (ethylene glycol) unit (**poly-3b**). Although SmI_2–THF is often used as a reductant for C=X bonds (X = C, N, O), *tert*-butoxycarbonyl (Boc) group was fully retained (**poly-3c**), and the subsequent deprotection gave a water-soluble arylopeptide (**poly-3d**) having cationic side chain. All of the multiple ester groups of (**poly-2h**) were also retained. The reductive reaction proceeded efficiently, even with bulky side chains such as saccharide moiety. Although **poly-3g** is an insoluble solid and NMR analysis was difficult, only CO-NH amide group absorption was observed in IR, so the reaction seemed to proceed. The samarium reagent exhibits a wide tolerance for various functional groups, although the reductive reaction of **poly-1** having C=C bonds did not produce desired product.

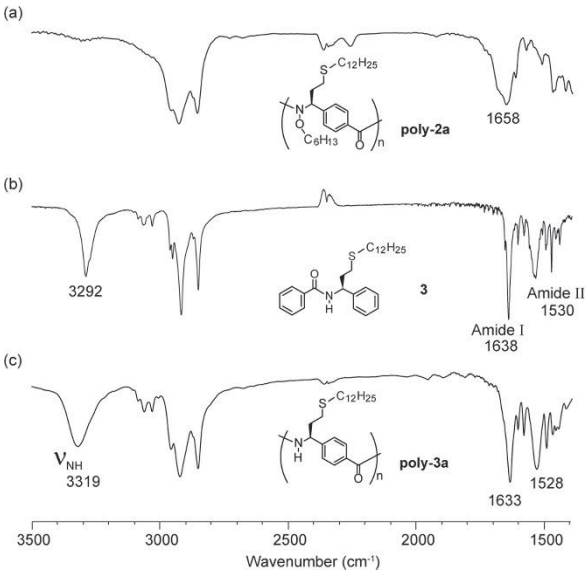

Figure 2-3. IR spectra of (a) **poly-2a**, (b) model compound **3**, and (c) **poly-3a** (KBr tablet).

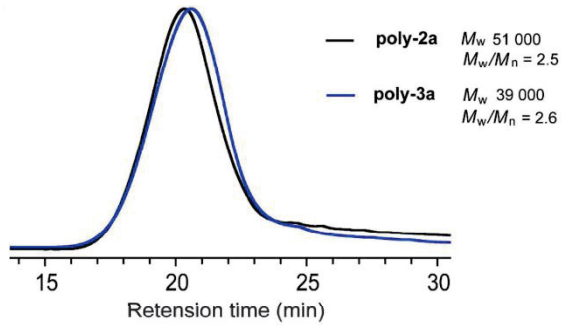

Figure 2-4. SEC chromatograms of (A) **poly-2a** and **poly-3a** in $CHCl_3$ at 40 °C

Structural Analysis of Synthesized Arylopeptide

The polymer conformation of isolated **poly-3a** was investigated by means of UV absorption and circular dichroism (CD) spectroscopies in THF at 25 °C (Figure 2-5a). The main chain of **poly-2a** is flexible than those of polypeptides because the rotational barrier of the N–C bonds in the *N*-alkoxyamide moiety is relatively low compared with that in amides. Therefore, the CD intensity of **poly-2a** in THF was weak (Figure 2-5a).[9] On the other hand, the CD spectrum of **poly-3a** showed a large bisignate Cotton effect at 238 and 258 nm that differed from those of the corresponding monomer (**4**) The CD and UV signals of **poly-3a** did not change over the concentration range of 0.034-32 mM or after the addition of the TFE as a hydrogen-bond competitor to a THF solution. These results indicate that the polymer chain does not form higher-order chiral aggregates at the concentration of CD measurements. Therefore, additional chirality derived from the asymmetric carbon in the main chain was present, which suggested a one-handed helical structure for **poly-3a.**

To reveal the origin of the Cotton effect of **poly-3a**, oligomers (n = 1, 2, 3, 4) were synthesized by step-wise elongation (See Experimental Section). The UV and CD spectroscopic analyses of oligomers **4**–**6** (n = 1, 2, 4) were conducted (Figure 2-5b). In monomer **4** (n = 1), two positive Cotton effects were observed at 241 and 274 nm. On the other hand, dimer **5** (n = 2) showed new bisignate Cotton effects at 229 and 250 nm, similar to that

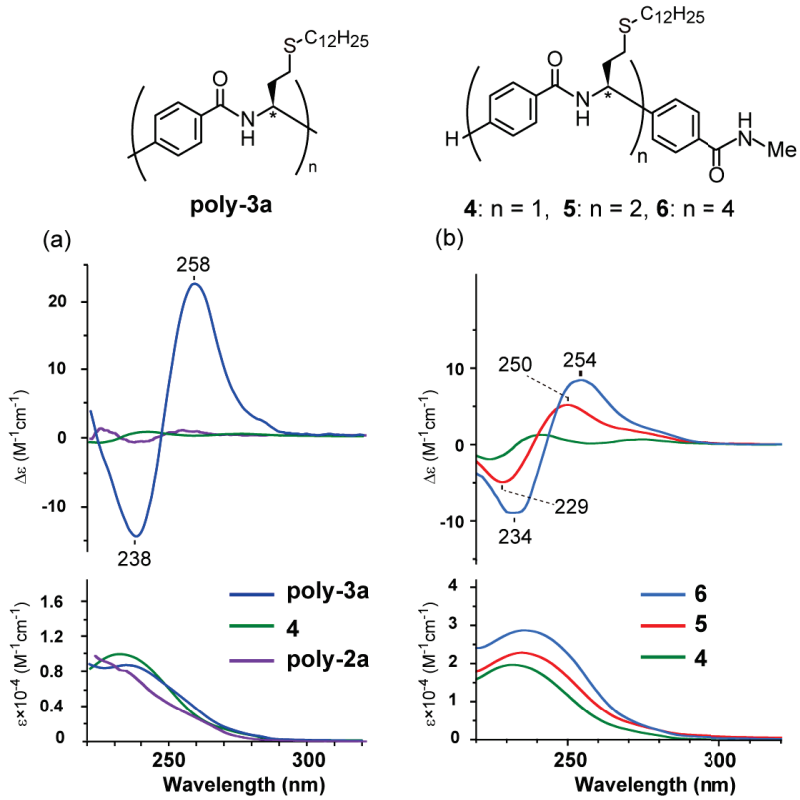

Figure 2-5. CD and UV spectra of (a) **poly-2a** (0.32 mM), **poly-3a** (0.30 mM), and model compound (0.21 mM), (b) **poly-3a** (0.32 mM) and 4 (0.17 mM) in THF at 25 °C

of **poly-3a**, which shifted to longer wavelengths as the monomer units were elongated (from n = 2 to 4). NMR studies were carried out to investigate the conformation in solution. In the ^{1}H NMR spectrum of **4**, applying the Karplus equation[3d,10] to the coupling constant of the internal NH proton $J_{HN–CH}$ indicates a HN–CH dihedral angle of $\phi = -87°$, which closely agrees with the dihedral angle observed in the crystal structure of **3′** ($\phi = -85°$) (Figure 2-6 and Table S2-1).

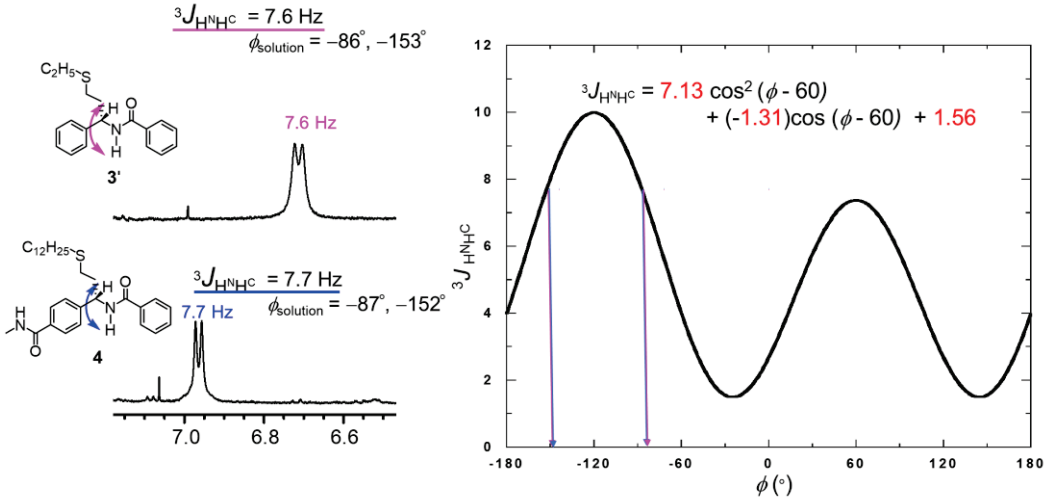

Figure 2-6. Partial ^{1}H NMR spectra of **3′** and **4** and its Karplus equation.

The density functional theory (DFT) and time-dependent density functional theory (TD-DFT) calculation of **4** was based on the crystal structure of **3′** and conducted at the B3LYP/6-31G** level of theory.[11] The calculated UV and CD spectra were in close agreement with those of **4**. Next, the spectra of dimer **5** (n = 2) were analyzed. Because the carbonyl group and benzene rings are generally regarded as coplanar, two different possible conformations based on the optimized structure of **4** can be assumed according to the orientation of the vicinal unit: *turn* (**5**$_{turn}$) and *zigzag* (**5**$_{zig}$) types (Figure 2-7). After geometrical optimizations of **5**$_{turn}$ and **5**$_{zig}$ by DFT calculation, TD-DFT calculation was conducted in the same manner as that for **4**. The calculated UV and CD spectra

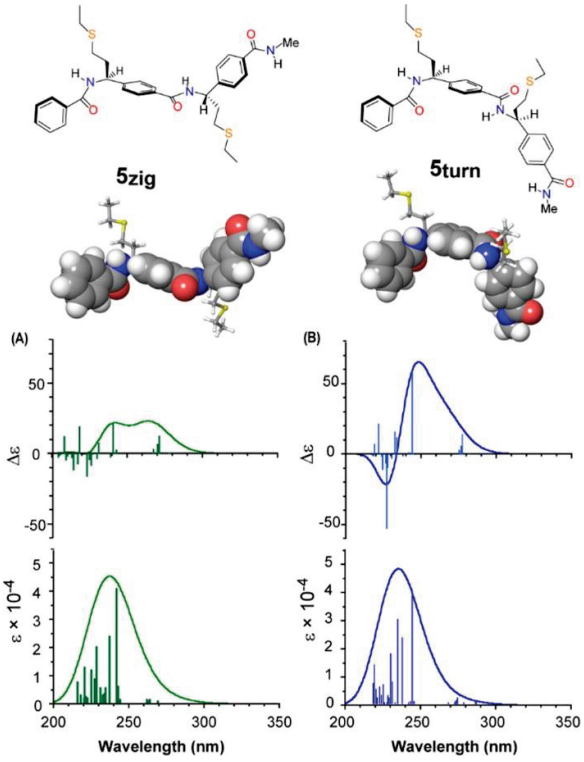

Figure 2-7. Simulated CD and UV spectra of (A) **5**$_{zig}$ and (B) **5**$_{turn}$ by TD-DFT (B3LYP/6-31**)

of **5**$_{\mathbf{turn}}$ were in close agreement with the observed spectra of **5** (Figure 2-5b), showing the positive and negative CD signals at 240–260 nm. Thus, the bisignate Cotton effect of **5** originated from the turn conformation (**5**$_{\mathbf{turn}}$). In Figure 2-5b, the peak of the positive Cotton effect was shifted to a longer wavelength (from 250 to 254 nm) with the elongation of the peptide chain (**5**, **6** (*n* = 2 to 4)) and approached the peak position observed for **poly-3a** (258 nm). The results indicated that longer oligomer lengths form the stable *turn* type conformation. A model structure of **poly-3a′** was constructed based on the optimized structure of **5**$_{\mathbf{turn}}$. As shown in Figure 2-8, **poly-3a** (*n* = 12) exhibits a right-handed (*P*)-3_1-helix structure. The helix did not form hydrogen bonds between the units, unlike natural polypeptides. The pitch was estimated to be 16 Å. The series of calculations for **poly-2a** did not give any results consistent with experimental values, indicating that the structure was flexible and undefined.

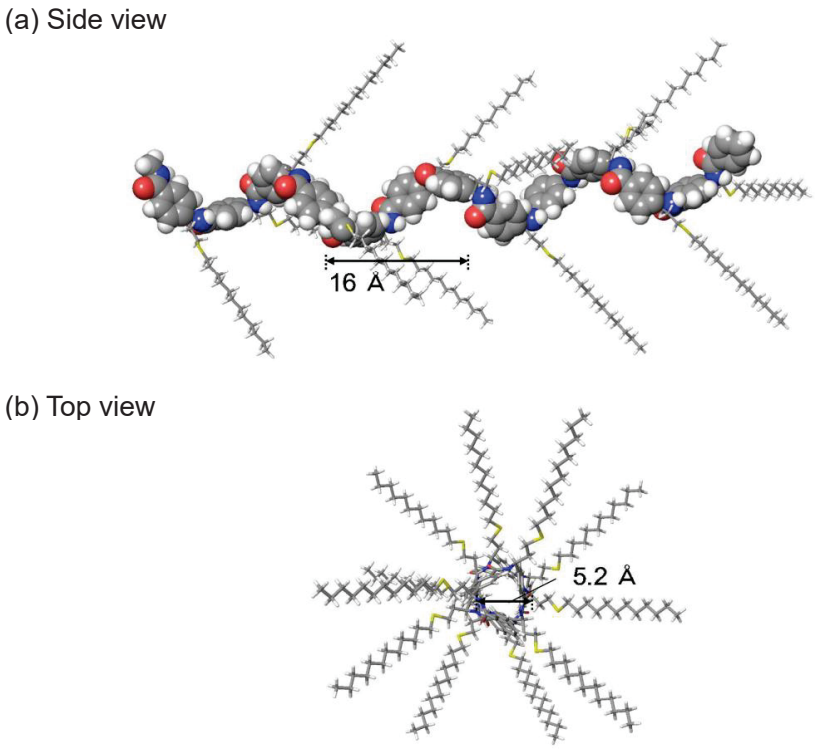

Figure 2-8. Plausible helical conformation of **poly-3a** (*n* = 12) based on the conformation of **5**$_{\mathbf{turn}}$.

Helical Property of Arylopeptide

The intensity of the Cotton effect at 258 nm showed a molecular-weight dependence (Figure 2-9a and 9b). The CD signals sharply increased with the apparent degree of polymerization (*n*) below 130 and leveled off to a constant value at higher *n*. The helix structure was more stable at $n > 130$, as the ratio of the flexible terminal moieties was reduced. Additionally, a small but significant change in the Cotton effect at 258 nm was observed at temperatures from −15 to 45 °C. All arylopeptides which the author synthesized so far show little temperature dependence and solvent dependence in any side chain. This finding suggests that the arylopeptide **poly-3a** shows tremendous helical stability.

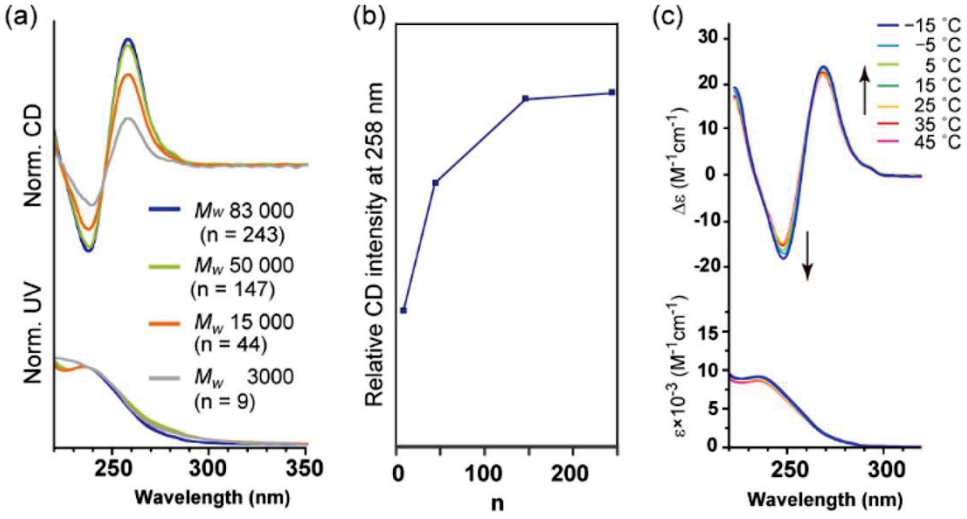

Figure 2-9. (a) The dependence of CD and UV spectra on molecular weight of **poly-3a**. The vertical axis is normalized on the basis of the absorption at 238 nm. (b) The dependence of CD intensity at 258 nm on polymerization degree (*n*) of **poly-3a**. (c) The temperature dependence of CD intensity.

In this synthetic approach, the reverse helix can be easily prepared from the same achiral monomer using the other chiral isomer of the catalyst. Indeed, (*M*)-**poly-3a** was prepared using (*S*)-**I** as the catalyst, and the resulting polymer exhibited a CD spectrum that was the mirror image of the right-handed helix (Figure 2-10).

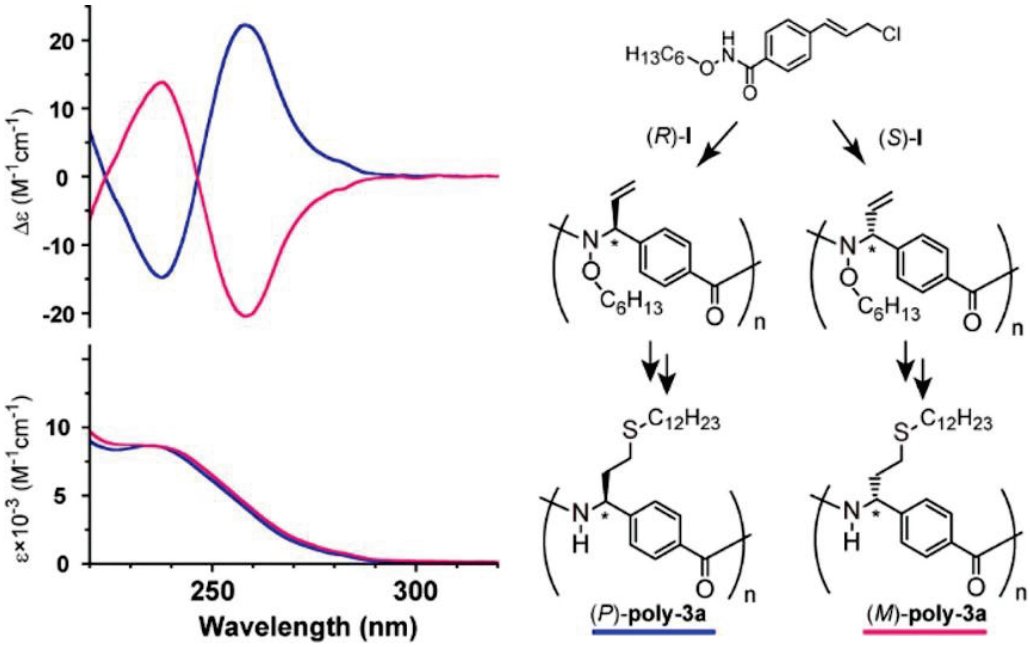

Figure 2-10. CD and UV spectra of nonnatural helical polypeptides (*P*)-**poly-3a** and (*M*)-**poly-3a** in THF at 25 °C

2-3: Conclusions

In conclusion, an innovative synthetic strategy to a novel type of non-natural polypeptide called "arylopeptide" was demonstrated, which involved the use of asymmetric polymerization and reduction of N–O bonds. The reaction proceeded smoothly regardless of the substituents on the side chains to afford an arylopeptide that contained a *p*-phenylene unit in the main chain. The secondary structure of the resulting polymer was analyzed by theoretical and computational approach, and it exhibited a one-handed helical conformation. This synthetic method did not require enantiomerically pure amino acids and its condensation on stepwise synthetic chemistry and afforded a long peptidic chain, whose asymmetric centers were controlled. The precursor polymer (**poly-2**) containing various arylene spacers (R) in the main chain and bearing a wide range of substituents on the side chain was synthesized. Since the cleavage of N–O bonds of *N*-alkoxyamide can be achieved with simple SmI_2–THF systems under very mild conditions with high chemoselectivity in organic synthesis, the present method was used to obtain numerous varieties of custom-made nonnatural polypeptides with various combinations of main chain and side chains.

2-4: Experimental Sections

General

Unless otherwise indicated, all reactions were carried out under an Ar atmosphere, whereas the workup was performed in air. ^{1}H NMR spectra were recorded in $CDCl_3$, toluene-d_8, and benzene-d_6 on a Bruker AVANCE700, JEOL JNM-ECS400, or JEOL JNM-ECA500 spectrometers using $SiMe_4$ as an internal standard. IR spectra were recorded on a SHIMADZU IR Prestige-21 spectrometer using KBr tablets. HR-MS and MS/MS (CID) measurements were carried out on a Thermo Fisher Scientific LTQ-Orbitrap XL mass spectrometer. Retention time of polymers were measured by SEC analyses using a SHIMAZU LC-10AS, SPD-10A UV-vis detector, and CTO-10A column oven equipped with two SEC columns TOSOH TSKgel GMH_{HR}-M carried out at 40 °C and a flow rate of 0.7 mL min^{-1} with $CHCl_3$ as the eluent. The enantiomeric excesses were determined by HPLC analysis using a Shimadzu LC-10 system equipped with an SPD-10AV detector and DAICEL Chiralcel OD-H, Chiralpak AD-H, or IA column. CD spectra were obtained by a JASCO J-720WO polarimeter with a cryostat thermostated at −75 to 85 °C. UV–vis spectra were obtained by a SHIMAZU UV 3100PC spectrophotometer.

Material

All solvents used for reactions were passed through purification columns just before use, and tetrahydrofuran was dried by sodium benzophenone and distilled under argon. Planar–chiral Cp′Ru complexes (*R*)-**I**, (*S*)-**I**, **poly-1**, **S1**, and **poly-2** were prepared as previous our report.[9] Cinamyl chloride was purchased from TCI.

Standard Method of Reductive Cleavage Using SmI_2-THF Complex

To a THF solution (0.15 M) of the polymer (**poly-2**) was added a THF solution of SmI_2-THF complex (4.6 equiv) at room temperature, dropwise via syringe. After stirring for 2.5 h at room temperature, the reaction was quenched with a 10% solution of $Na_2S_2O_3{\cdot}H_2O$. The mixture was then diluted with CH_2Cl_2 (15 mL). The layers were separated and the product was extracted from the aqueous layer with CH_2Cl_2 (3 × 10 mL). The combined solvent was removed under reduced pressure. The crude product was purified by SEC using two Shodex KF 2003 columns connected in series at a flow rate of 3.0 mL min^{-1}) to give the target product.

Characterization of Representative Compounds

Synthesis of poly-3a.

According to the standard method of reductive cleavage using SmI_2-THF complex, **poly-3a** was obtained as a pale brown solid (83%). ^{1}H NMR ($CDCl_3$, 500 MHz): δ 8.20-7.06 (br, 4H, Ar), 7.11–6.25 (br, 1H, NH), 5.69–

4.66 (br, 1H, –C*H*CH_2CH_2S–), 3.41-2.00 (br, 6H, –CHCHHCH_2S–, –$CHCH_2CH_2SCH_2$–) and –$CHCH_2CH_2S$–), 1.58 (br, 2H, $CHCH_2CH_2SCH_2CH_2$–), 1.42-1.10 (br, 18H, –CH_2–), 0.87 (br, 3H, CH_3). ^{13}C NMR ($CDCl_3$, 176 MHz): δ 168.2, 148.2, 132.1, 128.5, 126.5, 54.9, 36.5, 32.7, 32.3, 30.4, 29.7, 29.4, 23.0, 14.5. IR (KBr) 3319, 2922, 2850, 1633, 1530 cm^{-1}.

Synthesis of poly-3b.

According to the standard method of reductive cleavage using SmI_2-THF complex, **poly-3a** was obtained as a pale brown solid (65%). ^{1}H NMR ($CDCl_3$, 500 MHz): δ 8.00-7.06 (br, 4H, Ar), 6.90–6.51 (br, 1H, NH), 5.59-4.96 (br, 1H, –C*H*CH_2CH_2S–), 3.78–3.56 (br, 8H, –OCH_2CH_2O–), 355–3.45 (br, 2H, –SCH_2CH_2O–) 3.42–3.24 (br, 3H, OCH_3), 3.01–2.52 (br, 2H, –SCH_2CH_2O–), 2.70–2.48 (br, 2H, –$CHCH_2CH_2$S–), 2.34–2.22 (br, 2H, –$CHCH_2CH_2$S).

Synthesis of oligomer

Scheme 2-3. Synthetic pathway of dimer.

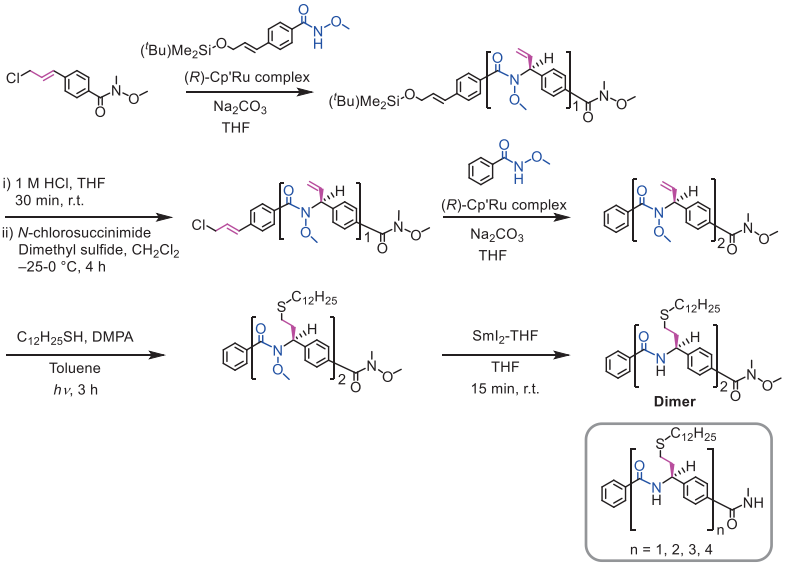

***N*-(1-(*N*-Methylamide)phenyl)3-thiododecyl)benzamide (4)**

A solution of SmI_2 (7.0 mL, 0.1 M in THF) was added dropwise using a syringe to a stirring solution of *N*-methoxy-*N*-(1-phenyl-3-thiododecyl)benzamide (30.5 mg, 0.054 mmol) in 0.5 mL of THF at room temperature. After stirring it for 15 min at room temperature, the reaction was rapidly quenched with a 10% aqueous solution of $Na_2S_2O_3{\cdot}H_2O$ (10 mL) then diluted with CH_2Cl_2 (40 mL). The organic layers was separated and the product was extracted from aqueous layer with CH_2Cl_2 (3 × 20 mL). The organic layers were combined. The combined

organic layer was dried with anhydrous Na_2SO_4. The Na_2SO_4 was removed by filtration. After the solvent was removed under reduced pressure, pale yellow solid was obtained. The product was purified by silica gel column chromatography (CH_2Cl_2/AcOEt = 1/1) to give a colorless solid (25.2 mg, 94%). ^{1}H NMR ($CDCl_3$, 400 MHz): δ 7.79 (d, 2H, *J* = 7.3 Hz, Ar), 7.49 (t, 1H, *J* = 7.6 Hz, Ar), 7.42–7.35 (m, 4H, Ar), 7.16 (d, 1H, *J* = 7.7 Hz, NH), 6.32 (brs, 1H, N*H*), 5.34 (td, 1H, *J* = 7.7, 7.0 Hz, –C*H*CH_2CH_2S–), 2.97 (d, 3H, *J* = 4.8 Hz, NCH_3), 2.47–2.58 (m, 4H, –$CHCH_2CH_2SCH_2$– and –$CHCH_2CH_2SCH_2$–), 2.58–2.53 (m, 3H, –CHCH*H*CH_2S– and –$CHCH_2CH_2$S–), 2.23–2.12 (m, 1H, –$CHCH_2CH_2$S–), 1.54 (quintet, 2H, *J* = 7.2 Hz, –$CHCH_2CH_2SCH_2CH_2$–), 1.34 (quintet, 2H, *J* = 7.2 Hz, –$CHCH_2CH_2SCH_2CH_2CH_2$–), 1.30–1.21 (m, 16H, –CH_2–), 0.88 (t, 3H, *J* = 6.7 Hz, –CH_3). ^{13}C NMR ($CDCl_3$, 101 MHz): δ 168.1, 167.0, 145.2, 134.3, 134.0, 131.8, 128.7, 127.5, 127.2, 126.8, 53.6, 35.5, 32.5, 32.0, 29.8, 29.8, 29.7, 29.7, 29.5, 29.4 29.0, 28.7, 27.0, 22.8, 14.2. HRMS (ESI): Calcd for $C_{30}H_{44}N_2NaO_2S$([M+Na]$^+$): *m*/*z* 519.3021, Found: *m*/*z* 519.3015. $[\alpha]^{24}_D$ −23.3 (c 0.7, $CHCl_3$). Chiralpak IA column, CH_2Cl_2 (v), 1.0 mL min^{-1}, 250 nm; major enantiomer: *t* = 9.0 min, minor enantiomer: *t* = 16.0 min, 93% ee.

5 (oligomer *n* = 2)

To a stirring solution of precursor (68.3 mg, 0.072 mmol) in 0.7 mL of THF, a solution of SmI_2 (4.75 mL, 0.1 M in THF) was added dropwise using a syringe at room temperature. After stirring it for 15 min at room temperature, the reaction was quenched with a 10% aqueous solution of $Na_2S_2O_3{\cdot}H_2O$ (10 mL). The mixture was then diluted with CH_2Cl_2 (30 mL). The layers were separated and the product was extracted from the aqueous layer with CH_2Cl_2 (3 × 20 mL). The combined organic layers were dried with anhydrous Na_2SO_4. The Na_2SO_4 was removed by filtration. After the solvent was removed under reduced pressure, pale yellow solid was obtained. The product was purified by silica gel column chromatography (CH_2Cl_2/AcOEt = 1/1) to a colorless solid (48.3 mg, 91%). ^{1}H NMR ($CDCl_3$, 500 MHz): δ 7.77 (d, 2H, *J* = 7.4 Hz, Ar), 7.68 (d, 4H, *J* = 7.7 Hz, Ar), 7.49 (t, H, *J* = 7.4 Hz, Ar), 7.44–7.30 (m, 6H, Ar), 7.27 (brs, 1H, N*H*), 7.14 (brs, 1H, N*H*), 6.13 (br, 1H, N*H*CH_3), 5.39–5.28 (m, 2H, –C*H*CH_2CH_2S–), 2.99 (d, 3H, *J* = 4.6 Hz, NCH_3), 2.64–2.42 (m, 8H, –$CHCH_2CH_2$S– and –$CHCH_2CH_2SCH_2$–), 2.26–2.18 (m, 4H, –$CHCH_2CH_2$S–), 1.44–1.15 (m, 40H, –CH_2–), 0.88 (t, 6H, CH_2CH_3). IR (KBr) 3335, 2923, 2852, 1634, 1532, 1316 cm^{-1}. HRMS (ESI): calcd for $C_{52}H_{79}N_3NaO_3S_2$ ([M + Na]$^+$): *m*/*z* 880.5461, found: *m*/*z* 880.5457. $[\alpha]^{24}_D$ +8.9 (c 0.7, $CHCl_3$).

6 (oligomer *n* = 4)

To a stirring solution of precursor (41 mg, 0.02 mmol) in 0.2 mL of THF, a solution of SmI_2 (2.7 mL, 0.1 M

in THF) was added dropwise using a syringe at room temperature. After stirring for 15 min at room temperature, the reaction was quenched with a 10% aqueous solution of $Na_2S_2O_3 \cdot H_2O$ (5 mL) then diluted with CH_2Cl_2 (10 mL). The layers were separated and the product was extracted from the aqueous layer with CH_2Cl_2 (3 × 10 mL). The organic layers were combined. After the solvent was removed under reduced pressure, pale yellow solid was obtained. The product was washed with *n*-hexane and methanol to give a colorless solid (28 mg, 77%). ^{1}H NMR ($CDCl_3$, 500 MHz) δ 7.83–7.61 (m, 10H, Ar), 7.55–7.30 (m, 13H, Ar and N*H*), 7.17 (brs, 1H, N*H*), 6.97 (brs, 1H, N*H*), 6.54 (brs, 1H, N*H*CH_3), 6.45 (brs, 1H, N*H*), 6.09 (brs, 1H, N*H*CH_3), 5.49–5.02 (brs, 4H, –C*H*CH_2CH_2S–), 3.00 (s, 3H, NCH_3). 2.52 (brs, 16H, –CHCHHCH_2S– and –$CHCH_2CH_2SCH_2$–), 2.19 (brs, 8H, –CHCH_2CH_2S–), 1.55 (s, 6H, $CHCH_2CH_2SCH_2CH_2$–), 1.42–1.10 (brs, 72H, –CH_2–), 0.88 (t, 12H, *J* = 6.4 Hz,CH_3). HRMS (ESI): calcd for $C_{96}H_{149}N_5NaO_5$ ([M + Na]$^+$): *m*/*z* 1603.0339, found: *m*/*z* 1603.0310.

Synthesis of model compound for X-ray crystallography (3')

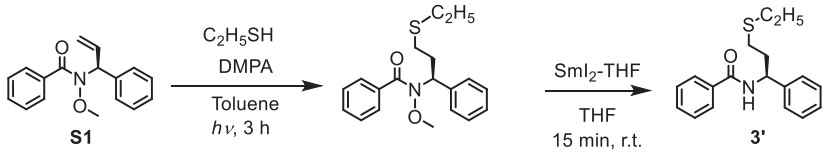

To a solution of **S1** (401 mg, 1.5 mmol) and DMPA (76.9 mg, 0.3 mmol) in toluene (1.5 mL) was added ethanethiol (1.21 g, 6.0 mmol). The solution was irradiated with a 500W high-pressure mercury lamp for 13h. The crude product was passed through a short column of SiO_2 (eluent: *n*-hexane and then *n*-hexane/diethyl ether = 10/1) to give colorless oil. To a stirring solution of the resulting oil in 1.0 mL of THF was added dropwise using a syringe to a solution of SmI_2 (3.9 mL, 0.1 M in THF). After stirring for 15 min at room temperature, the reaction was quenched with a 10% aqueous solution of $Na_2S_2O_3 \cdot H_2O$ (10 mL). The mixture was diluted with CH_2Cl_2 (50 mL). The organic layers was separated and the product was extracted from the aqueous layer with CH_2Cl_2 (3 × 20 mL). The organic layers were combined. The combined organic layer was dried with anhydrous Na_2SO_4. The Na_2SO_4 was removed by filtration. After evaporation of the solvent, colorless solid was obtained (395.2 mg, 86%). The solid was crystallized for X-ray crystallography from diethyl ether. ^{1}H NMR ($CDCl_3$, 400 MHz): δ 8.65 (dd, 2H, *J* = 8.0, 1.5 Hz, Ar), 7.0-7.15 (m, 8H, Ar), 6.23 (d, 1H, *J* = 8.1 Hz, NH), 5.42 (q, 1H, *J* = 7.3 Hz, C*H*$CH=CH_2$), 2.38 (t, 2H, *J* = 7.5 Hz, SCH_2CH_2CH), 2.35 (t, 2H, *J* = 7.4 Hz, $SCH_2CH_2CH_2$), 1.98 (m, 2H, SCH_2CH_2CH), 1.48 (quin, 2H, *J* = 7.3 Hz, OC*H*2), (br, 18H, C*H2*), 0.91 (t, 3H, CH_2CH_3). ^{13}C NMR (Toluene-

d_8, 101 MHz): δ 166.1, 142.5, 137.8, 137.2, 135.4, 131.2, 128.9, 128.5, 127.6, 127.5, 127.1, 53.6, 36.0, 32.5, 30.3, 30.24, 30.23, 30.2, 30.03, 30.0, 29.8, 29.4, 29.0, 23.2, 14.4). HRMS (ESI): calcd for $C_{18}H_{21}NNaOS$ ([M+Na] $^+$): *m*/*z* 322.1242, found: *m*/*z* 322.1236.

3. X-ray Crystallography

A colorless platelet crystal of $C_{18}H_{21}NOS$ (**3′**) having approximate dimensions of 0.250 × 0.050 × 0.020 mm was mounted on a MicroMount™ 200 μm. Data collection was made on a Rigaku Rapid II Imaging Plate area detector with Mo-Kα radiation (0.71075 Å) using a MicroMax-007HF microfocus rotating anode X-ray generator and VariMax-Mo optics. The structure was solved by direct methods[12] and expanded Fourier techniques using a SHELXL-2014/7 software.[13] Non-hydrogen atoms were refined anisotropically. The H atoms were generated by the riding model.

Table S2-1. Crystallographic Data (**3'**)

formula	$C_{18}H_{21}NOS$
fw	299.43
Crystal syst	orthorhombic
Space group	$Pca2_1$
a, Å	16.9235(14)
b, Å	9.5861(7)
c, Å	9.9959(7)
α, deg	90
β, deg	90
γ, deg	90
V, Å^3	1621.3(2)
Z	4
d_{calc}, g cm^{-3}	1.226
μ, mm^{-1}	1.983
GOF	1.021
$R_1{}^a$ [I > 2σ(I)]	0.0579
w$R_2{}^b$ (all data)	0.1097

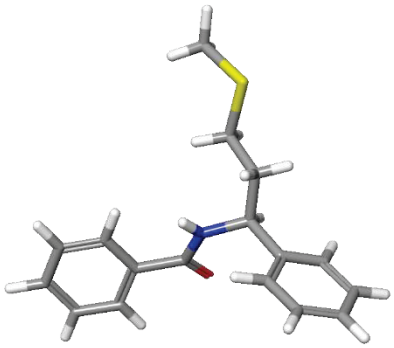

$^aR_1 = \Sigma||F_o| - |F_c||/\Sigma|F_o|$.

$^bwR_2 = \{\Sigma[w(F_o^2 - F_c^2)^2]/\Sigma[w(Fo^2)^2]\}^{1/2}$

References

(1) (a) Gellman, S. H. *Acc. Chem. Res.* **1998**, *31*, 173. (b) Hill, D. J.; Mio, M. J.; Prince, R. B.; Hughes, T. S.; Moore, J. S. *Chem. Rev.* **2001**, *101*, 3893. (c) Goodman, C. M.; Choi, S.; Shandler, S.; DeGrado, W. F. *Nat. Chem. Biol.* **2007**, *3*, 252. (d) Hecht, S.; Huc, I.; Diederich, F. *Foldamers: Structure, Properties, and Applications*; Wiley-VCH: Weinheim, 2007.

(2) (a) Cheng, R. P.; Gellman, S. H.; DeGrado, W. F. *Chem. Rev.* **2001**, *101*, 3219. (b) Arndt, H. D.; Ziemer, B.; Koert, U. *Org. Lett.* **2004**, *6*, 3269. (c) Chi, Y.; Guo, L.; Kopf, N. A.; Gellman, S. H. *J. Am. Chem. Soc.* **2008**, *130*, 5608. (d) Vasudev, P. G.; Chatterjee, S.; Shamala, N.; Balaram, P. *Acc. Chem. Res.* **2009**, *42*, 1628.

(3) (a) Huc, I. *Eur. J. Org. Chem.* **2004**, *2004*, 17. (b) Okamura, T.; Iwamura, T.; Seno, S.; Yamamoto, H.; Ueyama, N. *J. Am. Chem. Soc.* **2004**, *126*, 15972. (c) Zhang, D. W.; Zhao, X.; Hou, J. L.; Li, Z. T. *Chem. Rev.* **2012**, *112*, 5271. (d) Kudo, M.; Maurizot, V.; Kauffmann, B.; Tanatani, A.; Huc, I. *J. Am. Chem. Soc.* **2013**, *135*, 9628. (e) Okamura, T.; Seno, S. *Macromolecules* **2017**, *50*, 3500.

(4) (a) Berl, V.; Huc, I.; Khoury, R. G.; Krische, M. J.; Lehn, J. M. *Nature* **2000**, *407*, 720. (b) Porter, E. A.; Wang, X.; Lee, H. S.; Weisblum, B.; Gellman, S. H. *Nature* **2000**, *404*, 565. (c) Liu, D.; DeGrado, W. F. *J. Am. Chem. Soc.* **2001**, *123*, 7553. (d) Mowery, B. P.; Lee, S. E.; Kissounko, D. A.; Epand, R. F.; Epand, R. M.; Weisblum, B.; Stahl, S. S.; Gellman, S. H. *J. Am. Chem. Soc.* **2007**, *129*, 15474. (e) Müller, M. M.; Windsor, M. A.; Pomerantz, W. C.; Gellman, S. H.; Hilvert, D. *Angew. Chem., Int. Ed.* **2009**, *48*, 922. (f) Gan, Q.; Ferrand, Y.; Bao, C.; Kauffmann, B.; Grélard, A.; Jiang, H.; Huc, I. *Science* **2011**, *331*, 1172. (g) Jewginski, M.; Granier, T.; Langlois d'Estaintot, B.; Fischer, L.; Mackereth, C. D.; Huc, I. *J. Am. Chem. Soc.* **2017**, *139*, 2928.

(5) Hashimoto, K. *Prog. Polym. Sci.* **2000**, *25*, 1411.

(6) (a) Kanbayashi, N.; Okamura, T.; Onitsuka, K. *Macromolecules* **2014**, *47*, 4178. (b) Kanbayashi, N.; Okamura, T.; Onitsuka, K. *Macromolecules* **2015**, *48*, 8437. (c) Kanbayashi, N.; Hosoda, K.; Okamura, T.; Aoshima, S.; Onitsuka, K. *Polym. Chem.* **2016**, *7*, 3691.

(7) (a) Kanbayashi, N.; Takenaka, K.; Okamura, T.; Onitsuka, K. *Angew. Chem., Int. Ed.* **2013**, *52*, 4897. (b) Kanbayashi, N.; Hosoda, K.; Kato, M.; Takii, K.; Okamura, T.; Onitsuka, K. *Chem. Commun.* **2015**, *51*, 10895. (c) Kanbayashi, N.; Yamazawa, A.; Takii, K.; Okamura, T.; Onitsuka, K. *Adv. Synth. Catal.* **2016**, *358*, 555.

(8) (a) Keck, G. E.; McHardy, S. F.; Murry, J. A. *J. Am. Chem. Soc.* **1995**, *117*, 7289. (b) Keck, G. E.; McHardy, S. F.; Wager, T. T. *Tetrahedron Lett.* **1995**, *36*, 7419. (c) Chiara, J. L.; Destabel, C.; Gallego, P.; Marco-Contelles, J. *J. Org. Chem.* **1996**, *61*, 359.

(9) Kanbayashi, N.; Miyamoto, S.; Ishido, Y.; Okamura, T.; Onitsuka, K. *Polym. Chem.* **2017**, *8*, 985.

(10) Habeck, M.; Rieping, W.; Nilges, M. *J. Magn. Reson.* **2005**, *177*, 160.

(11) Frisch, M. J.; Trucks, G. W.; Schlegel, H. B.; Scuseria, G. E.; Robb, M. A.; Cheeseman, J. R.; Scalmani, G.; Barone, V.; Mennucci, B.; Petersson, G. A.; Nakatsuji, H.; Caricato, M.; Li, X.; Hratchian, H. P.; Izmaylov, A. F.; Bloino, J.; Zheng, G.; Sonnenberg, J. L.; Hada, M.; Ehara, M.; Toyota, K.; Fukuda, R.; Hasegawa, J.; Ishida, M.; Nakajima, T.; Honda, Y.; Kitao, O.; Nakai, H.; Vreven, T.; J. A, M.; Peralta, J. E.; Ogliaro, F.; Bearpark, M.; Heyd, J. J.; Brothers, E.; Kudin, K. N.; Staroverov, V. N.; Keith, T.; Kobayashi, R.; Normand, J.; Raghavachari, K.; Rendell, A.; Burant, J. C.; Iyengar, S. S.; Tomasi, J.; Cossi, M.; Rega, N.; Millam, J. M.; Klene, M.; Knox, J. E.; Cross, J. B.; Bakken, V.; Adamo, C.; Jaramillo, J.; Gomperts, R.; Stratmann, R. E.; Yazyev, O.; Austin, A. J.; Cammi, R.; Pomelli, C.; Ochterski, J. W.; Martin, R. L.; Morokuma, K.; Zakrzewski,

V. G.; Voth, G. A.; Salvador, P.; Dannenberg, J. J.; Dapprich, S.; Daniels, A. D.; Farkas, O.; Foresman, J. B.; Ortiz, J. V.; Cioslowski, J.; Fox, D. J. *Gaussian 09*, 2010.

(12) Altomare, A.; Burla, M. C.; Camalli, M.; Cascarano, M.; Giacovazzo, C.; Guagliardi, A.; Polidori, G. *J. Appl. Crystallogr.* **1994**, *27*, 435.

(13) Sheldrick, G. M. *Acta Crystallogr., Sect. A: Found. Crystallogr.* **2008**, *64*, 112.

Chapter 3

Folding Control of Nonnatural Glycopeptide Using Saccharide-Coded Structural Information for Polypeptide

3-1: Introduction

Glycosylation of natural peptides is a common bioprocess to lead the polypeptide chain to desired molecules, and one of the most widespread post-translation modifications in many peptide chains. Glycosylated polypeptide (glycopeptide) plays an irreplaceable role in a series of biological events (Figure 3-1a).[1] The saccharide moieties not only determine the physicochemical properties, such as the solubility and stability of polypeptides, but also provide significant information about the folding/unfolding of polypeptides and molecular recognition involving in other molecules.[2] For instance, one nascent peptide translated in ribosome is modificated with triglucosyl high-mannose typeoligosaccharide ($Glc_3Man_9GlcNAc_2$, G3M9) in endoplasmic reticulum, and the sugar chain commands the appropriate folding of the peptide. Then the peptide molecule is transported to Golgi apparatus and shows appropriate functions only if the peptide folds correctly, while mis-translating glycopeptide is re-modified or degraded. The interesting knowledge of saccharides has inspired chemists to utilize saccharide units to artificial polypeptides and glycopolymers.[3,4] In general, synthetic glycopolymers are known to show enhanced interactions with cells and have potential applications in cell sensing,[5] drug delivery,[6] molecular recognitions[7] and others (Figure 3-1b). Whitesides et al.[8] have reported that the glycopolymers having polyacrylamide, polystyrene, and poly(glutamate) interact with influenza viruses to inhibit agglutination of erythrocytes. As noted above, extensive efforts are spent on the application using glycopolymers including polypeptides. However, there are only a few studies that have investigated the relationship between saccharide structures and folding behavior of glycopolymers, although lectins precisely distinguish the slight differences between monosaccharides and disaccharides in oligosaccharide chains.[9] The reason is that the saccharides have similar hydrophilic properties and may only differ in the configuration of a single or a few stereogenic centers and the number of OH groups and from the standpoint of organic chemistry. Therefore, it is difficult to design an artificial molecular system that recognizes slight structural differences in saccharides.

Chapter 2 presented a novel type of peptidemimetic polyamide is called “arylopeptide”. Arylopeptide with the asymmetric center (*S*) adopt right-handed helical structures, which is maintained at temperatures ranging from -80 to 110 °C in various solvents, including water. The author became interested in the possibility of extending the structural features of our nonnatural polypeptides not only by the component of the main chain but also by substituents on the side chains. Althouth many types of side chain produce similar helices descrided in Chapter

2, the author focused on saccharides as a substituent on the side chain based on the phenomena that saccharide compounds command global conformation in nature. Chapter 3 presents a glycosylated arylopeptide called glyco-arylopeptide. This arylopeptide recognize the saccharide moieties depending on the length of the saccharide chain and the epimers with a slight differences in the configuration of a single stereogenic center to form distinct well-defined structures (Figure 3-1c). Complicated saccharide chain sequences in natural glycopeptides are simplified to glucose and some derivatives, and even simple saccharides commanded the helical structure and screw-sense of arylopeptides.

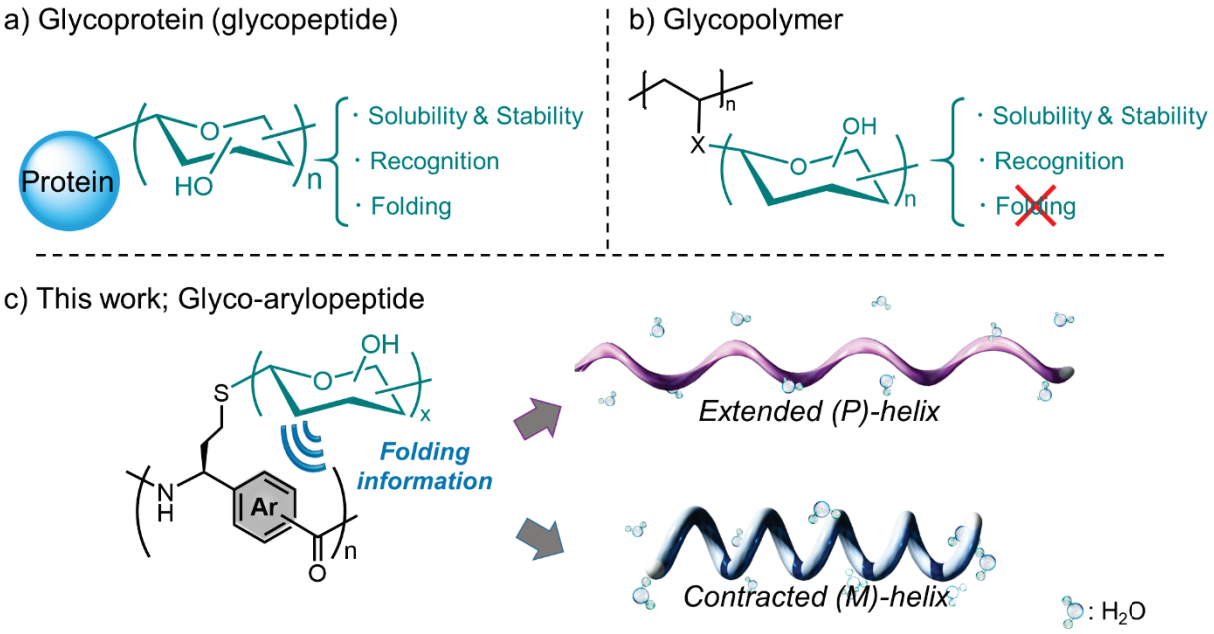

Figure 3-1. Schematic diagram of (a) glycoprotein and (b) glycopolymer. (c) This work; **c**hemical structure of glycol-arylopeptide and folding control using saccharide-coded folding information.

3-2: Results and Discussion

Synthesis of Glycoarylopeptide

As shown in Scheme 3-1, we synthesized poly-*N*-alkoxyamide (M_w 19 000) as a precursor via asymmetric polymerization catalyzed by (*R*)-**1** according to Chapter 2. Arylopeptides **poly-1a–d** (M_w 29,000–32,000) were synthesized by post-polymerization, the introduction of saccharide derivatives by using thiol-ene reaction and reductive cleavage of the *N*–O bonds of *N*-hexyloxyamide. Thiols with D-glucose, D-xylose, D-cellobiose and D-mannose moieties were synthesized with β-conformer (β/α >>99, *cf.* Scheme 3-S1). All reactions were done using the optimized procedures and proceeded quantitatively. **Poly-1a–d** are soluble in ordinary solvents such as THF, acetonitrile, ethanol, and water though it needed small amount of DMSO to prevent aggregation. The ^{1}H NMR spectrum of **poly-1a** in DMSO-d_6 at 25 °C is shown in Figure 3-2, in comparison with those of precursors. The thiol-ene reaction was confirmed by the absence of the proton signals (*a*-H, *c*-H, and *d*-H) and presence of *a′*-H, and 1H–6H of saccharide moiety. A full

Scheme 3-1. Synthetic pathway of glycoarylopeptides

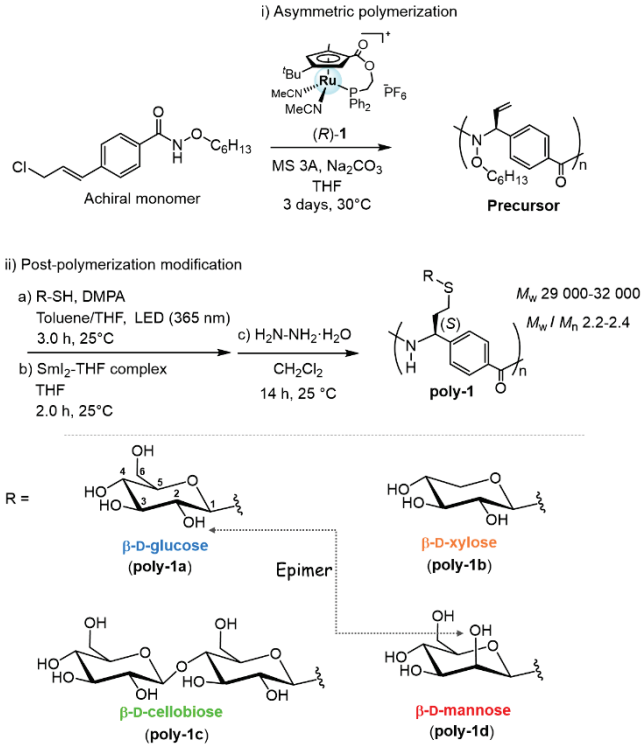

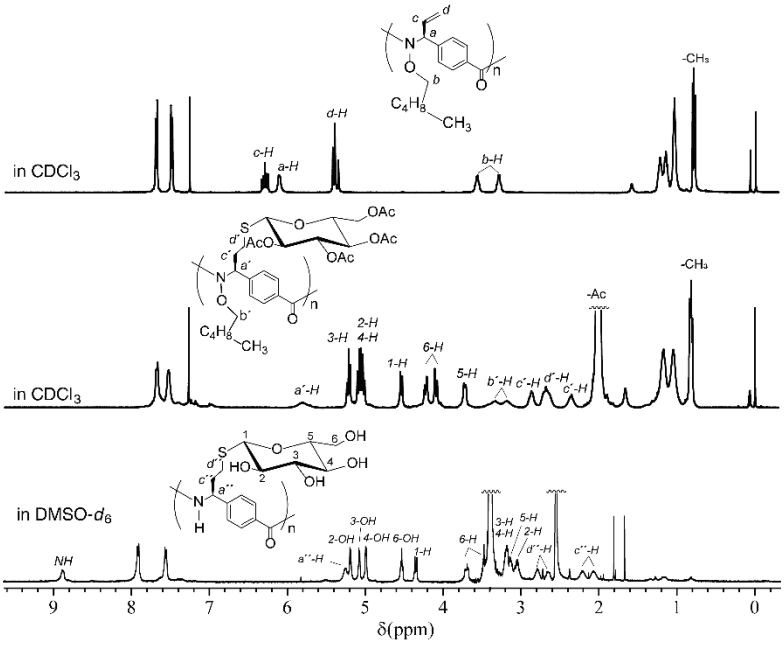

Figure 3-2. ^{1}H NMR Spectra of precursors and **poly-1a** (500 MHz, $CDCl_3$ and DMSO-d_6, 298 K).

assignment of ^{1}H NMR of **poly-1a** including signals of OH groups was conducted using by ^{1}H-^{1}H correlation spectroscopy (COSY) (Figure 3-3) and total correlation spectroscopy (TOCSY).

As shown in Figure 3-4, the enantio-selectivity of asymmetric centers on the main chain were evaluated.

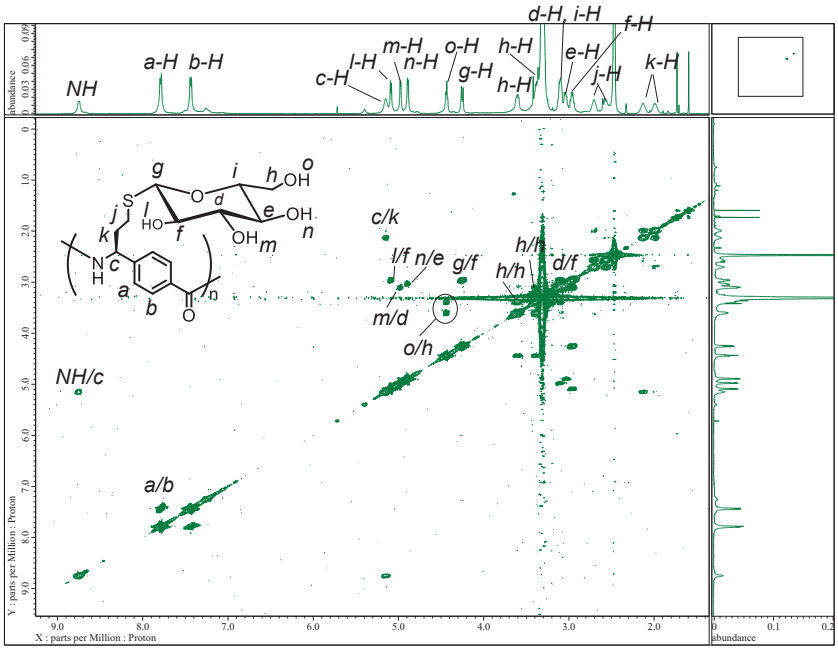

Figure 3-3. ^{1}H-^{1}H COSY spectrum of **poly-1a** (500 MHz, DMSO-d_6, 298 K).

The ^{1}H NMR spectrum of (*rac*)-precursor which was polymerized using a racemic catalyst (*rac*)-**I**, has two peaks at 4.57 (d, 1-H) and 4.53 ppm (d, 1-H) with a ratio of 50 : 50. In contrast, the spectra of (*S*)- and (*R*)-precursors, which were polymerized from (*R*)-**I** and (*S*)-**I**, showed only one peak (at 4.53 or 4.57 ppm), indicating that **poly-1a-1d** were strictly controlled.

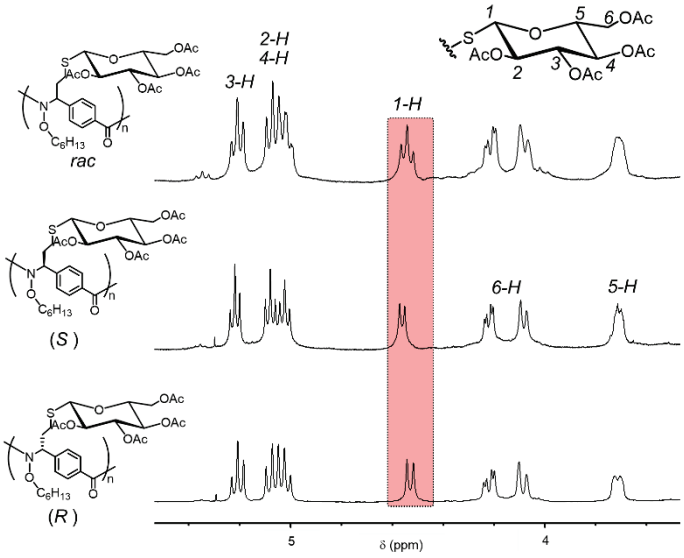

Figure 3-4. ^{1}H NMR spectra of (*S*/*R*) and (*rac*)-precursors ($CDCl_3$, 298 K).

Analysis of Secondary Structure of Glycoarylopeptide

To investigate the global conformation of **poly-1**, circular dichroism (CD) spectroscopy was conducted using water as the solvent. As shown in Figure 3-6a, CD spectra of **poly-1a** in organic solvents showed a plus to minus bisignate Cotton effects, indicating that the formation of (*P*)-helix caused by the asymmetric carbon (*S*) in the main chain ((*P*): right-handed, (*M*): left-handed). This is consistent with Chapter 2.[10] In water, however, the CD spectrum of **poly-1a** showed the opposite bisignate Cotton effect between 240 and 259 nm (Figure 3-5a, blue line). The computational analysis of the oligomers suggested that the minus to plus Cotton effect corresponded to the (*M*)-twisted conformation (Figure 3-5b). The simulated CD spectra of oligomers (n = 2) in water and THF using TD-DFT were very similar to the observed spectra of **poly-1a**. The major differences between the optimized structures of (*P*)-twist and (*M*)-twist are the reversal in the sign of dihedral angles (ϕ and θ) in the local structures and the formation of cyclic intramolecular C6-OH ···O=C hydrogen bonding in the (*M*)-twist.

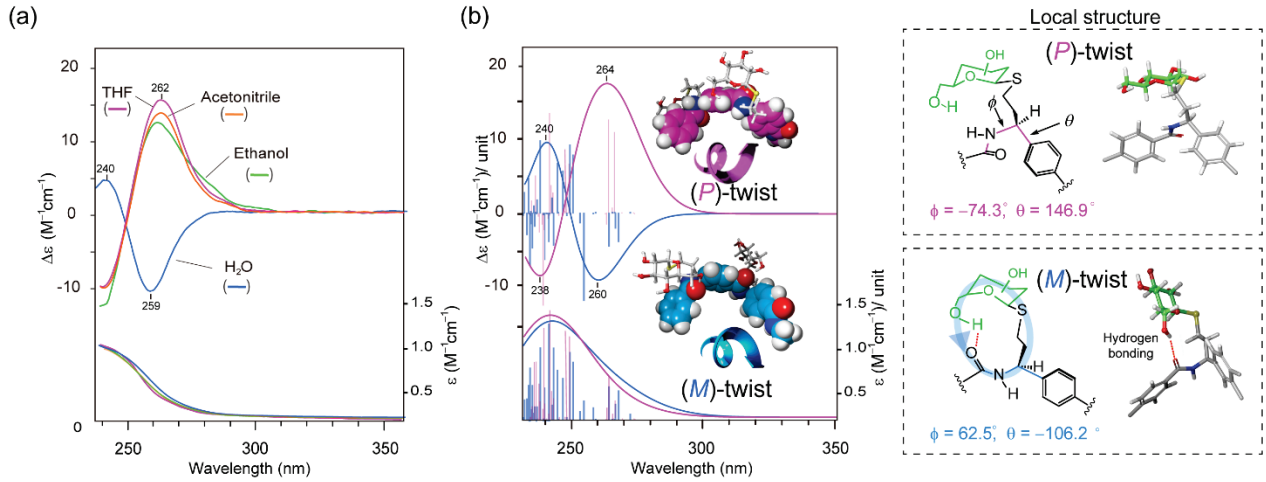

Figure 3-5. (a) Solvent effect of CD spectra of **poly-1a** in 1% (v/v) DMSO/(solvent) at 298 K. Solvent; THF (pink), acetonitrile (orange), ethanol (green) and H_2O (blue). Concentration: [**poly-1a**] = 0.30-32 mM. (b) Simulated Structures and CD spectra of oligomer (n = 3), (*P*)-twist and (*M*)-twist by TD-DFT calculation (B3LYP/6-31**) in THF (pink curve) and water (blue curve) and their local structures.

To investigate the role of the C6-OH, CD spectra of the analogs were measured in water. The CD spectrum of **poly-1b** without C6-OH showed ordinary (*P*)-conformation (Figure 3-6). It is surprising that **poly-1c** having D-cellobiose, a disaccharide of glucose, also formed the (*P*)-conformation, although the D-glucose moiety is connected to the main chain in the same manner as that in **poly-1a**. The C6-OH of D-cellobiose in the optimized structure was easily incorporated into the hydrogen bond with the adjacent pyranose ring and did not interact with the main chain (Figure 3-7). Interestingly, **poly-1d** also formed the (*P*)-conformation with the epimer of D-

glucose at the C2-position. The axial C2-OH of mannose and its hydration probably disrupts the preferred conformation through intramolecular hydrogen bonding (Figure 3-8).[11] In glycopeptides, a few saccharides near the glycosylated site are known to determine the stability of the peptide backbone via hydrogen bonding between the saccharide and the carbonyl group in the main chain.[12] Therefore, the intramolecular hydrogen bonding of D-glucose in the glycoarylopeptide also play an important role in the folding behavior similar to that observed in glycopeptides.

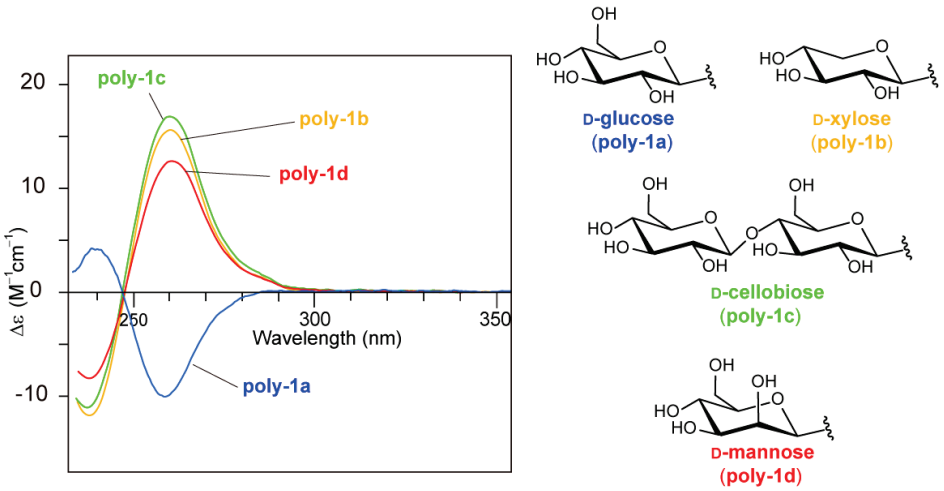

Figure 3-6. CD spectra of **poly-1a–d** in 1% (v/v) DMSO/H_2O at 25 ºC. Concentration/unit: [**poly-1a**] = 0.31 mM, [**poly-1b**] = 0.30 mM, [**poly-1c**] = 0.37 mM, and [**poly-1d**] = 0.38 mM.

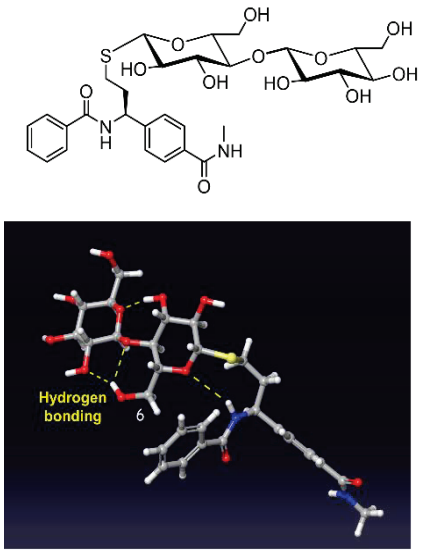

Figure 3-7. The optimized structure of oligomer (n = 1) in H_2O whose side chain is a β-D-cellobiose derivative.

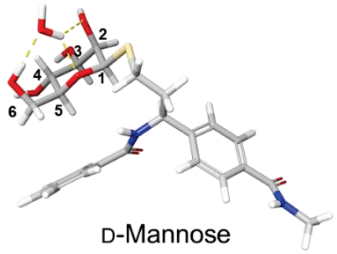

Figure 3-8. The optimized structure of a monomer conformer containing a H_2O molecule on the D-mannose subsutituent. Such a hydration structure is formed in the literature.[12]

The above experimental results and computational simulations lead us to propose two global conformations (Figures 3-9a-b)—(*P*)- and (*M*)-helices. The (*P*)-helix is 3_1-like helical structure formed by successive formation of a (*P*)-twist with a pitch of 5.1 Å. The (*M*)-helix is more contracted 4_1-like helix with a pitch of 3.0 Å. Hydrophobic/hydrophilic map suggests that hydrophobic helical pore of the left-handed helix is efficiently covered with hydrophilic saccharide unit like a rod micelle and this contracted form increases the solubility in water. The structural study using atomic force microscopy (AFM) revealed detailed insights the glycopeptide.[13] The AFM image of pyridine/THF solution on mica exhibited a height of about 1.2 nm (Figure 3-10). This agreed

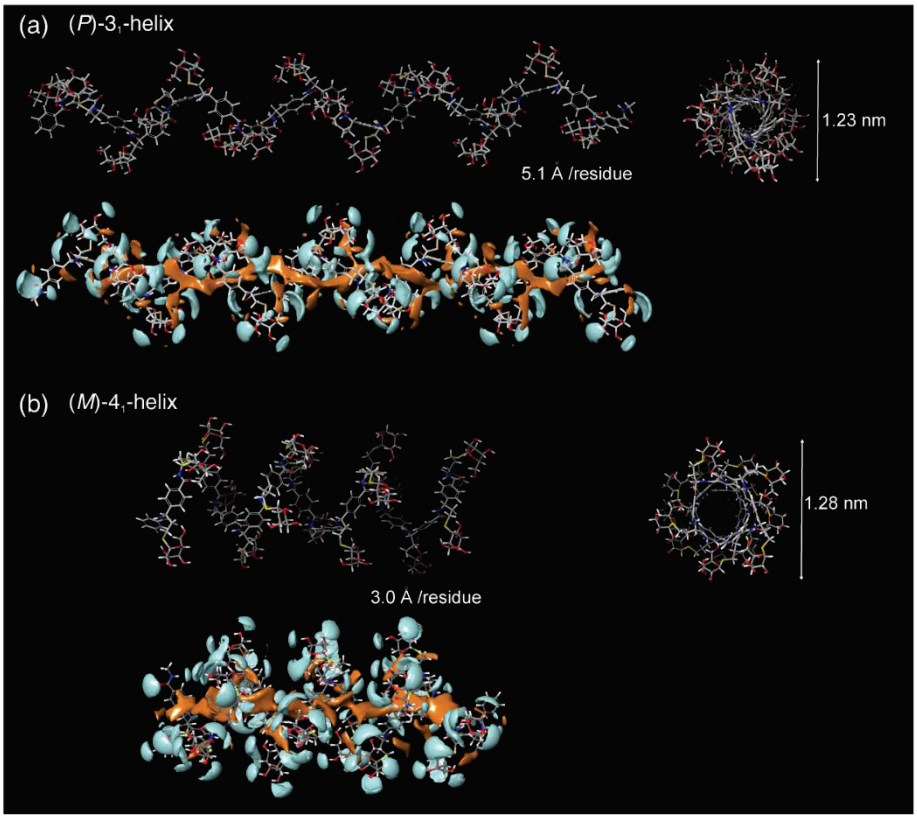

Figure 3-9. Two plausible 3D helical conformations and hydrophobic/hydrophilic maps (brown; hydrophobic, blue; hydrophilic) of poly-1a (n = 17) in (a) THF and (b) water.

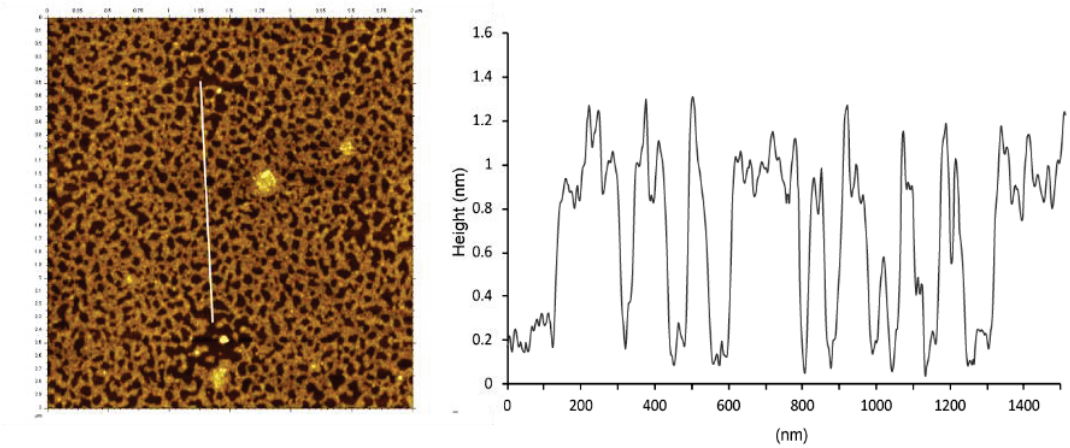

Figure 3-10. AFM image of **poly-1a** by casting 1% pyridine/THF solution (topography) and the height profile.

with the height of the proposed structure of **poly-1a** (Figure 3-9). The difference of distance between both polymer chain ends is of importance because saccharide units have a good affinity to water, but the moiety of the main chain has not good affinity. Hydrophobic/hydrophilic map suggesting that hydrophobic helical pore of the left-handed helix is efficiently covered with hydrophilic saccharide unit like rod micelle, and this contracted form is ahead of the solubility in water.

Although **poly-1a** having asymmetric carbon (*S*) in the main chain were focused so far ((*S*)-**poly-1a**), β-D-glucose substituent has an ability changing the screw-sense of (*R*)-**poly-1a** having asymmetric center (*R*) on the main chain, implying that β-D-glucose substituent is tag for arylopeptide to induce helical inversion (Figure 3-11).

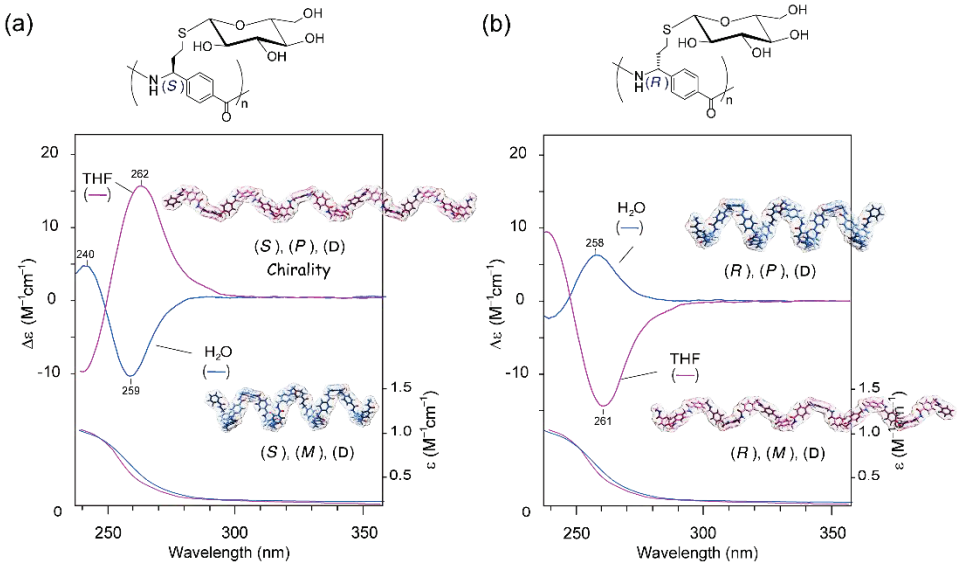

Figure 3-11. CD/UV spectra of diastereomers of (a) (*S*)-**poly-1a** and (b) (*R*)-**poly-1a** in 1% DMSO/THF and 1% DMSO/H_2O solution at 25 °C. (*S* /*R*); chirality of asymmetric carbon, (*P*/*M*); helicity, (D); chirality of saccharide.

Property of Helical Structures

L-Amino acid residues induce only a right-handed α-helix; however, the residues of glycoarylopeptide form helices with both screw-senses.[14] Thus, the helical stability of **poly-1a** was investigated in detail. The molecular weight-dependences of the helical formation were examined by CD measurements in THF and H_2O (Figure 3-12a). The CD intensity of **poly-1a** increased nonlinearly as a function of the degree of polymerization (*n*) and plateaued at higher *n* values. The results indicate that a long polymer chain fixes the (*P*)- or (*M*)-helicity. Actually, the CD spectra of oligomer (n = 1, 2) in THF and H_2O show similar Cotton effects (Figure 3-13).

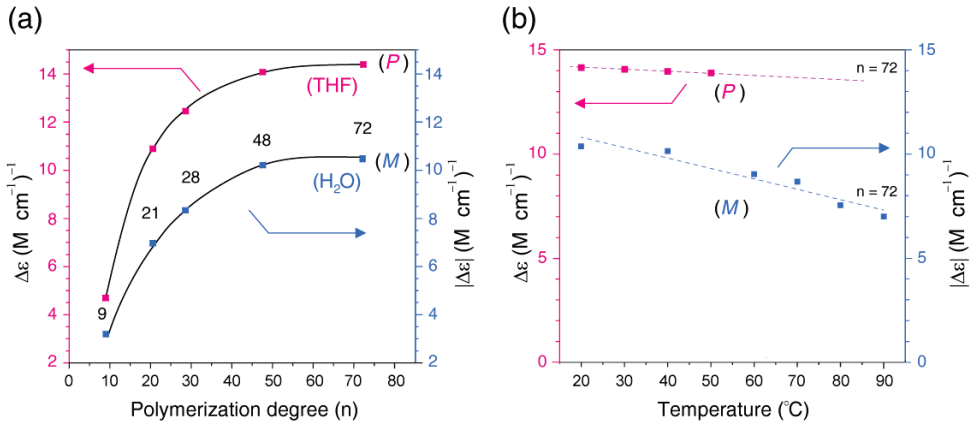

Figure 3-12. (a) CD intensity of poly-1a at 260 nm in THF (pink plots, left vertical axis) and at 259 nm in H_2O (blue plots, right vertical axis) as a function of the polymerization degree *n*. (b) Temperature dependence (20 to 90 °C) of the CD intensity of **poly-1a** at 260 nm in THF (pink plots, left vertical axis) and at 259 nm in H_2O (blue plots, right vertical axis).

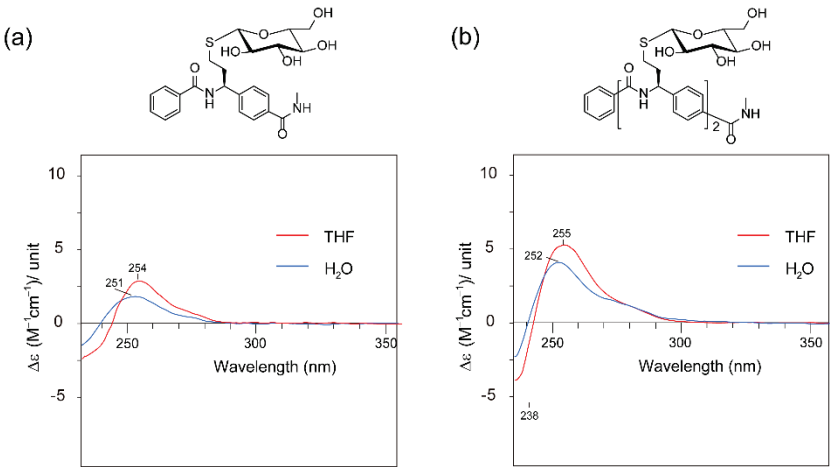

Figure 3-13. CD/UV spectra of oligomers in 1% DMSO/THF and 1% DMSO/H_2O solution at 25 °C. (a) oligomer (*n* = 1) (b) oligomer (*n* = 2).

Helical and Chiral Tuning of Glycoarylopeptide

As described above, the author revealed the synthesis, structure, and properties of glycoarylopeptides. The next purpose is to interconvert these two helical structures freely. Glycopeptides in nature change their structures and functions by various modification and interaction/recognition with other molecules. For example, acetylation of the OH groups in sialic acid is a popular modification *in vivo* (Figure 3-14), and acetylation of sialic acid is known to be related to the regulation of many life phenomena.[15] Sialic acid is usually present at the non-reducing end of the sugar chain and plays important functions such as cell recognition.

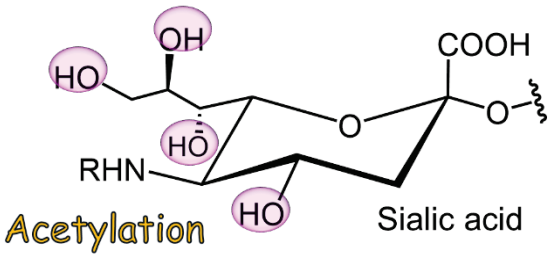

Figure 3-14. Chemical structure of sialic acid.

Thus, acetylation of the hydroxyl groups on **poly-1a** was carried out using acetic anhydride. Acetylation of **poly-1a** proceeded quantitatively, and the CD spectrum of acetylated **poly-1a** showed a plus to minus Cotton effect originated from the (*P*)-helix (Figure 3-15a). The other acetylated glycoarylopeptides (**poly-1b-d**) showed no inversion in the Cotton effect, indicating that acetyl groups disrupted the delicate energy balance of (*M*)-helix of **poly-1a**, which is an unstable diastereomer. Acetylation is a very easy chemical modification, and deacetylation also proceeded quantitatively. Therefore, the author succeeded in the development of tunable bimodal helical structures and chirality switching system using acetylation and deacetylation. On the other hand, boronic acid moieties are known to show favorable interaction with saccharides.[16] Adding the 4-carboxy-phenylboronic acid to the **poly-1a** in aqueous solution resulted in a drastic change from the contracted (*M*)-4_1-helix to the extended (*P*)-3_1-helix (Figure 3-15b). Upon increasing the fraction of 4-carboxyphenylboronic acid (0 to 60 eq /unit), the Cotton effect originated from the (*M*)-4_1-helix, which is contracted helix, systematically changed to that of extended the (*P*)-3_1-helix (Figure 3-15c). The CD spectral changes shown in Figure 4b have a clearly isodichroic point and were represented by the linear combination of the Cotton effects for (*P*)- and (*M*)-helices of **poly-1a**, indicating the existence of mainly two kinds of chiral architectures (*P*)-and (*M*)-helices.

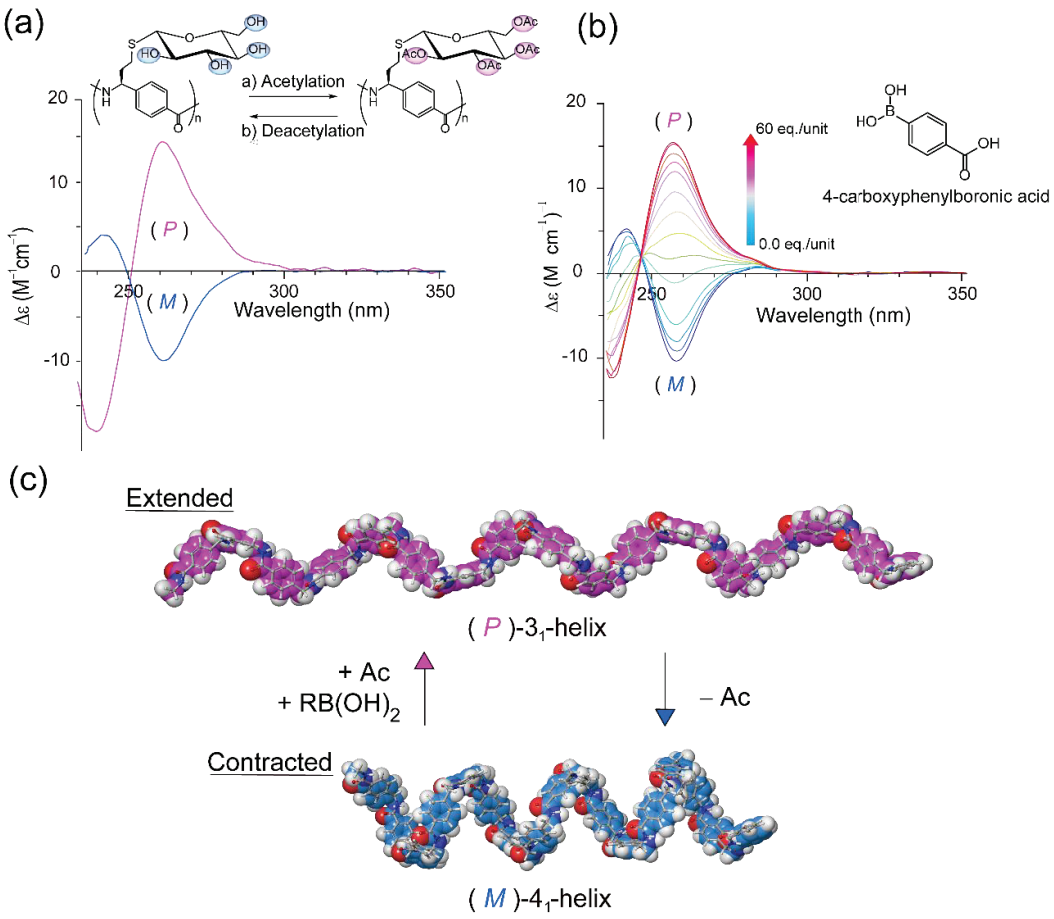

Figure 3-15. (a) CD spectra of **poly-1a** with acetylation and deacetylation. ([**poly-1a**] = 0.31 mM/unit, 1% DMSO/H_2O solution, 298 K). (b) CD titration experiment of **poly-1a** in THF at 298 K in the presence of 0, 4, 8,…, 60 equiv of 4-carboxyphenylboronic acid. (Initial concentration: [**poly-1a**] = 0.25 mM/unit, 1% DMSO/ 10 mM NH_3 solution, pH = 10.5). (c) Helix to Helix transition of **poly-1a**. The chain-length from (*M*)-4_1-helix to (*P*)-3_1-helix extend about 1.7 times of its length (pitch per residue; [(*P*)-3_1-helix] 5.1 Å and [(*M*)-4_1-helix] 3.0 Å). Side chains are omitted for clarity.

3-3: Conclusions

In conclusion, we succeeded in establishing a folding control in a glycoarylopeptide using saccharide-coded folding information for a peptide backbone. The arylopeptide distinguished the configuration of a single stereogenic center in the epimers—D-glucose and D-mannose—and formed a completely distinct and well-defined architecture ((*P*)-3_1-helix or (*M*)-4_1-helix) in aqueous solutions. Similar to the recently reported mechanism for glycopeptides, the saccharides near the glycosylated site determine the properties of the peptide backbone via hydrogen bonding.[12] (*P*/*M*)-helix was easily converted to the other structure via simple chemical modification (acetylation/de-acetylation) or by using additives. These results indicate that the properties of completely artificial polypeptide molecules are also dominated by the type of saccharides; this is analogous to

the behavior of natural polypeptides.

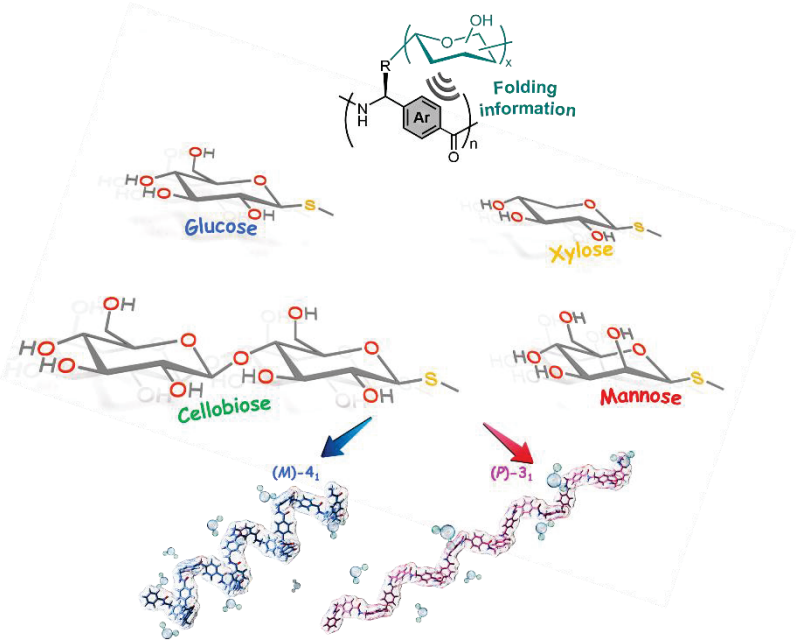

Figure 3-16. Summary of this Chapter.

3-4: Experimental Sections

General

Unless otherwise indicated, all reactions were carried out under an Ar atmosphere, whereas the workup was performed in air. ^{1}H NMR spectra were recorded in $CDCl_3$, DMSO-d_6, methanol-d_4 and D_2O on a JEOL JNM-ECS400, or JEOL JNM-ECA500 spectrometers using $SiMe_4$ as an internal standard. IR spectra were recorded on a SHIMADZU IR Prestige-21 spectrometer using KBr tablets. HR-MS and MS/MS (CID) measurements were carried out on a Thermo Fisher Scientific LTQ-Orbitrap XL mass spectrometer. Retention time of polymers were measured by SEC analyses using a SHIMAZU LC-10AS, SPD-10A UV-vis detector, and CTO-10A column oven equipped with two SEC columns TOSOH TSKgel GMH_{HR}-M carried out at 40 °C and a flow rate of 0.7 mL min^{-1} with $CHCl_3$ as the eluent. CD spectra were obtained by a JASCO J-720WO polarimeter with a cryostat thermostated at −75 to 85 °C. UV–vis spectra were obtained by a SHIMAZU UV 3100PC spectrophotometer. Samples for the AFM measurements of **poly-1a** were prepared by drop casting (about 20 μL) of dispersions onto freshly cleaved mica substrates at room temperature (about. 25 °C), and the substrates were then dried under vacuum for 1 h. The AFM images were obtained in air by tapping mode on an Agilent Technology Agilent PicoPlus 5100 microscope.

Materials

All solvents used for reactions were passed through purification columns just before use and tetrahydrofuran was dried by sodium-benzophenone and distilled under argon. Planar-chiral Cp′Ru complexes were prepared as reported previously.[17]

Standard Method of Asymmetric Polymerization

To a mixture of molecular sieve 3A, Na_2CO_3 (1.2 eq), monomer (1.0 eq) and (*R/S*) or (*rac*)-**I** (2 mol%) were added THF (0.5 mmol/ 1 mL), which was stirred at 30 °C. After 3days, dichloromethane was added to the reaction mixture. The insoluble part was filtered through Celite. The combined organic layer was washed with water. After drying with anhydrous Na_2SO_4, the solvent was removed under reduced pressure. The product was purified by silica gel column chromatography with CH_2Cl_2 and dried under vacuum to give a pale-yellow solid.

Standard Method of Post-Polymerization Modification

To a toluene solution (5 mL) of the polymer (0.15 mmol of C=C groups) and 2,2-dimethoxy-2-phenylacetophenone (DMPA) (38.4 mg, 0.15 mmol) was added thiol (0.90 mmol), and the reaction mixture was irradiated at 365 nm with LED lamp (365 nm) for 5 h. The crude product was purified by using an SEC column (Shodex; KF 2003 × 2; flow rate 3.0 mL min^{-1}) to give the pale brown solid. To a THF solution (0.10 M) of the resulting polymer was added THF solution of SmI_2–THF complex (2.3 equiv) at 25 °C, dropwise via syringe. After stirring it for 1.5 h at 25 °C, the reaction was rapidly quenched with a 10% solution of $Na_2S_2O_3 \cdot H_2O$ and then diluted with CH_2Cl_2. The organic layers was separated, and the aqueous layer was extracted with CH_2Cl_2. The combined organic layers were concentrated in vacuo. The crude product was purified by using an SEC column (Shodex; KF 2003 × 2; flow rate 3.0 mL min^{-1}), and washed with n-hexane to give white powder. To a THF solution (2.0 mL) of resulting powder was added hydrazine·H_2O (20.0 eq/ unit) at 0°C, and the reaction mixture was stirred at 25 °C. After 17 h, the reaction was quenched with acetone. After the solvent was removed under reduced pressure, ether was added to give white solid. The solid was purified by washing with DCM to give target compounds.

Characterization of Representative Compounds

Synthesis of poly-1a.

According to the standard method of asymmetric polymerization and post-polymerization modification, **poly-**

1a was obtained as a white powder (M_w = 29,000, M_w/M_n = 2.1). ^{1}H NMR (DMSO-d_6, 500 MHz): δ 8.91 (bs, 1H, NH), 7.90 (d, J = 8.4 Hz, 2H, Ar), 7.90 (d, J = 7.5 Hz, 2H, Ar), 5.26 (bs, 1H, –C*H*CH_2CH_2S–), 5.19 (d, J = 5.8 Hz, 1H, OH-H2), 5.08 (d, J = 4.5 Hz, 1H, OH-H3), 4.99 (d, J = 4.5 Hz, 1H, OH-H4), 4.59 (t, J = 5.7 Hz, 1H, OH-H6), 4.36 (d, J = 9.3 Hz, 1H, H-1), 3.70 (m, 1H, H-6a), 3.49 (m, 1H, H-6b), 3.22–3.19 (m,, 2H, H-3, H-5), 3.16–3.13 (m, 1H, H-4), 3.09–3.06 (m, 1H, H-2), 2.85–2.78 (m, 1H, –$CHCH_2C$*H*$_2$S), 2.70–2.62 (m, 1H, –$CHCH_2C$*H*$_2$S), 2.30–2.19 (m, 1H, –CHC*H*$_2CH_2$S), 2.18–2.20 (m, 1H, –CHC*H*$_2CH_2$S). IR (KBr): 3387, 1652, 1548 cm^{-1}.

Synthesis of poly-1b.

According to the standard method of reductive cleavage using SmI_2-THF complex, **poly-1b** was obtained as a white solid (M_w = 31,000, M_w/M_n = 2.3). ^{1}H NMR (DMSO-d_6, 500 MHz): δ 8.99 (brs, 1H, NH), 7.90 (br, 2H, Ar), 7.54 (br, 2H, Ar), 5.21 (br, 1H, –C*H*CH_2CH_2S–), 5.19 (m, 3H, OH-H2, OH-H3, OH-H4), 4.47 (br, 1H, OH-H6), 4.17 (bs, 1H, H-1), 3.80–3.68 (br, 2H, H-2, H-6a), 3.54 (br, 1H, H-6b), 3.18–3.13 (br, 1H, H-4), 2.81–2.70 (m, 2H, –$CHCH_2C$*H*$_2$S), 2.31–2.20 (m, 1H, –CHC*H*$_2CH_2$S), 2.15–2.07 (m, 1H, –CHC*H*$_2CH_2$S). Two peaks was missing to overlap with water. IR (KBr): 3373, 1642, 1548 cm^{-1}.

Synthesis of poly-1c.

According to the standard method of reductive cleavage using SmI_2-THF complex, **poly-1b** was obtained as a white solid (M_w = 33,000, M_w/M_n = 2.4). ^{1}H NMR (DMSO-d_6, 500 MHz): δ 8.89 (bs, 1H, NH), 7.88 (d, J = 8.4 Hz, 2H, Ar), 7.53 (d, J = 7.5 Hz, 2H, Ar), 5.26–5.20 (br, 2H, –C*H*CH_2CH_2S– and OH-H2), 5.12 (br, 1H, OH-H3), 5.05 (br, 1H, OH-H4), 4.34 (d, J = 8.9 Hz, 1H, H-1), 4.27–4.25 (br, 1H, H-5a), 4.42–4.14 (br, 1H, H-5b), 3.72, 3.21–3.02 (m, 3H, H-2, H-3, H-4), 2.74–2.69 (m, 2H, –$CHCH_2C$*H*$_2$S), 2.22(br, 1H, –CHC*H*$_2CH_2$S), 2.15 (br, 1H, –CHC*H*$_2CH_2$S). IR (KBr): 3350, 1640, 1549 cm^{-1}.

Synthesis of poly-1d.

According to the standard method of asymmetric polymerization and post-polymerization modification, **poly-1d** was obtained as a white powder (M_w = 29,000, M_w/M_n = 2.7). ^{1}H NMR (DMSO-d_6, 500 MHz): δ 8.98 (bs, 1H, NH), 7.89 (br, 2H, Ar), 7.55 (br, 2H, Ar), 5.37 (bs, 1H, –C*H*CH_2CH_2S–), 5.29–4.32 (7H, OH), 5.29–4.32 (14H, CH and CH_2), 2.85–2.78 (m, 1H, –$CHCH_2C$*H*$_2$S), 2.70–2.62 (m, 1H, –$CHCH_2C$*H*$_2$S), 2.30–2.19 (m, 1H, –CHC*H*$_2CH_2$S), 2.18–2.20 (m, 1H, –CHC*H*$_2CH_2$S). IR (KBr): 3372, 1642, 1549 cm^{-1}.

Synthesis of poly-1a (stereochemistry on main chain is (*R*)).

According to the asymmetric polymerization with (*S*)-**I** and post-polymerization modification, **poly-1a** was obtained as a white powder (M_w = 30,000, M_w/M_n = 2.4). ^{1}H NMR (DMSO-d_6, 500 MHz): δ 8.91 (bs, 1H, NH), 7.90 (d, *J* = 8.4 Hz, 2H, Ar), 7.90 (d, *J* = 7.5 Hz, 2H, Ar), 5.26 (bs, 1H, –C*H*CH_2CH_2S–), 5.19 (d, *J* = 5.8 Hz, 1H, OH-H2), 5.08 (d, *J* = 4.5 Hz, 1H, OH-H3), 4.99 (d, *J* = 4.5 Hz, 1H, OH-H4), 4.59 (t, *J* = 5.7 Hz, 1H, OH-H6), 4.41 (d, *J* = 9.3 Hz, 1H, H-1), 3.70 (m, 1H, H-6a), 3.49 (m, 1H, H-6b), 3.22–3.19 (m,, 2H, H-3, H-5), 3.16–3.13 (m, 1H, H-4), 3.09–3.06 (m, 1H, H-2), 2.85–2.78 (m, 1H, –$CHCH_2C$*H*$_2$S), 2.70–2.62 (m, 1H, –$CHCH_2C$*H*$_2$S), 2.30–2.19 (m, 1H, –CHC*H*$_2CH_2$S), 2.18–2.20 (m, 1H, –CHC*H*$_2CH_2$S).

Synthesis of Oligomer (*n* = 1)

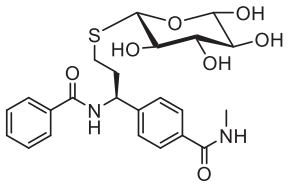

To a THF solution (2.0 mL) of precursor (62 mg, 0.09 mmol) was hydrazine·H_2O (20.0 eq) at 0°C, and the reaction mixture was stirred at room temperature. After 17 h, the reaction was quenched with acetone. After the solvent was removed under reduced pressure, the residue was purified by washing with dichloromethane (DCM) and ethyl acetate to give colorless solid (43 mg, quant). ^{1}H NMR (DMSO-d_6, 400 MHz): δ 8.88 (d, *J* = 8.4 Hz, 1H, NH), 8.43 (q, *J* = 4.8 Hz, 1H, NH), 7.94 (d, *J* = 8.2 Hz, 2H, Ar), 7.84 (d, *J* = 8.3 Hz, 2H, Ar), 7.64–7.50 (m, 5H, Ar), 5.26 (q, *J* = 6.9 Hz, 1H, –C*H*CH_2CH_2S–), 5.17 (d, *J* = 6.2 Hz, 1H, OH-H2), 5.06 (d, *J* = 4.8 Hz, 1H, OH-H3), 4.98 (d, *J* = 4.8 Hz, 1H, OH-H4), 4.52 (t, *J* = 5.8 Hz, 1H, OH-H6), 4.36 (d, *J* = 9.5 Hz, 1H, H-1), 3.58(s, 1H, H-6), 3.42 (s, 1H, H-6), 3.26–3.07 (m,, 4H, H-2, H-3, H-4, H-5), 2.83 (d, *J* = 4.8 Hz, 3H, NCH_3), 2.85–2.75 (m, 1H, –$CHCH_2C$*H*$_2$S), 2.30–2.20 (m, 1H, –CHC*H*$_2CH_2$S), 2.18–2.11 (m, 1H, –CHC*H*$_2CH_2$S). One proton peak (–$CHCH_2C$*H*$_2$S) was missing due to overlap with solvent. IR (KBr): 3333, 1652, 1547 cm^{-1}. HRMS (ESI): Calcd for $C_{23}H_{28}N_2NaO_7S$ ([M+Na]$^+$): m/z 499.1515, Found: m/z 499.1516.

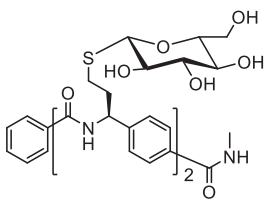

Synthesis of Oligomer (*n* =2)

To a THF solution (2.0 mL) of precursor (97 mg, 0.083 mmol) was hydrazine·H_2O (30.0 eq) at 0°C, and the reaction mixture was stirred at room temperature. After 17 h, the reaction was quenched with acetone. After the solvent was removed under reduced pressure, the residue was purified by washing with DCM and ethyl acetate to give white solid (67.6 mg, 98%). ^{1}H NMR (DMSO-d_6, 500 MHz): δ 8.91 (d, J = 7.8 Hz, 1H, NH), 8.83 (d, J = 8.02 Hz, 1H, NH), 8.43 (q, J = 4.8 Hz, 1H, NH), 7.97–7.82 (m, 6H, Ar), 7.60–7.50 (m, 7H, Ar), 5.25 (q, J = 3.9 Hz, 2H, –C*H*CH_2CH_2S–), 5.29–4.83 (br, 6H, OH-H2, OH-H3, OH-H4), 4.52 (br, 2H, OH-H6), 4.36 (m, 2H, H-1), 3.58 (s, 1H, H-6), 3.68 (m, 2H, H-6a), 3.25–3.05 (m,, 8H, H-2, H-3, H-4, H-5), 2.83 (d, J = 4.8 Hz, 3H, NCH_3), 2.85–2.60 (m, 4H, –$CHCH_2$CH_2S), 2.30–2.21 (m, 2H, –CHCH_2CH_2S), 2.20–2.11 (m, 2H, –CHCH_2CH_2S). One proton peak (H-6b) was missing due to overlap with H_2O. IR (KBr): 3328, 1653, 1548 cm$^-$ ^{1}HRMS (ESI): Calcd for $C_{40}H_{51}N_3NaO_{13}S_2$ ([M+Na]$^+$): m/z 868.2761, Found: m/z 868.9661.

Scheme 3-S3. Synthesis of thiols

The C-1 position in saccharide was selectively thiolated and the other OH groups were protected with acetyl

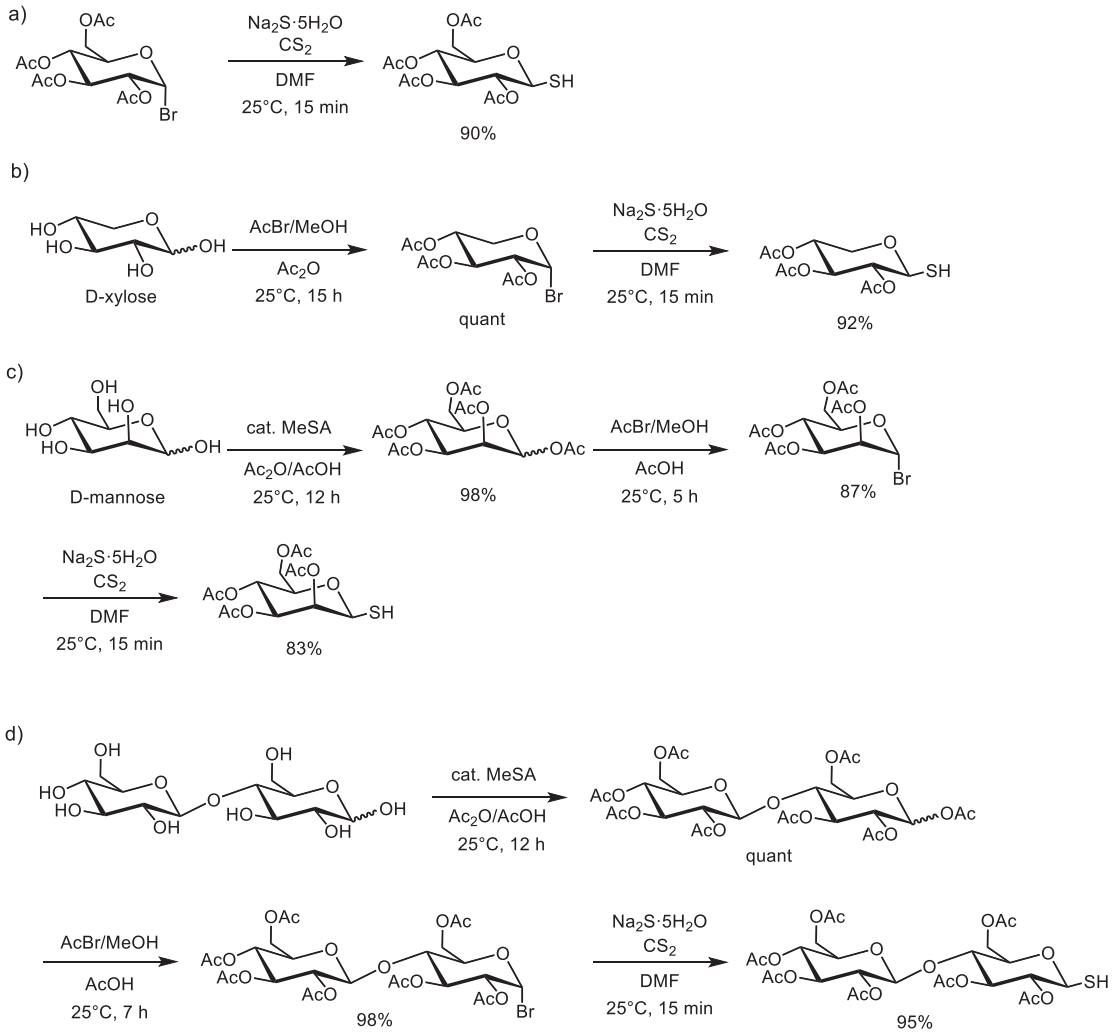

groups.

Appendix

Computational Study

Several attempts have been made to analyze the conformations of glycoarylopeptide. The crystal structure of **3'** in Chapter 2 was used for the initial structures. As shown Figures 3-S1a,b, the energy diagrams for dihedral angle change around the asymmetric carbon on the main chain in $CHCl_3$ and H_2O were examined by two coordination scan program using a MacroModel software. In H_2O, there are several local minima, especially, the local minimums in the area opposite to the global minimum (*P*)-conformation can be are allowed. The energy gap of each form in H_2O is much smaller than that of in $CHCl_3$, indicating that left-handed helix is formed easily in H_2O.

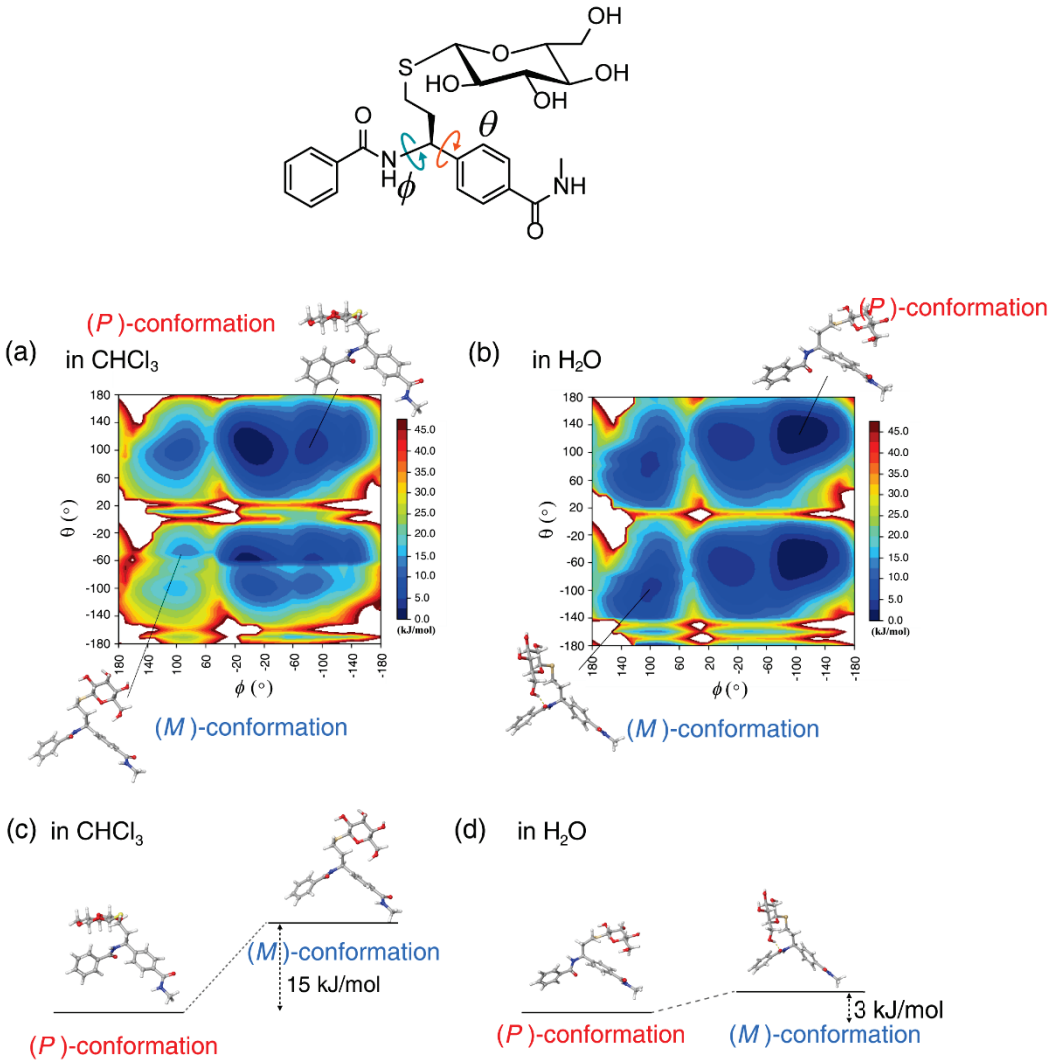

Figure 3-S1. Energy diagrams for dihedral angle change around asymmetric carbon on the main chain in (a) $CHCl_3$ and (b) H_2O. (c, d) Optimized structures obtained by molecular mechanics calculation in $CHCl_3$ and H_2O.

Next, oligomer (n = 2) was made from above (*P*)-form in THF and (*M*)-form in H_2O by fusing the arylene rings. Conformational searches of the oligomer by a MacroModel software vided mainly two types of conformer, which is zig-zag and twist types. The seven conformers from the most stable order based on the conformational searches are showed in Figure 3-S2. Therefore, the geometry optimizations of the two conformations were performed in both cases in THF and H_2O (Figure 3-S3).

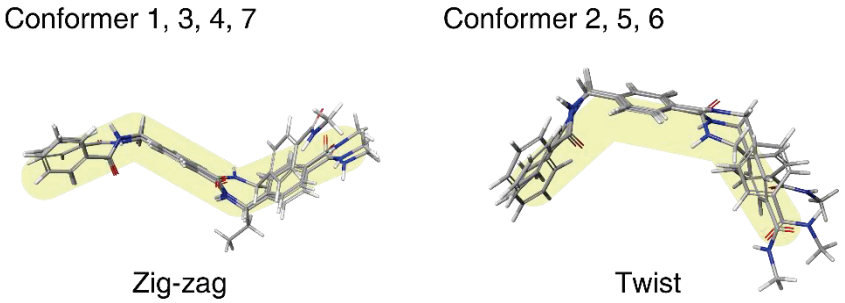

Figure 3-S2. Conformational search of oligomer (n = 2) calculated by MacroModel program (condition; H_2O, 298 K). Side chains are omitted for clarity.

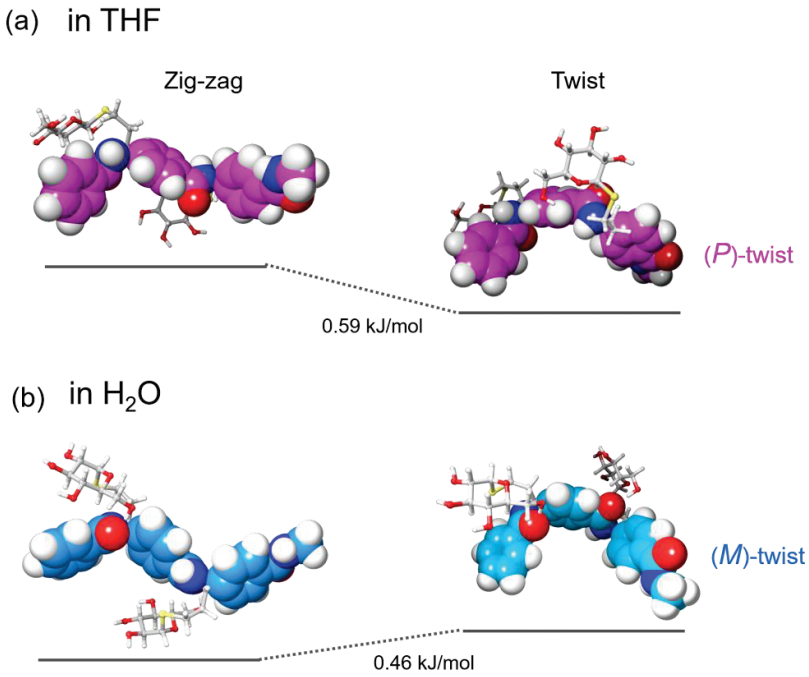

Figure 3-S3. Energy diagram of oligomer (n = 2) obtained by DFT calculation (B3LYP/6-31G (d, p)) in THF and H_2O at 25°C.

The simulated CD and UV spectra of the two conformers by TD DFT calculations. The result for zig-zag conformer was shown in Figure 3-S4. This simulation did not agree with the experimental results of polymers. Conversely, as shown in Figure 3-5, the simulated spectra of twist type is very similar to the experimental results.

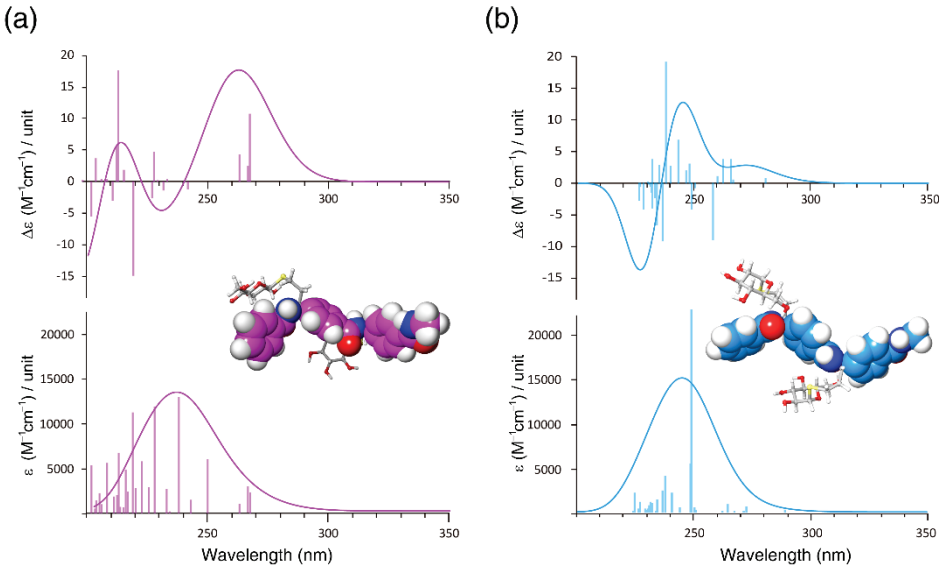

Figure 3-S4. The simulated CD/UV spectra of zig-zag type in (a) THF and (b) H_2O calculated by TD-DFT calculation (B3LYP/6-31G (d, p)) in THF and H_2O

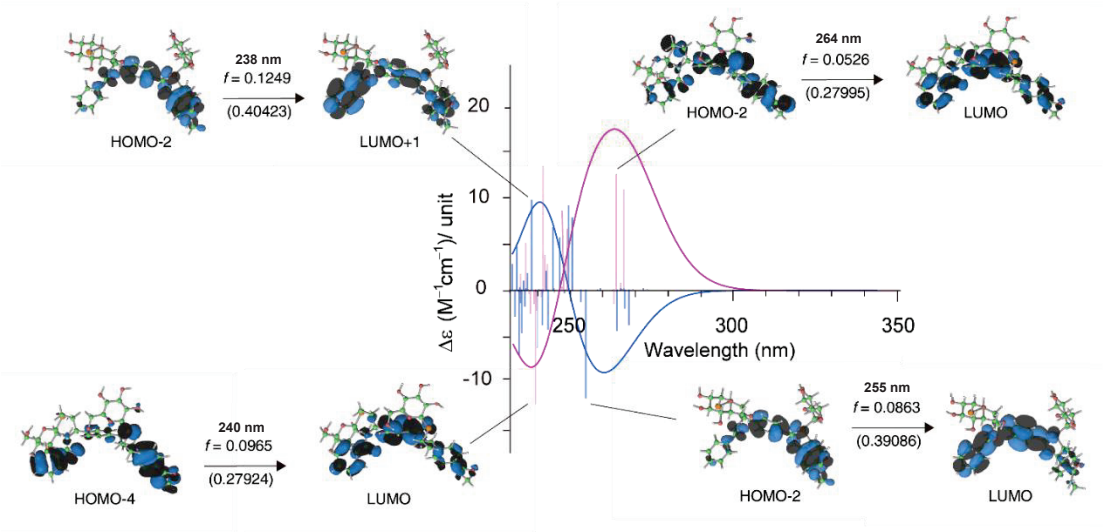

Figure 3-S5. The calculated predominant transitions for the absorption bands (wavelength, nm), oscillator strength (*f*) and the molecular orbitals (MOs) for oligomer (n = 2) of twist type. The coefficients indicating their contributions to the excitation are shown in the parentheses under arrows.

References

(1) Hubbard, S. C.; Ivatt, R. J. *Ann. Rev. Biochem.* **1981**, *50*, 555.

(2) (a) Shinkawa, T.; Nakamura, K.; Yamane, N.; Shoji-Hosaka, E.; Kanda, Y.; Sakurada, M.; Uchida, K.; Anazawa, H.; Satoh, M.; Yamasaki, M. *J. Biol. Chem.* **2003**, *278*, 3466. (b) Taylor, M. E.; Drickamer, K. *Introduction to glycobiology* (3rd ed); Oxford University press, 2011.

(3) (a) Kramer, J. R.; Deming, T. J. *J. Am. Chem. Soc.* **2012**, *134*, 4112. (b) Huang, J.; Heise, A. *Chem. Soc. Rev.* **2013**, *42*, 7373. (c) Krannig, K.-S.; Doriti, A.; Schlaad, H. *Macromolecules* **2014**, *47*, 2536. (d) Krannig, K.-S.; Sun, J.; Schlaad, H. *Biomacromolecules* **2014**, *15*, 978.

(4) (a) Albertin, L.; Stenzel, M. H.; Barner-Kowollik, C.; Foster, L. J. R.; Davis, T. P. *Macromolecules* **2005**, *38*, 9075. (b) Miura, Y.; Hoshino, Y.; Seto, H. *Chem. Rev.* **2016**, *116*, 1673. (c) Ohno, K.; Tsujii, Y.; Miyamoto, T.; Fukuda, T.; Goto, M.; Kobayashi, K.; Akaike, T. *Macromolecules* **1998**, *31*, 1064.

(5) (a) Jelinek, R.; Kolusheva, S. *Chem. Rev.* **2004**, *104*, 5987. (b) Toyoshima, M.; Miura, Y. *J. Polym. Sci., Part A: Polym. Chem.* **2009**, *47*, 1412. (c) Takara, M.; Toyoshima, M.; Seto, H.; Hoshino, Y.; Miura, Y. *Polym. Chem.* **2014**, *5*, 931.

(6) Suriano, F.; Pratt, R.; Tan, J. P.; Wiradharma, N.; Nelson, A.; Yang, Y. Y.; Dubois, P.; Hedrick, J. L. *Biomaterials* **2010**, *31*, 2637.

(7) (a) Percec, V.; Leowanawat, P.; Sun, H. J.; Kulikov, O.; Nusbaum, C. D.; Tran, T. M.; Bertin, A.; Wilson, D. A.; Peterca, M.; Zhang, S. *J. Am. Chem. Soc.* **2013**, *135*, 9055. (b) Zhang, S.; Moussodia, R.-O.; Sun, H.-J.; Leowanawat, P.; Muncan, A.; Nusbaum, C. D.; Chelling, K. M.; Heiney, P. A.; Klein, M. L.; André, S.; Roy, R.; Gabius, H.-J.; Percec, V. *Angew. Chem., Int. Ed.* **2014**, *53*, 10899. (c) Zhang, S.; Xiao, Q.; Sherman, S. E.; Muncan, A.; Ramos-Vicente, A. D. M.; Wang, Z.; Hammer, D. A.; Williams, D.; Chen, Y.; Pochan, D. J.; Vértesy, S.; André, S.; Klein, M. L.; Gabius, H. J.; Percec, V. *J. Am. Chem. Soc.* **2015**, *137*, 13334.

(8) (a) Sigal, G. B.; Mammen, M.; Dahmann, G.; Whitesides, G. M. *J. Am. Chem. Soc.* **1996**, *118*, 3789. (b) Spaltenstein, A.; Whitesides, G. M. *J. Am. Chem. Soc.* **1991**, *113*, 686.

(9) Hasegawa, T.; Kondoh, S.; Matsuura, K.; Kobayashi, K. *Macromolecules* **1999**, *32*, 6595.

(10) Ishido, Y.; Kanbayashi, N.; Okamura, T.; Onitsuka, K. *Macromolecules* **2017**, *50*, 5301.

(11) Carçabal, P.; Jockusch, R. A.; Hünig, I.; Snoek, L. C.; Kroemer, R. T.; Davis, B. G.; Gamblin, D. P.; Compagnon, I.; Oomens, J.; Simons, J. P. *J. Am. Chem. Soc.* **2005**, *127*, 11414.

(12) (a) Coltart, D. M.; Royyuru, A. K.; Williams, L. J.; Glunz, P. W.; Sames, D.; Kuduk, S. D.; Schwarz, J. B.; Chen, X.-T.; Danishefsky, S. J.; Live, D. H. *J. Am. Chem. Soc.* **2002**, *124*, 9833. (b) Imperiali, B.; O'Connor, S. E. *Curr. Opin. Chem. Biol.* **1999**, *3*, 643.

(13) (a) Kumaki, J.; Sakurai, S.-i.; Yashima, E. *Chem. Soc. Rev.* **2009**, *38*, 737. (b) Freire, F.; Quiñoá, E.; Riguera, R. *Chem. Rev.* **2016**, *116*, 1242.

(14) (a) Karlson, R. H.; Norland, K. S.; Fasman, G. D.; Blout, E. R. *J. Am. Chem. Soc.* **1960**, *82*, 2268. (b) Goodman, M.; Boardman, F.; Listowsky, I. *J. Am. Chem. Soc.* **1963**, *85*, 2491. (c) Watanabe, J.; Okamoto, S.; Satoh, K.; Sakajiri, K.; Furuya, H.; Abe, A. *Macromolecules* **1996**, *29*, 7084.

(15) (a) Varki, A. *Glycobiology* **1992**, *2*, 25. (b) Angata, T.; Varki, A. *Chem. Rev.* **2002**, *102*, 439.

(16) (a) Lorand, J. P.; Edwards, J. O. *J. Org. Chem.* **1959**, *24*, 769. (b) Suenaga, H.; Mikami, M.; Sandanayake, K. S.; Shinkai, S. *Tetrahedron Lett.* **1995**, *36*, 4825. (c) Springsteen, G.; Wang, B. *Tetrahedron* **2002**, *58*, 5291.

(d) Sun, X.; James, T. D. *Chem. Rev.* **2015**, *115*, 8001.

(17) (a) Dodo, N.; Matsushima, Y.; Uno, M.; Onitsuka, K.; Takahashi, S. *Dalton Trans.* **2000**, 35. (b) Matsushima, Y.; Komatsuzaki, N.; Ajioka, Y.; Yamamoto, M.; Kikuchi, H.; Takata, Y.; Dodo, N.; Onitsuka, K.; Uno, M.; Takahashi, S. *Bull. Chem. Soc. Jpn.* **2001**, *74*, 527. (c) Kanbayashi, N.; Onitsuka, K. *Angew. Chem., Int. Ed.* **2011**, *50*, 5197.

Chapter 4

Synthesis of Arylopeptide Bearing 2,6-Naphthylene Unit and Side Chain-Driven Dual System of Helical Conformation.

4-1: Introduction

Natural polypeptides comprise α-amino acids with perfectly controlled asymmetric carbon centers in highly specific sequences, allowing them to form the corresponding well-defined secondary structures (e.g., α-helix and β-sheet) for constructing the higher-order structures that dictate their biological functions. Accordingly, the design of synthetic folded molecular architectures[1] has received considerable research attention, and several types of folded oligomers, helices,[2] or sheet-like motifs[3] have been created in recent decades. Moreover, research into bistable synthetic foldamers capable of adopting two well-defined secondary structures like some natural polypeptides has been developed as an understanding of the structure–property relationship and the development of novel functional materials, including molecular machines and molecular switches.[4] Aromatic amides are often used in the field of foldamer as ideal backbone to form the specific structures. Their rigidity, dipole, and capacity of hydrogen-donor or acceptor enable the accurate construction of specific structure. In the case of aromatic oligoamides,[5] the aryl amide moieties (aryl-CONH) exhibit stable geometrical isomers (*syn*- and *anti*-conformations) in relation to the direction of translational axis; the control of each conformer is crucial for realizing aromatic polyamides with distinct well-defined specific global conformations. Some studies have been reported to control these geometrical conformations by specific attractive and repulsive interactions using the design of the aromatic amide moieties.[6] However, the molecular design of a backbone that forms dual-folded systems remains a highly challenging topic due to requirement of high-sophisticated backbones for predictability of the distinct structures.

The field of polymer chemistry often involves cooperative phenomena, which are based on the amplification of small energy differences in local structures that result in a specific global structure.[7] The most representative examples of such systems are helical polymers with their achiral main chains and side chains with optically active substituents.[8] For shorter polymer chains of this type, the energy gap between the right- and the left-handed helices is smaller than the thermal energy supplied, whose two helical conformation are in a balanced state. However, increasing the chain length leads predominately to a one-handed conformer with cooperative amplification, where the preference of the helical sense is determined by the thermodynamic stabilization.[9] In some cases, distinct helical conformations having different helical parameters, such as pitch [10] and chirality,[11] are

generated from the same backbone.

The author presented a peptidic aromatic polyamide, "arylopeptide" in Chapter 2, which comprises axially symmetric *p*-phenylene amide spacers between residues by combining asymmetric polymerization[12] and post-polymerization modification (Scheme 4-1a).[13] Importantly, this main chain has dominantly two types of local conformers, turn and zig-zag, but successive formation of turn conformer predominates with elongation of the peptide chain to afford the 3_1-helix. The CD intensity of **poly-1**, which originates from the global conformation, increases nonlinearly as a function of the degree of polymerization, *n*, indicating cooperative convergence of plural conformers.

Because the axial symmetric *p*-phenylene spacer formed the stable 3_1-helix, the author paid attention to axial unsymmetrical 2,6-naphthylene spacer (Scheme 4-1b). When 2,6-naphthylene spacer is adopted in arylopeptide, the rotating operation of arylene ring gives geometrically non-equivalent isomers (*syn* and *anti*). Thus, plural rotational isomers and similar energy levels are produced, and the bistable structure was formed depending on

Scheme 4-1. (a) Previous Work and (b) This work: Geometrical Property of 2,6-Naphthylene Amide and This Concept

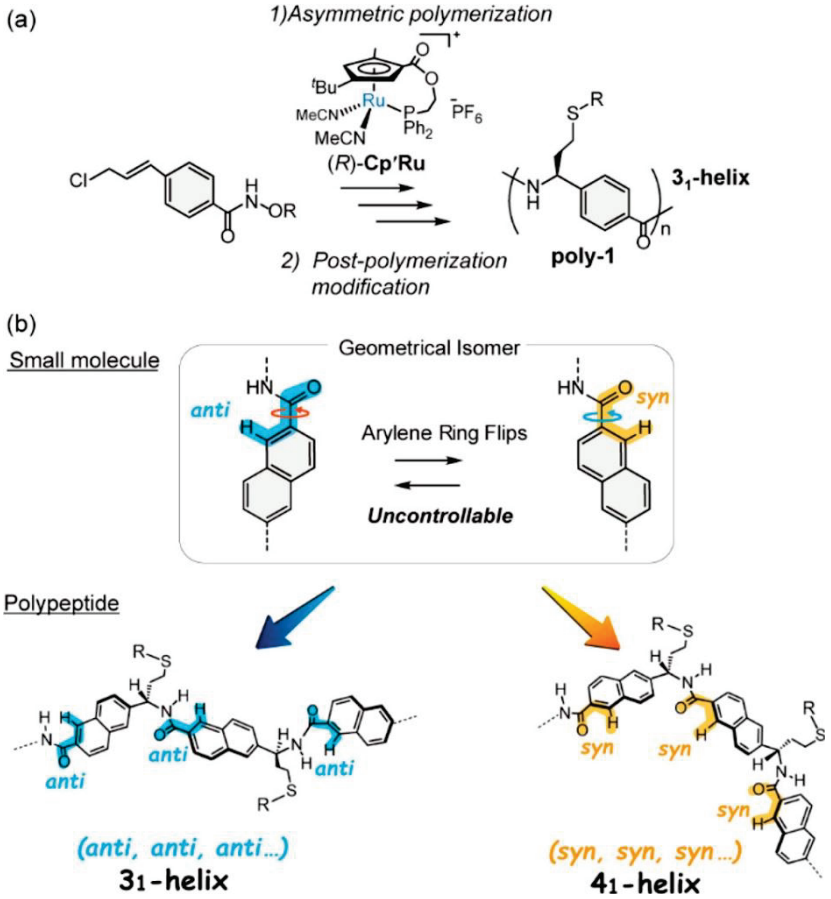

the conditions. The author presents herein novel dual structural systems of macromolecules in solution derived from aromatic ring flips. The structural control is based on the orientation of 2,6-naphthylene spacer, and folding selectivity is controlled by the side chain. Furthermore, the *anti*- to *syn*-transition also appears upon adding a small amount of additive with the identical molecule, which indicates that a structural transition occurs between well-defined macromolecular architectures. The bimodal system based on simple unsymmetrical geometry on local structure of peptide is a promising candidate for constructing bistable architectures.

4-2: Results and Discussion

Synthesis of Arylopeptide Bearing 2,6-Naphthylene Unit

As shown in Scheme 4-2, we synthesized poly-*N*-alkoxyamide as a precursor via asymmetric polymerization catalyzed by the planar–chiral ruthenium complex (*R*)-**I**.[12a] The arylopeptides **poly-2a** (R = $C_{12}H_{25}$) and **poly-2b** (R = $(CH_2CH_2O)_3CH_3$) were then synthesized by post-polymerization, the introduction of long-alkyl or ether side chains, and the subsequent reductive cleavage of the N–O bonds of *N*-hexyloxyamide. All reactions were done using the optimized procedures in Chapter 2 and proceeded quantitatively.[14]

Scheme 4-2. Synthetic Pathway of Arylopeptide

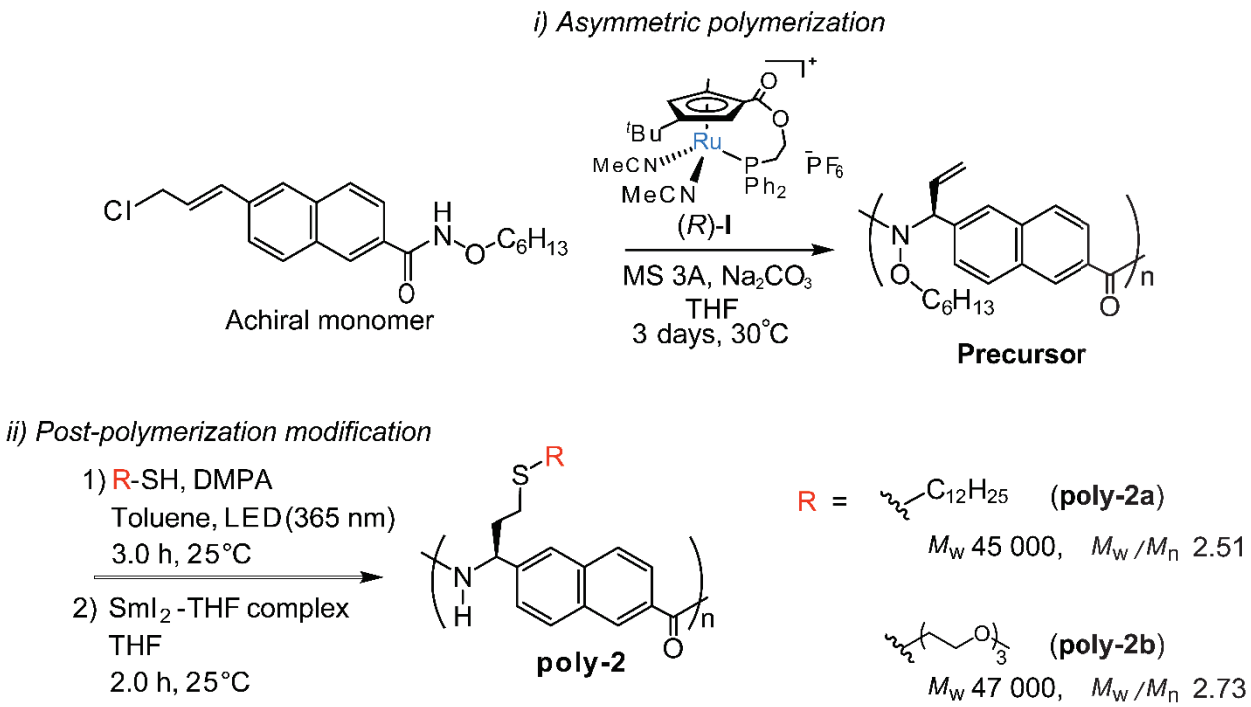

The ^{1}H NMR spectrum of **poly-2a** in $CDCl_3$ at 25 °C is shown in Figure 4-1, in comparison with those of precursors. The thiol-ene reaction was confirmed by the disappearance of the proton signals (*a*-H, *c*-H, and *d*-H) and appearance of a new broad signal (*a*′-H). The reductive reaction was confirmed by the absence of the proton signals (*a*′-H, *b*′-H, and –CH_3).

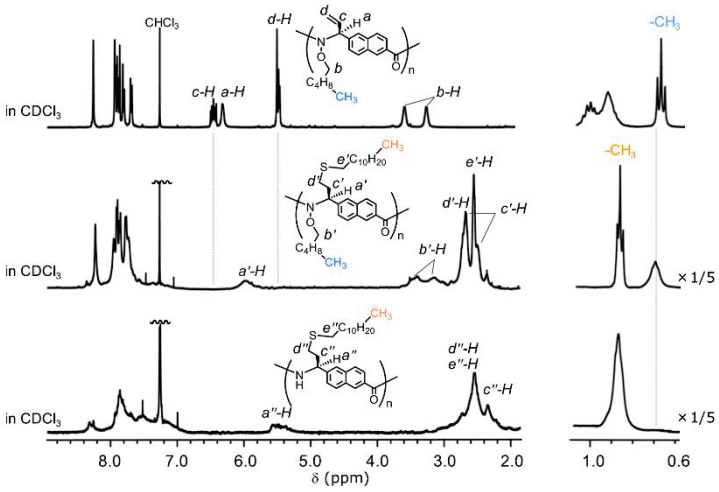

Figure 4-1. ^{1}H NMR spectra of precursors and **poly-2a** (500 MHz, $CDCl_3$, 298 K).

The ^{1}H NMR signals of **poly-2a** were broad, presumably because of intermolecular aggregation of the polymer at the concentration of NMR measurements ([**poly-2a**] = 23.8 mM/unit) similar to arylopeptide containing a *p*-phenylene spacer. Addition of 2,2,2-trifluoroethanol-d_3 (TFE-d_3) as a hydrogen-bond competitor to a $CDCl_3$ solution of **poly-2a**, the signals became sharper (Figure 4-2). The spectrum was similar to the model compound.

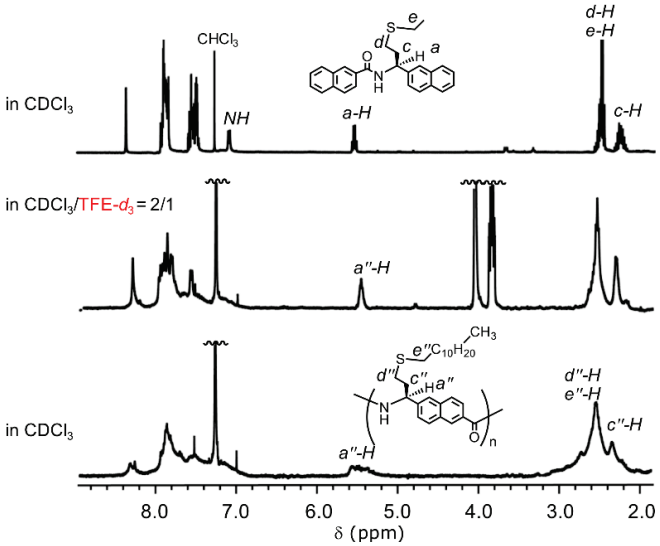

Figure 4-2. ^{1}H NMR spectra of model compound in $CDCl_3$ and **poly-2a** in $CDCl_3$ and $CDCl_3$ /TFE-d_3 = 2/1. [model compound] = 14.7 mM, [**poly-2a**] = 9.8 g/L (23.8 mM/unit).

Amide group was confirmed by IR spectrometry. NH stretching band was detected at 3309 cm^{-1} in the IR spectrum of **poly-2a** (Figure 4-3). This case also agrees with the result of model compound. The M_w and M_w/M_n values of **poly-2a** was determined by SEC using with calibration polystyrene standards (M_w = 45 000, M_w/M_n = 2.51).

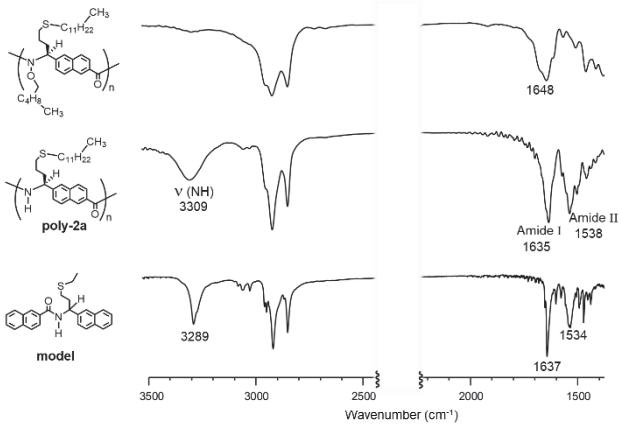

Figure 4-3. IR spectra of precursor, model compound **3** and **poly-3a** (KBr tablet).

Structural Analysis

CD and UV spectroscopy studies were carried out to investigate the conformation of **poly-2** with different side chains. The CD spectra of **poly-2a** and **poly-2b** in THF at 25 °C exhibit very different Cotton effects (Figure 4-4a). The CD spectrum of **poly-2a** shows a plus-to-minus bisignate Cotton effect between 252 and 231 nm, which is similar to that of **poly-1** (*cf.* Chapter 2 and ref.14). Conversely, **poly-2b** presents a minus-to-plus bisignate curve exhibiting a negative Cotton effect at 257 nm and a positive Cotton effect at 238 nm. Since the CD and UV signals of **poly-2a** and **poly-2b** did not change over the concentration range of 1.2–120 μM, the polymers did not adopt a higher-order chiral aggregation at the concentration of CD measurements. These results

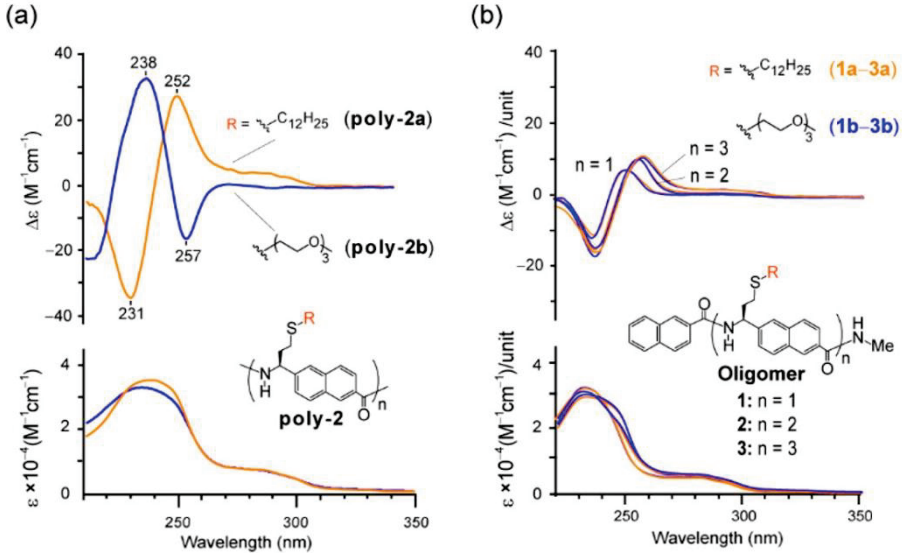

Figure 4-4. (a) CD spectra of **poly-2a** and **poly-2b** in THF, 25 °C. Concentration: [**poly-2a**]/unit = 0.32 mM and [**poly-2b**] = 0.30 mM. (b) CD spectra of oligomers (n = 1–3) in THF at 25 °C. The orange spectra are for a compound with the dodecyl group and the blue spectra are for a compound with an oligoether group on the side chain. Concentration: [n = 1] = 0.30 and 0.34 mM, [n = 2] = 0.30 and 0.32 mM, and [n = 3] = 0.38 and 0.44 mM.

indicate that the polypeptides adopt different specific structures in solution, whereas **poly-1**, which contains *p*-phenylene spacers without geometrical isomers, forms a stable 3_1-helix, regardless of the side chain. Additionally, we synthesized oligomers **1**–**3** (n = 1–3) with the dodecyl or triethylene glycol group as side chains to model the local structure of the polymer chain (Figure 4-4b). The CD features of the oligomers are independent of the side chains, which indicates that the drastic change in CD of **poly-2** is related to the secondary structure of the polymer, not to the local conformation.

DFT and time-dependent DFT calculations[15] (B3LYP/6-31G**) were done to understand the origin of the each Cotton effect for **poly-2** in THF. Initially, the calculation of **1′** coressponding the monomer unit of **poly-2** was conducted (Figure 4-5a). The author employed the crystal structure data of model compound **1** as initial structure for **1′**. In the ^{1}H NMR spectrum of synthesized oligomer **1′**, applying the Karplus equation[16,17] to coupling constant of the internal NH proton $J_{\text{HN-CH}}$ indicates an HN-CH dihedral angle of $\phi = -87°$, which is consistent with the observed dihedral angle in the crystal structure of **1** (−86°). Therefore, this crystal structure is suitable as a model of **1′** the solution state. Next, initial structures for calculating dimer **2** were constructed based on the optimized structure of **1′** as a local structure, and geometry optimizations were conducted for each structure. The optimization revealed that two type of conformers ($\mathbf{2}_{\text{anti}}$ and $\mathbf{2}_{\text{syn}}$) which can be assumed according to the orientation of the vicinal unit were most energetically stable. The difference in energy of $\mathbf{2}_{\mathbf{anti}}$ and $\mathbf{2}_{\mathbf{syn}}$ is only 0.02 kJ/mol evaluated by DFT to be regarded as the almost the same stabilities. Interestingly, the TD-DFT calculation in THF of $\mathbf{2}_{\mathbf{anti}}$ and $\mathbf{2}_{\mathbf{syn}}$ reproduced the different type of Cotton effects as observed for **poly-2a** and **poly-2b** (Figure 4-5b). Furthermore, oligomer **3** was also optimized in the same manner. The calculated CD

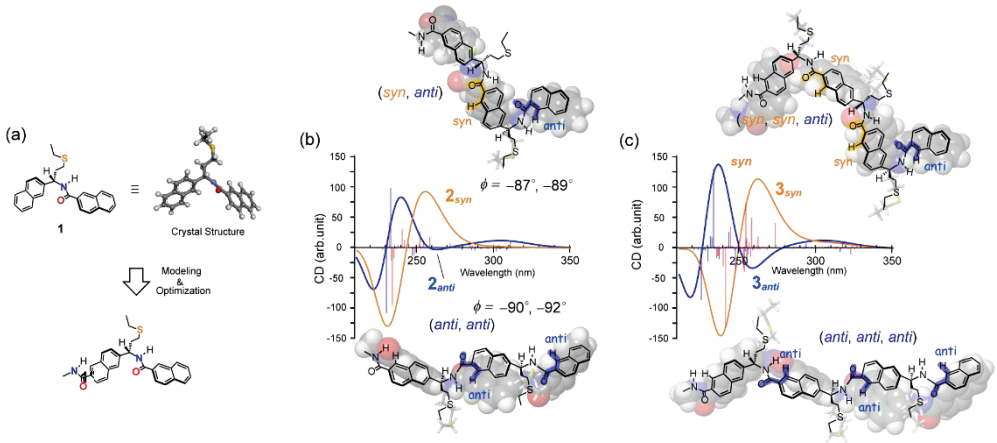

Figure 4-5. (a) Chemical structure of **1** and **1′**. (b, c) Simulated structures and CD spectra of oligomer $\mathbf{2}_{syn}$ and $\mathbf{2}_{anti}$, $\mathbf{3}_{syn}$ and $\mathbf{3}_{anti}$ by TD-DFT calculation (B3LYP/6-31**) in THF

spectra of **3** by TD-DFT resembles those of **poly-2** (Figure 4-5c). These calculations strongly indicate that the dodecyl side chain induces the successive *syn* units (*syn*, *syn*, *syn*, ...) and that the oligo(ethylene glycol) group induces successive *anti* units (*anti*, *anti*, *anti*, ...), leading to the proposal of two global conformations (Figure 4-6). **Poly-2a** exhibits a right-handed 4_1-helix by the successive formation of $\mathbf{3}_{syn}$, and **poly-2b** adopts a right-handed 3_1-helix in THF. The author estimated the pitch per residue of the 3_1-helix to be 8.2 Å, and the pitch is more extended than that of the 4_1-helix (5.5 Å) and has no cavity.

The Structural study by atomimc force microscopy (AFM) revealed detailed insights into the structure of **poly-2a**. AFM images of **poly-2a** film casted by THF solution on mica exhibited a hight of about 0.8 nm. Judging from the calculated structure of the polymer, which matched well with the height of the proposed helical conformation of **poly-1a** (Figure 4-7).

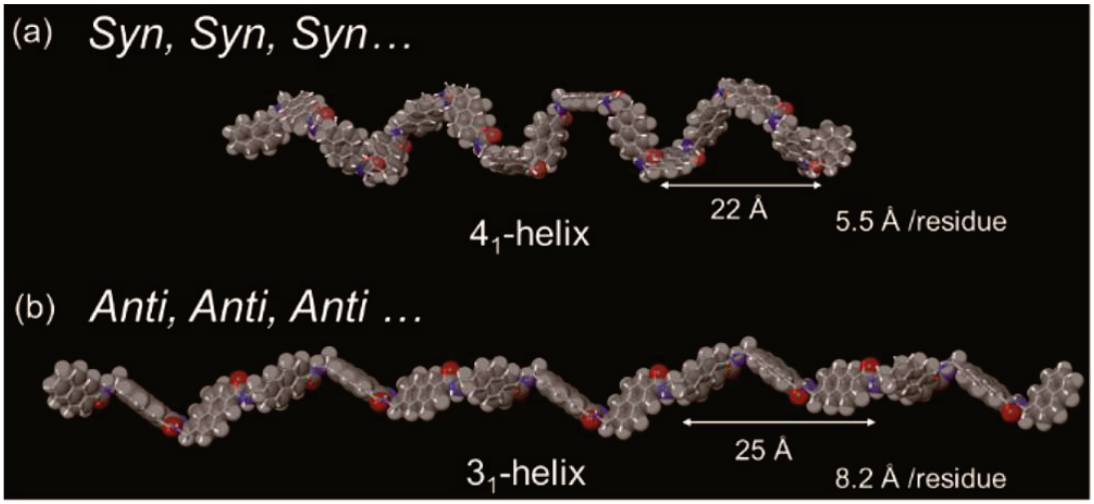

Figure 4-6. Two plausible helical conformations of **poly-2** (n = 15) based on results of 3_{syn} and 3_{anti}. The upper structure corresponds to **poly-2a** and the lower structure corresponds to **poly-2b**. Side chains are omitted for clarity.

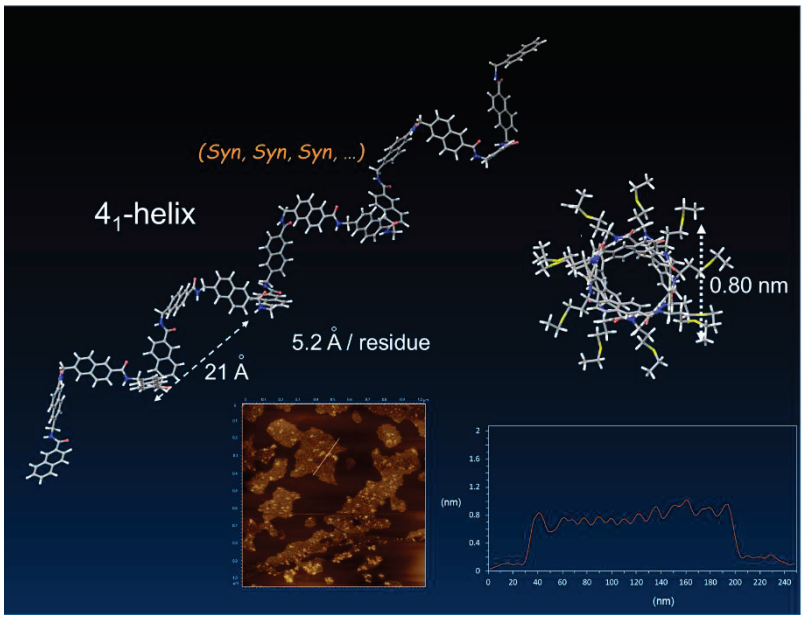

Figure 4-7. AFM image of **poly-2a**. (1.0 um ×1.0 um, topography, HOPG)

Property of Helical Structures

VT-CD spectroscopic measurements of two helical structure were carried out. As shown Figure 4-8, these helices adopt the main proposed conformation in THF at temperatures ranging from −80 to 50 °C, although some conformational fluctuation were observed. Furthermore, the CD spectra are identical even after the solution is maintained at 30 °C for 5 days. Next, CD spectrometry was used to study the helical formation depending on the molecular weight (Figure 4-9). The CD signals of **poly-2a** and **poly-2b** increased nonlinearly as a function of the degree *n* of polymerization and plateaued at higher *n* value. The CD spectra of **poly-2a** was red-shifted with the higher degree of polymerization, similar to that of the oligomers (**1**–**3**; Figure 4-4b). Therefore, the formation of 4_1-helix is preferable for the main

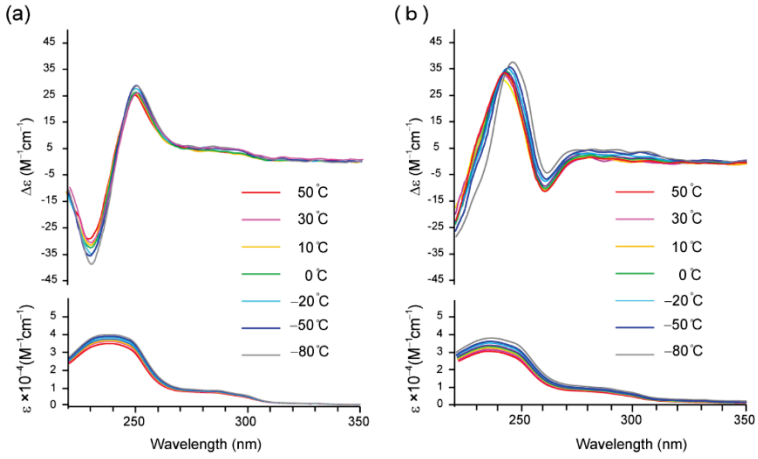

Figure 4-8. VT-CD and UV measurement (–80–50 °C). (a) **poly-2a** (0.40 mM), (b) **poly-2b** (0.39 mM) in THF.

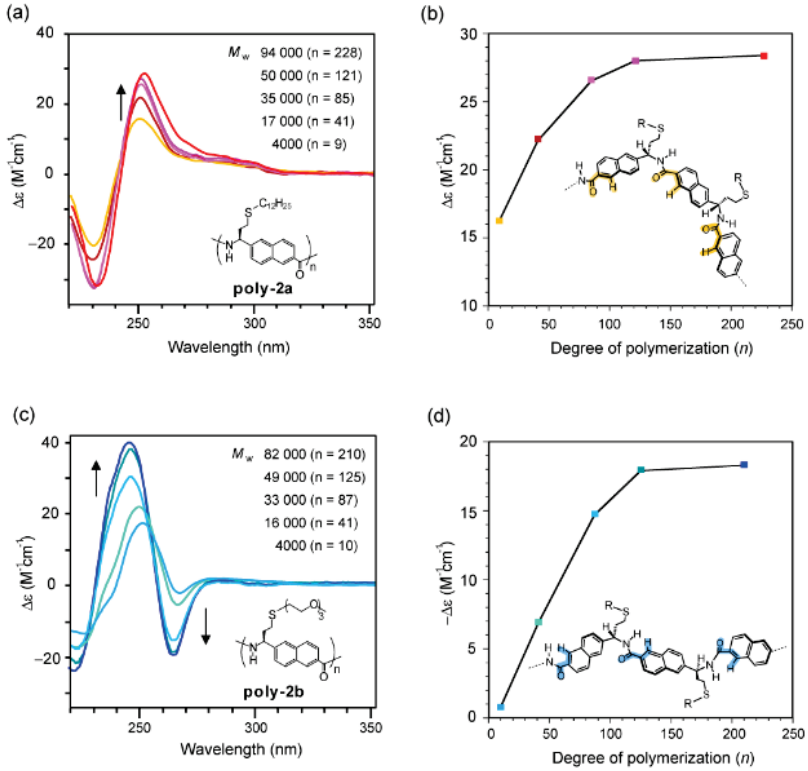

Figure 4-9. (a) CD spectra of **poly-2a** of different M_w in THF at 25 °C. (b) CD intensity of **poly-2a** at 252 nm as a function of polymerization degree *n*. (c) CD spectra of **poly-2b** in THF at 25 °C for several molecular weights. (d) CD intensity at 257 nm as a function of polymerization degree *n* of **poly-2b**. Concentration/unit: [**poly-2a**] = 0.28–0.41 mM and [**poly-2b**] = 0.32–0.48 mM.

chain. Conversely, the development of long chains gradually leads to the formation of backbones to form a 3_1-helix in **poly-2b**, which is undesirable for the main chain itself. The underlying mechanism of the changing thermodynamic stability dependence on the side chain is unclear. Probably, the difference in solvation of a side chain can be attributed to the thermodynamic stability of **poly-2**,[11g,18] and for the side chain of the oligo(ethylene glycol) groups, the more extended 3_1-helix is a preferable structure compared to the 4_1-helix for efficient solvation by THF, whereas the main chain originally prefers to form the 4_1-helix. These results indicate that the entire peptide chain thermodynamically prefers to fold into one of the two helical structures, resulting in *anti* and *syn* control.

4-3: Conclusions

In conclusion, we have developed unique dual structural systems of poly arylopeptide by using the energy difference between geometrical *anti* and *syn* conformations of the 2,6-naphthalene spacer. Although the formations of the *syn* and *anti* conformers of the 2 6-naphthalene ring was out of control within the oligomers, longer polymeric chains adopted either the contracted 4_1-helix or the expanded 3_1-helix in response to the conditions and without specific interactions. This geometrical control of the local structure is due to the relative thermodynamic stability of the polymers. The 4_1- and 3_1-helices was selectively formed by the appropriate the side chain, and the polypeptide reselects the geometrical isomers. The presented results utilize a small energy difference of the monomer units to create stable particular secondary structures in polymer by polymer effects, which are expected to be a new guideline for designing the primary structure of synthetic polymers. Polypeptide chain would create branching point and allow to control conformers under various conditions.

4-4: Experimental Sections

General

Unless otherwise indicated, all reactions were carried out under an Ar atmosphere, whereas the workup was performed in air. ^{1}H NMR spectra were recorded in $CDCl_3$, toluene-d_8, and benzene-d_6 on JEOL JNM-ECS400 or JEOL JNM-ECA500 spectrometers using $SiMe_4$ as an internal standard. IR spectra were recorded on a SHIMADZU IR Prestige-21 spectrometer using KBr tablets. HR-MS and MS/MS (CID) measurements were carried out on a Thermo Fisher Scientific LTQ-Orbitrap XL mass spectrometer. Retention time of polymers were measured by SEC analyses using a SHIMAZU LC-10AS, SPD-10A UV-vis detector, and CTO-10A column oven equipped with two SEC columns TOSOH TSKgel GMH_{HR}-M carried out at 40 °C and a flow rate of 0.7 mL min^{-1} with $CHCl_3$ as the eluent. The enantiomeric excesses were determined by HPLC analysis using a Shimadzu LC-10 system equipped with an SPD-10AV detector and DAICEL Chiralpak AD-H. CD spectra were obtained by a

JASCO J-720WO polarimeter with a cryostat thermostated at −75 to 85 °C. UV–vis spectra were obtained by a SHIMAZU UV 3100PC spectrophotometer. Samples for the AFM measurements of **poly-2a** were prepared by drop casting (about 20 μL) of dispersions onto freshly cleaved mica substrates at room temperature (about. 25 °C), and the substrates were then dried under vacuum for 1 h. The AFM images were obtained in air by tapping mode on an Agilent Technology Agilent PicoPlus 5100 microscope.

Materials

All solvents used for reactions were passed through purification columns just before use and tetrahydrofuran was dried by sodium-benzophenone and distilled under argon. Planar-chiral Cp′Ru complexes were prepared as reported previously.[19]

Standard Method of Asymmetric polymerization

To a mixture of molecular sieve 3A, Na_2CO_3 (1.2 eq), a monomer (1.0 eq) and (*R*) or (*rac*)-**Cp′Ru** (1 mol%) were added THF (0.5 mmol/ 1 mL), which was stirred at 30 °C. After 3days, dichloromethane was added to the reaction mixture. The insoluble part was removed by filtration through Celite. The combined organic layer was washed with water. After drying with anhydrous Na_2SO_4, the solvent was removed under reduced pressure. The product was purified by silica gel column chromatography with CH_2Cl_2 and dried under vacuum to give a pale-yellow solid.

Standard Method of Post-Polymerization Modification

To a toluene solution (5 mL) of the polymer (0.15 mmol of C=C groups) and 2,2-dimethoxy-2-phenylacetophenone (DMPA) (38.4 mg, 0.15 mmol) was added thiol (0.90 mmol), and the reaction mixture was irradiated at 365 nm with LED lamp (365 nm) for 5 h. The product was purified by SEC using two Shodex KF 2003 columns connected in series at a flow rate of 3.0 mL min^{-1} to give the pale brown solid. To a THF solution (0.10 M) of the resulting polymer, THF solution of SmI_2–THF complex (4.0 equiv) was added dropwise using a syringe at room temperature. After stirring for 2.0 h, the reaction was rapidly quenched with a 10% solution of $Na_2S_2O_3 \cdot H_2O$. The mixture was diluted with CH_2Cl_2 (20 mL). The organic layer was separated, and the product was extracted from the aqueous layer with CH_2Cl_2 (3 × 20 mL). The organic layers were combined. The combined organic layer was dried with anhydrous Na_2SO_4. The Na_2SO_4 was removed by filtration. After the solvent was removed under reduced pressure, the product was purified by SEC column using two Shodex KF

2003 columns connected in series at a flow rate of 3.0 mL min^{-1}, and washed with *n*-hexane to give the target product.

Characterization of Representative Compounds

Synthesis of poly-2a.

According to the standard method of asymmetric polymerization and post-polymerization modification, **poly-2a** was obtained as a pale brown solid. ^{1}H NMR ($CDCl_3$/trifluoroethanol-d_3 = 2/1, 500 MHz): δ 8.20 (brs, 1H, Ar), 7.89–7.55 (m, 5H, Ar), 5.47 (br, 1H, –C*H*CH_2CH_2S–), 2.55 (br, 4H, –$CHCH_2CH_2$S– and –$CHCH_2CH_2SCH_2$–), 2.33 (br, 2H, –$CHCH_2CH_2S$–), 1.56 (br, 2H, –$CHCH_2CH_2SCH_2CH_2$–), 1.42-1.10 (br, 18H, –CH_2–), 0.84 (br, 3H, CH_3). IR (KBr) 3309, 2922, 2850, 1635, 1538 cm^{-1}.

Synthesis of poly-2b.

According to the standard method of reductive cleavage using SmI_2-THF complex, **poly-2b** was obtained as a pale brown solid. ^{1}H NMR (DMSO-d_6, 500 MHz): δ 9.10 (brs, 1H, NH), 8.48 (brs, 1H, Ar), 8.18-7.97 (br, 4H, Ar), 7.70 (br, 1H, Ar), 5.38 (br, 1H, –C*H*CH_2CH_2S–), 3.54–3.37 (br, 8H, –OCH_2CH_2O–), 3.16 (br, 3H, OCH_3), 2.67 (br, 2H, –SCH_2CH_2O–), 2.32 (br, 2H, –$CHCH_2CH_2S$). the peak of (–SCH_2CH_2O–) and (–$CHCH_2CH_2S$) overlap with solvent. IR (KBr) 3296, 3040, 2971, 2920, 2868, 1639, 1531, 1260 cm^{-1}.

(*E*)-6-(3-Chloroprop-1-en-1-yl)-*N*-(hexyloxy)-2-naphthamide (Monomer)

(*E*)-6-(3-chloroprop-1-en-1-yl)-*N*-(hexyloxy)-2-naphthamide was synthesized based on the previously reported method. [20] ^{1}H NMR ($CDCl_3$, 400 MHz): δ 8.66 (s, 1H, N*H*), 8.21 (s, 1H, Ar), 7.87 (d, 1H, *J* = 8.4 Hz, Ar), 7.86 (d, *J* = 8.4 Hz, 1H, Ar), 7.77 (d, 1H, *J* = 8.1 Hz, Ar), 7.76 (d, 1H, *J* = 8.1 Hz, Ar), 6.82 (d, 1H, *J* = 16.0 Hz, C*H*=$CHCH_2$–), 6.49 (dt, 1H, *J* = 16.0, 7.1 Hz, CH=C*H*CH_2–), 4.30 (d, 2H, *J* = 7.1 Hz, CH=$CHCH_2$–), 4.08 (t, 2H, *J* = 6.8 Hz, –OCH_2CH_2–) 1.75 (quin, 2H, *J* = 6.8 Hz, –OCH_2CH_2–), 1.44 (quin, 2H, *J* = 6.8 Hz, –$OCH_2CH_2CH_2$–), 1.36–1.32 (m, 4H, –$CH_2CH_2CH_3$ and –$CH_2CH_2CH_3$, 0.90 (t, *J* = 6.8 Hz, 3H, –CH_2CH_3).^{13}C NMR ($CDCl_3$, 101 MHz): δ 165.5, 134.2, 133.9, 132.7, 131.3, 131.1, 131.0, 128.3, 127.6, 127.5, 125.6, 125.4, 123.4, 123.0, 44.2, 30.6, 27.1, 24.5, 21.5, 13.0. HRMS (ESI+): Calcd for $C_{20}H_{24}NNaO_2$ ($[M+Na]^+$): m/z 368.1393, Found: m/z 368.1390.

(*S*)-6-(1-(2-Naphthamido)-3-(dodecylthio)propyl)-*N*-methyl-2-naphthamide (1a)

To a stirring solution of precursor (50.2 mg, 0.076 mmol) in 0.5 mL of THF was added at 25°C a solution of

SmI_2-THF complex (2.1 mL, 0.1 M in THF). After stirring for 15 min at 25°C, the reaction was quickly quenched with a 10% aqueous solution of $Na_2S_2O_3 \cdot H_2O$ (10 mL). The mixture was then diluted with CH_2Cl_2 (30 mL). The layers were separated and the product was extracted from the aqueous layer with CH_2Cl_2 (3 × 20 mL). The combined organic layers were dried with anhydrous Na_2SO_4. The Na_2SO_4 was removed by filtration. After the solvent was removed under reduced pressure, pale yellow solid was obtained. The product was washed with *n*-hexane to give a colorless solid (44.8 mg, 99%). ^{1}H NMR ($CDCl_3$, 500 MHz): δ 8.34 (s, 1H, Ar), 8.24 (s, 1H, Ar), 7.93–7.76 (m, 8H, Ar), 7.60–7.52 (m, 3H, Ar), 7.24 (d, 1H, J = 7.4 Hz, N*H*CHCH$_2$), 6.34 (q, 1H, J = 4.8 Hz, N*H*CH$_3$), 5.57 (q, 1H, J = 7.4 Hz –C*H*CH$_2$CH$_2$S–), 3.06 (d, 3H, J = 4.8 Hz, NHC*H*$_3$), 2.65–2.54 (m, 4H, –CHCH$_2$CH$_2$SC*H*$_2$– and –CHCH$_2$C*H*$_2$SCH$_2$–), 2.36–2.30 (m, 2H, –CHC*H*$_2$CH$_2$S–), 1.56 (quintet, 2H, J = 7.2 Hz, –CHCH$_2$C*H*$_2$SCH$_2$C*H*$_2$–), 1.30–1.21 (m, 16H, –CH$_2$–), 0.87 (t, 3H, J = 7.1 Hz, –C*H*$_3$). ^{13}C NMR ($CDCl_3$, 101 MHz): δ 168.1, 167.5, 141.4, 135.4, 135.2, 133.2, 132.6, 132.4, 131.9, 130.2, 129.5, 129.1, 129.1, 129.0, 129.0, 128.3, 128.1, 127.6, 127.3, 126.1, 125.7, 124.5, 124.2, 54.4, 52.3, 35.9, 32.9, 32.4, 30.2, 30.2, 30.1, 30.1, 29.9, 29.8, 29.4, 29.2, 27.5. HRMS (ESI+): calcd for $C_{38}H_{48}N_2NaO_2S$([M+Na]$^+$): *m*/*z* 619.3334, found: *m*/*z* 619.3339.

Synthesis of 1b

To a stirring solution of precursor (47.4 mg, 0.075 mmol) in 0.5 mL of THF was added dropwise using a syringe at 25°C a solution of SmI_2-THF complex (1.9 mL, 0.1 M in THF). After stirring for 15 min at 25°C, the reaction was quickly quenched with a 10% aqueous solution of $Na_2S_2O_3 \cdot H_2O$ (10 mL). The mixture was then diluted with CH_2Cl_2 (30 mL). The layers were separated and the product was extracted from the aqueous layer with CH_2Cl_2 (3 × 20 mL). The combined organic layers were dried with anhydrous Na_2SO_4. The Na_2SO_4 was removed by filtration. After the solvent was removed under reduced pressure, pale yellow solid was obtained. The product was washed with *n*-hexane to give a colorless solid (42.8 mg, 97%). ^{1}H NMR ($CDCl_3$, 400 MHz): δ 7.93–7.74 (m, 2H, Ar), 7.7.3–7.64 (m, 2H, Ar), 7.53-7.30 (m, 9H, Ar), 7.23 (d, 1H, J = 8.2 Hz, NH), 6.45 (q, 1H, J = 4.3 Hz, NHC*H*$_3$), 5.31 (q, 1H, J = 8.2 Hz, –C*H*CH$_2$CH$_2$S–), 3.75–3.57 (s, 8H, –OC*H*$_2$C*H*$_2$O–), 3.50 (t, 2H, J = 6.7 Hz, –SCH$_2$C*H*$_2$O–), 3.30 (s, 3H, OC*H*$_3$), 2.97 (d, 1H, J = 4.3 Hz, NHC*H*$_3$), 2.75-2.70 (m, 4H, –CHCH$_2$C*H*$_2$S– and –CHC*H*$_2$CH$_2$S–). ($CDCl_3$, 101 MHz): 168.0, 167.1, 145.3, 134.3, 133.9, 131.7, 128.6, 127.7, 127.5, 127.2, 126.8, 72.0, 72.0, 71.1, 70.6, 70.5, 70.5, 70.4, 70.4, 68.5, 59.1, 59.0, 53.3, 38.5, 35.6, 31.7, 29.2, 26.9, 26.6. Four carbon peaks were missing due to overlap. HRMS (ESI+): calcd for $C_{33}H_{38}N_2NaO_5S$ ([M + Na]$^+$): *m*/*z* 597.2399, found: *m*/*z* 597.2390.

Synthesis of 2a

To a stirring solution of precursor (68.3 mg, 0.062 mmol) in 0.5 mL of THF was added dropwise using a syringe at 25°C a solution of SmI_2-THF solution (4.28 mL, 0.1 M in THF). After stirring for 15 min at 25°C, the reaction was quickly quenched with a 10% aqueous solution of $Na_2S_2O_3{\cdot}H_2O$ (10 mL). The mixture was then diluted with CH_2Cl_2 (30 mL). The layers were separated and the product was extracted from the aqueous layer with CH_2Cl_2 (3 × 10 mL). The combined organic layers were dried with anhydrous Na_2SO_4. The Na_2SO_4 was removed by filtration. After the solvent was removed under reduced pressure, pale yellow solid was obtained. The product was washed with ether to give a colorless solid (61.8 mg, 99%). ^{1}H NMR ($CDCl_3$, 400 MHz): δ 8.34–8.25 (br, 3H, Ar), 7.88–7.86 (br, 12H, Ar), 7.55 (brs, 4H, Ar), 6.72 (brs, 1H, N*H*CH_3), 5.56 (t, 2H, *J* = 5.7 Hz, C*H*CH_2CH_2S), 3.06 (brs, 3H, NHC*H*$_3$), 2.69–2.44 (brs, 8H, –$CHCH_2CH_2SCH_2$– and –$CHCH_2CH_2SCH_2$–), 2.43–2.17 (brs, 4H, –$CHCH_2CH_2S$–), 1.56 (brs, 4H, –$CHCH_2CH_2SCH_2CH_2$–), 1.30–1.21 (brs, 36H, –CH_2–), 0.86 (t, 6H, *J* = 6.41 Hz, –CH_2CH_3). ^{13}C NMR ($CDCl_3$/methanol-d_4 = 9/1, 101 MHz): δ 169.1, 167.9, 167.9, 141.4, 141.3, 134.7, 134.6, 132.4, 1311.8, 131.8, 131.3, 131.2, 131.1, 129.4, 128.7, 128.2, 128.1, 127.6, 127.5, 127.5, 127.4, 127.1, 126.5, 125.5, 125.5, 125.0, 125.0, 123.9, 123.8, 123.5, 53.5, 39.9, 35.3, 35.3, 32.0, 32.0, 29.4, 29.3, 29.3, 29.3, 29.2, 29.2, 29.1, 29.1, 29.0, 28.9, 28.6, 28.6, 26.3, 22.1, 13.7. Thirteen carbon peaks were missing due to overlap. (ESI+): calcd for $C_{64}H_{85}N_3NaO_3S_2$([M+Na]$^+$): *m*/*z* 1030.5930, found: *m*/*z* 1030.5925.

Synthesis of 2b

To a stirring solution of precursor (84.7 mg, 0.09 mmol) in 0.5 mL of THF was added dropwise using a syringe at 25°C a solution of SmI_2-THF solution (6.0 mL, 0.1 M in THF). After stirring for 15 min at 25°C, the reaction was quickly quenched with a 10% aqueous solution of $Na_2S_2O_3{\cdot}H_2O$ (10 mL). The mixture was then diluted with CH_2Cl_2 (30 mL). The layers were separated and the product was extracted from the aqueous layer with CH_2Cl_2 (3 × 10 mL). The combined organic layers were dried with anhydrous Na_2SO_4. The Na_2SO_4 was removed by filtration. After the solvent was removed under reduced pressure, pale yellow solid was obtained. The product was purified by silica gel column chromatography (eluent: dichloromethane /methanol = 93/7.) to give a colorless solid (82.0 mg, 91%). ^{1}H NMR ($CDCl_3$, 400 MHz): δ 8.35–8.25 (m, 3H, Ar), 7.86–7.77 (br, 12H, Ar), 7.55 (br, 4H, Ar), 6.37 (brs, 1H, N*H*CH_3), 5.56 (m, 2H, C*H*CH_2CH_2S–), 3.57 (m, 16H, –OCH_2CH_2O–), 3.48 (s, 4H, –SCH_2CH_2O–), 3.07 (s, 3H, NC*H*$_3$), 2.75 (m, 4H, –SCH_2CH_2O–), 2.74–2.69 (m, 4H, –$CHCH_2CH_2$S–), 2.69–2.67 (m, 4H, –$CHCH_2CH_2$S). ^{13}C NMR ($CDCl_3$, 101 MHz): δ 168.7, 167.6, 161.8, 135.0, 134.8, 1346,

134.2, 132.8, 132.7, 132.4, 132.5, 131.9, 131.5, 131.3, 131.0, 129.9, 139.1, 139.0, 128.7, 128.4, 128.1, 127.5, 127.2, 126.8, 126.4, 126.2, 125.8, 125.4, 125.1, 124.5, 123.9, 123.6, 59.1, 59.0, 53.9, 53.7, 53.3, 38.5, 32.1, 31.8, 31.6, 31.1, 30.5, 30.4, 29.8, 29.7, 29.4, 28.9, 28.6, 28.1, 27.5, 27.0, 26.8. HRMS (ESI+): calcd for $C_{64}H_{85}N_3NaO_3S_2$([M+Na]$^+$): *m*/*z* 1030.5930, found: *m*/*z* 1030.5925.

Synthesis of 3a

To a toluene solution (4.0 mL) of precursor (26.6 mg, 0.028 mmol) and DMPA (7.1 mg, 0.025 mmol) was added 1-dodecanethiol (0.1 mL, 0.51 mmol), and the reaction mixture was irradiated at 365 nm by an LED lamp (365 nm) for 3 h at 25 °C. The reaction mixture was concentrated under reduced pressure. The residue was purified by silica gel column chromatography (eluent: *n*-hexane/ethyl acetate = 1/1 then dichloromethane /ethyl acetate = 1/1) to give a colorless oil. To a stirring solution of resulting oil in 0.5 mL of THF, a solution of SmI_2-THF complex (2.57 mL, 0.1 M in THF) was added. After stirring for 15 min at 25 °C, the reaction was quickly quenched with a 10% aqueous solution of $Na_2S_2O_3{\cdot}H_2O$ (10 mL). The mixture was then diluted with CH_2Cl_2 (30 mL). The layers were separated and the product was extracted from the aqueous layer with CH_2Cl_2 (3 × 20 mL). The combined organic layers were dried with anhydrous Na_2SO_4. The Na_2SO_4 was removed by filtration. After the solvent was removed under reduced pressure, pale yellow solid was obtained. The product was washed with diethyl ether to afford colorless powder (34.5 mg, 87%). ^{1}H NMR ($CDCl_3$, 400 MHz): δ 8.41–8.18 (br, 4H, Ar), 7.88–7.46 (br, 21H, Ar), 7.35 (br, 1H, N*H*), 7.08 (br, 1H, N*H*), 6.37 (br, 1H, N*H*CH_3), 5.56 (br, 3H, C*H*CH_2CH_2S), 3.05 (br, 3H, NHC*H*$_3$), 2.69–2.44 (br, 12H, –$CHCH_2CH_2SCH_2$– and –$CHCH_2CH_2SCH_2$–), 2.43–2.17 (br, 6H, –$CHCH_2CH_2S$–), 1.55 (br, 6H, –$CHCH_2CH_2SCH_2CH_2$–), 1.30–1.21 (br, 54H, –CH_2–), 0.87 (t, 9H, *J* = 6.6 Hz, –CH_2CH_3). IR (KBr) 3312, 2922, 2950, 1633, 1530 cm^{-1}. HRMS (ESI+): calcd for $C_{90}H_{22}N_4NaO_8S_3$ ([M + Na]$^+$): *m*/*z* 1441.8526, found: *m*/*z* 1441.8521.

Synthesis of 3b

To a toluene (3.0 mL) and THF (1 mL) solution of precursor (92.4 mg, 0.1 mmol) and DMPA (25.3 mg, 0.1 mmol) was added 2-((methoxymethoxy)-methoxy)ethane-1-thiol (0.3 mL), and the reaction mixture was irradiated at 365 nm by an LED lamp for 5 h at 25 °C. The reaction mixture was concentrated under reduced pressure. The residue was purified by silica gel column chromatography (eluent: dichloromethane /ethyl acetate = 1/1 then dichloromethane /methanol = 93/7) to give a colorless oil. To a stirring solution of resulting oil in 0.5 mL of THF was added a solution of SmI_2-THF complex (9.1 mL, 0.1 M in THF). After stirring for 15 min at

25 °C, the reaction was quickly quenched with a 10% aqueous solution of $Na_2S_2O_3 \cdot H_2O$ (10 mL). The mixture was then diluted with CH_2Cl_2 (30 mL). The layers were separated and the product was extracted from the aqueous layer with CH_2Cl_2 (3 × 10 mL). The combined organic layers were dried with anhydrous Na_2SO_4. The Na_2SO_4 was removed by filtration. After the solvent was removed under reduced pressure, pale yellow solid was obtained. The product was washed with diethyl ether to afford colorless powder (90.6 mg, 67%). ^{1}H NMR ($CDCl_3$, 400 MHz): δ 8.34–8.23 (br, 4H, Ar), 7.86–7.22 (br, 21H, Ar), 7.01 (br, 1H, N*H*), 6.76–6.47 (br, 2H, N*H*), 6.23 (br, 1H, N*H*CH_3), 5.52 (br, 3H, –C*H*CH_2CH_2S), 3.57 (m, 24H, –OC*H*$_2$C*H*$_2$O–), 3.47 (brs, 6H, –SCH_2C*H*$_2$O–), 3.38 (s, 3H, NC*H*$_3$), 3.30 (s, 9H, OC*H*$_3$), 2.75–2.15 (m, 18H, –SC*H*$_2$$CH_2O$–, –$CHCH_2$C*H*$_2$S and –CHC*H*$_2$$CH_2S$–). IR (KBr) 3302, 1635, 1530, 1262 cm^{-1}. HRMS (ESI+): calcd for $C_{90}H_{22}N_4NaO_8S_3$ ([M + Na]$^+$): *m*/*z* 1375.5721, found: *m*/*z* 1375.5720.

Synthesis of X-ray model 1

To a stirring solution of precursor (212 mg, 0.49 mmol) in 5.0 mL of THF was added at 25°C a solution of SmI_2-THF complex (11.3 mL, 0.1 M in THF). After stirring for 15 min at 25°C, the reaction was quickly quenched with a 10% aqueous solution of $Na_2S_2O_3 \cdot H_2O$ (10 mL). The mixture was then diluted with CH_2Cl_2 (30 mL). The layers were separated and the product was extracted from the aqueous layer with CH_2Cl_2 (3 × 20 mL). The combined organic layers were dried with anhydrous Na_2SO_4. The Na_2SO_4 was removed by filtration. After the solvent was removed under reduced pressure, pale yellow solid was obtained. The product was purified by silica gel column chromatography (eluent: *n*-hexane /ethyl acetate = 4/1.) to give a colorless solid (183.8 mg, 94%). The product was recrystallized from toluene. ^{1}H NMR ($CDCl_3$, 400 MHz): ^{1}H NMR ($CDCl_3$, 400 MHz): δ 8.31 (s, 1H, Ar), 7.91–7.80 (m, 8H, Ar), 7.57–7.44 (m, 5H, Ar), 7.07 (d, 1H, *J* = 8.25 Hz, N*H*), 5.57 (q, 1H, *J* = 8.25 Hz, C*H*CH_2CH_2S), 2.63–2.52 (m, 4 H, $CHCH_2CH_2SC$*H*$_2CH_3$, and $CHCH_2$C*H*$_2$$SCH_2CH_3$), 2.39–2.28 (m, 2H, CHC*H*$_2CH_2SCH_2CH_3$),1.24 (t, 3H, *J* = 7.2 Hz, CHC*H*$_2CH_2SCH_2$C*H*$_3$). HRMS (ESI+): calcd for $C_{26}H_{25}NNaOS$ ([M+Na] $^+$): *m*/*z* 422.1555, found: *m*/*z* 422.1561.

X-ray Crystallography

Structural determination: A colorless platelet crystal of $C_{26}H_{25}NOS$ (X-ray model) having approximate dimensions of 0.250 x 0.050 x 0.020 mm was mounted on MicroMount™ 200 µm. Data collection was made on a Rigaku Rapid II Imaging Plate area detector with Mo-Kα radiation (0.71075 Å) using a MicroMax-007HF microfocus rotating anode X-ray generator and VariMax-Mo optics. The structure was solved by the direct method[21] and expanded Fourier techniques using a SHELXL-2014/7 software.[22] Non-hydrogen atoms were refined anisotropically. The H atoms were generated by the riding model.

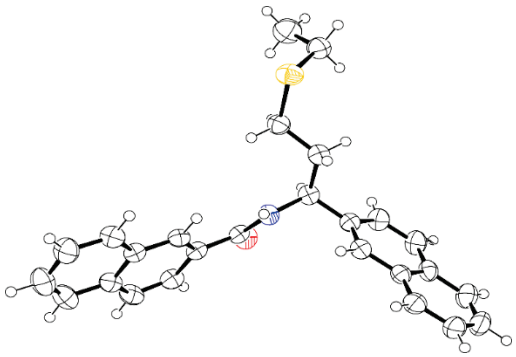

formula	$C_{26}H_{25}NOS$
fw	399.55
Crystal syst	monoclinic
Space group	$P\ 2_{1}/c$
a, Å	11.2135(5)
b, Å	21.5420(9)
c, Å	9.8888(4)
α, deg	90
β, deg	114.207(8)
γ, deg	90
V, Å^3	2178.71
Z	4
d_{calc}, g cm^{-3}	1.218
μ, cm^{-1}	1.649
GOF	1.030
$R1^a$ [I > 2σ(I)]	0.0514
w$R2^b$ (all data)	0.1079

$^aR1 = \Sigma||F_o| - |F_c||/\Sigma|F_o|$. $^bwR2 = \{\Sigma[w(F_o^2 - F_c^2)^2]/\Sigma[w(Fo^2)^2]\}^{1/2}$

APPENDIX

DFT Calculation

Computational Details

Geometry optimization and frequency calculation were performed using Becke's three parameter hybrid functionals (B3LYP) in Gaussian 09 program packages. 6-31G** basis set was employed. The crystal structure of the X-ray model compound was used for the initial structures of oligomer (n = 1, 2 and 3). Oligomer (n = 1) was made from the X-ray model by adding $CONHCH_3$ group. Oligomers (n = 2 and 3) were made from oligomer (n = 1 or 2) and X-ray model by fusing the naphthylene group of oligomer and naphthylene ring of oligomer (n = 1 or 2). All initial structures are manipulated on MacroModel (Schrödinger) and ChemBio3D (ver. 13.0.2.3021, Cambridge Soft) softwares. The optimized geometry was analyzed by MolStudio R4.0 (NEC Corp., Japan) and GaussView 5.0 (Gaussian, Inc.) softwares. The CD and UV spectra of oligomers were simulated by time-dependent (TD) DFT calculations after the geometrical optimization in tetrahydrofuran using the polarizable continuum model (PCM) as the self-consistent reaction field (SCRF) method.

Structual Optimization of Oligomer (n = 1)

The crystal structure of **1** was used for the initial structures, Oligomer (n = 1) was made from the crystal structure by adding $CONHCH_3$ group with an *anti* geometry. Geometry optimization was performed in THF (= Conformer B).We constructed the rotational isomers (Conformer A to D) by flipping the arylene ring or terminal $CONHCH_3$ group, then similar optimizations were carried out. We also calculated the CD and UV spectra of conformers by TD-DFT calculations.

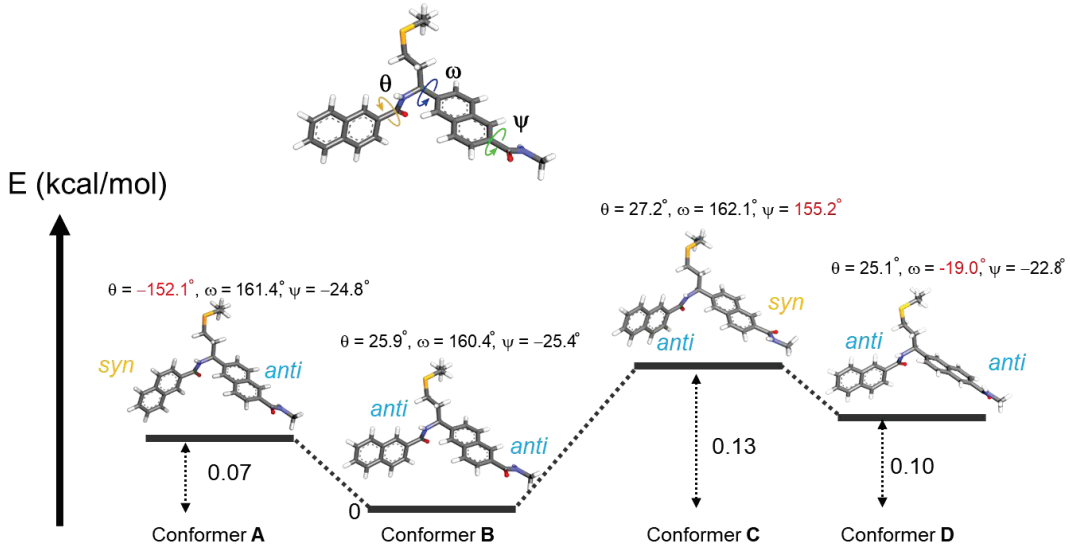

Figure 4-S1 Energy diagram of oligomer (n = 1) obtained by DFT calculation in THF.

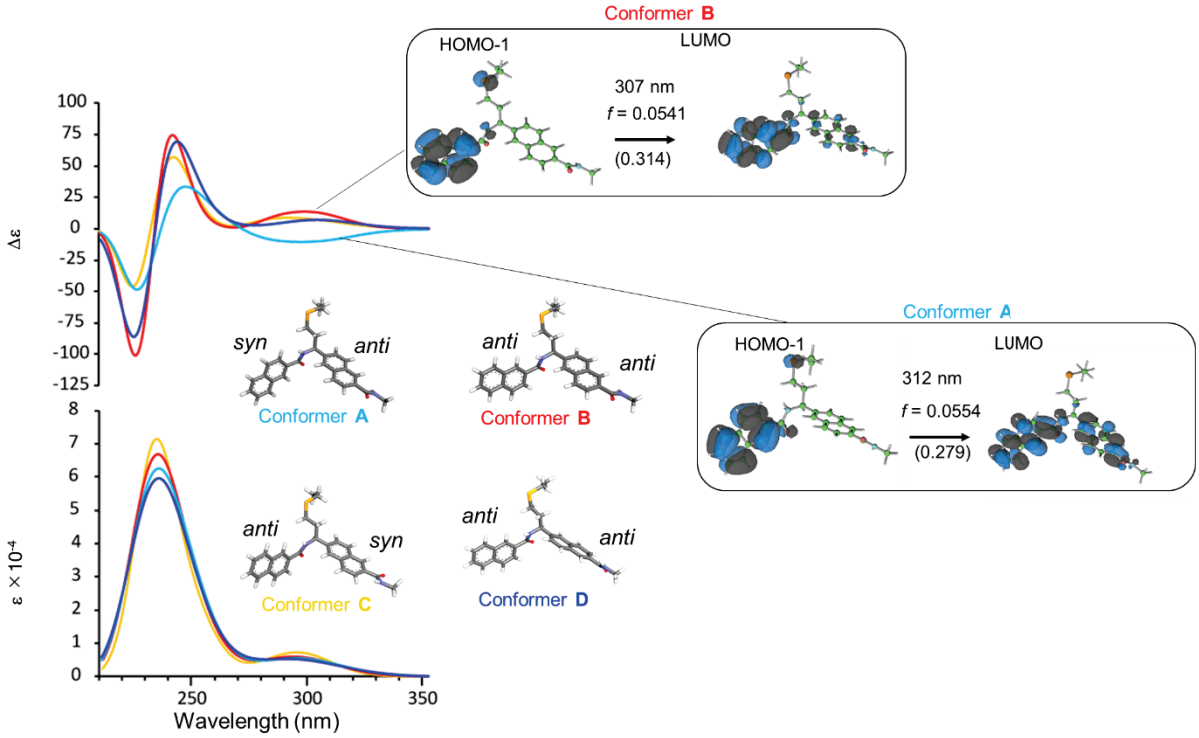

Figure 4-S2. The calculated CD/UV spectra of oligomer (n = 1) obtained by TD-DFT calculation and predominant transitions for the absorption bands, oscillator strength (f) and the molecular orbitals (MOs) for Conformers A and B. The coefficients indicating their contributions to the excitation are shown in parentheses under arrows.

.

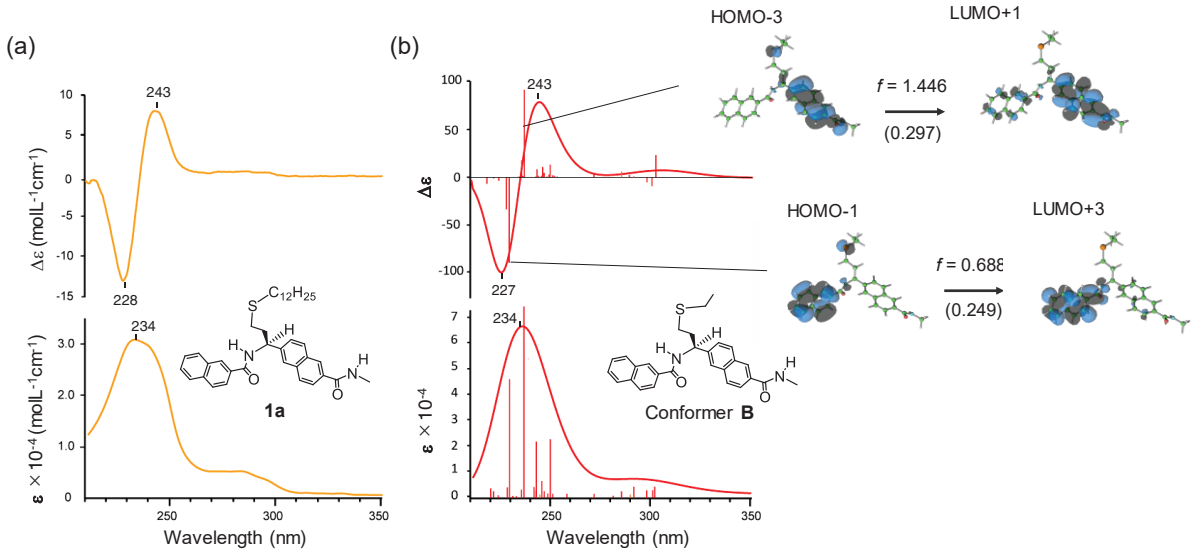

Figure 4-S3. (a) CD/UV spectrum of **1a** in THF at 25 °C. (b) Calculated CD/UV spectra of oligomer (n = 1, R = Et), The calculated predominant transitions for the absorption bands (nm), oscillator strength (f) and the molecular orbitals (MOs). The coefficients indicating their contributions to the excitation are shown in the parentheses under arrows

Structual Optimization of Oligomer (n = 2)

Oligomer (n = 2) was made from two molecules of oligomer (n = 1, conformer B) by fusing the arylene rings. The dihedral angle of internal θ in oligomer (n = 2) can be freely determined because terminal $\psi = (\theta)$ in conformer B has a negative value and internal θ has a positive value (Figure 4-S4).

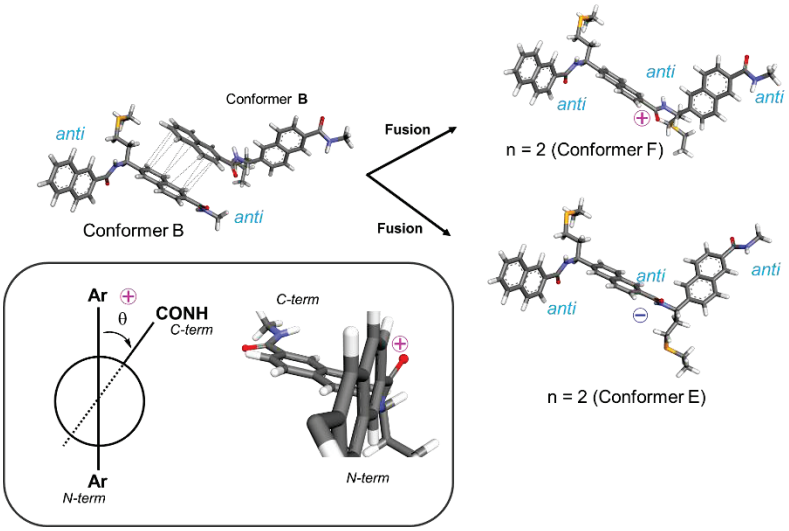

Figure 4-S4. Construction of oligomer (n = 2) by fusion of conformer B and definition of sign.

Therefore, geometry optimization was performed in both cases in THF (Conformers E to G), and we found that rotational state with a positive value of internal θ and negative values of terminal ψ is more preferred (Figure 4-S5).

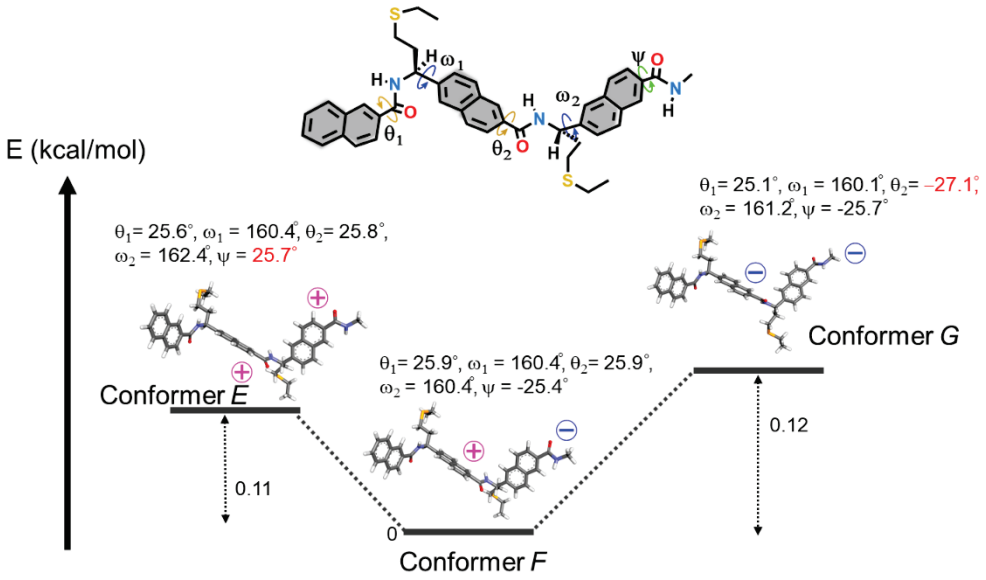

Figure 4-S5. Energy diagram of oligomer (n = 2) obtained by DFT calculation in THF.

As shown in Figure 4-S6, the arylene flip for θ is most likely to occur because the energy gap between conformers A and B is smallest. Based on the result, we constructed the rotational isomers (Conformer I) by arylene ring flipping the angle of θ_2. Conformer H was obtained by rotating of ω_1, which is based on the conformer D. Then same optimization were carried out. We also calculated the CD and UV spectra of conformers by TD- DFT calculations.

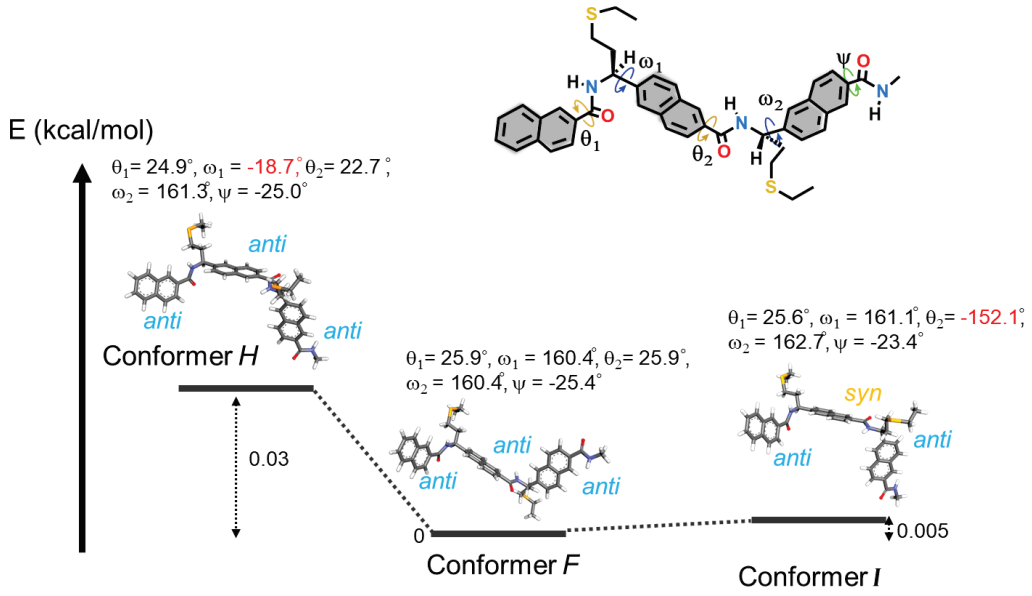

Figure 4-S6. Energy diagram of rotational isomer in oligomer (n = 2) obtained by DFT calculation in THF.

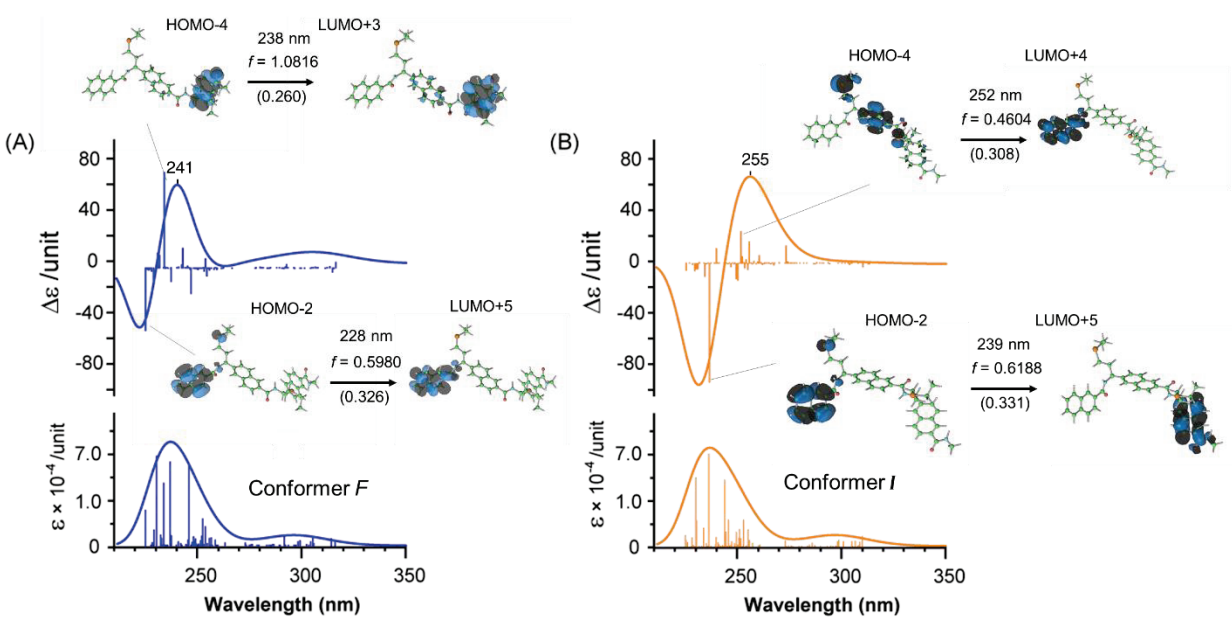

Figure 4-S7. The calculated predominant transitions for the absorption bands (wavelength, nm), oscillator strength (*f*) and the molecular orbitals (MOs) for (A) Conformer F and (B) Conformer I. The coefficients indicating their contributions to the excitation are shown in the parentheses under arrows.

Structual Optimization of Oligomer (*n* = 3)

Oligomer (*n* = 3) was made from oligomer (*n* = 1, conformer B) and oligomer (*n* = 2, conformers F and I) by the same manner. Geometry optimizations were performed in THF, then calculated the CD and UV spectra of conformers by TD-DFT calculations.

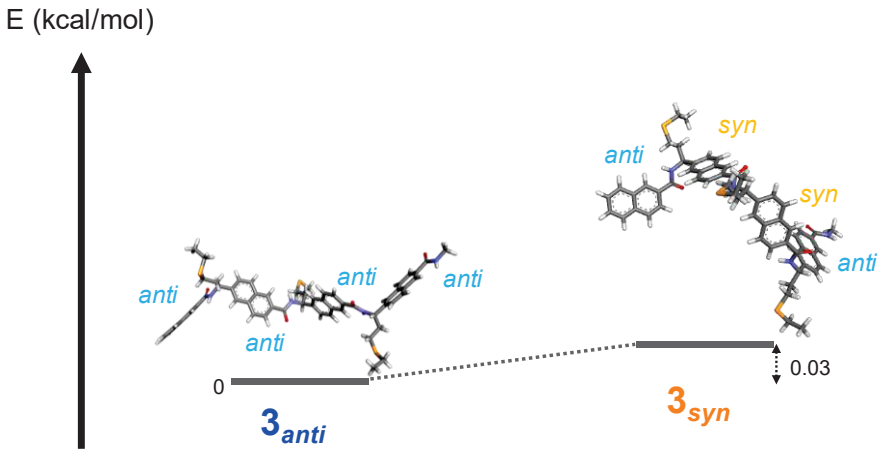

Figure 4-S8. Energy diagram of rotational isomer in oligomer (*n* = 3) obtained by DFT calculation in THF.

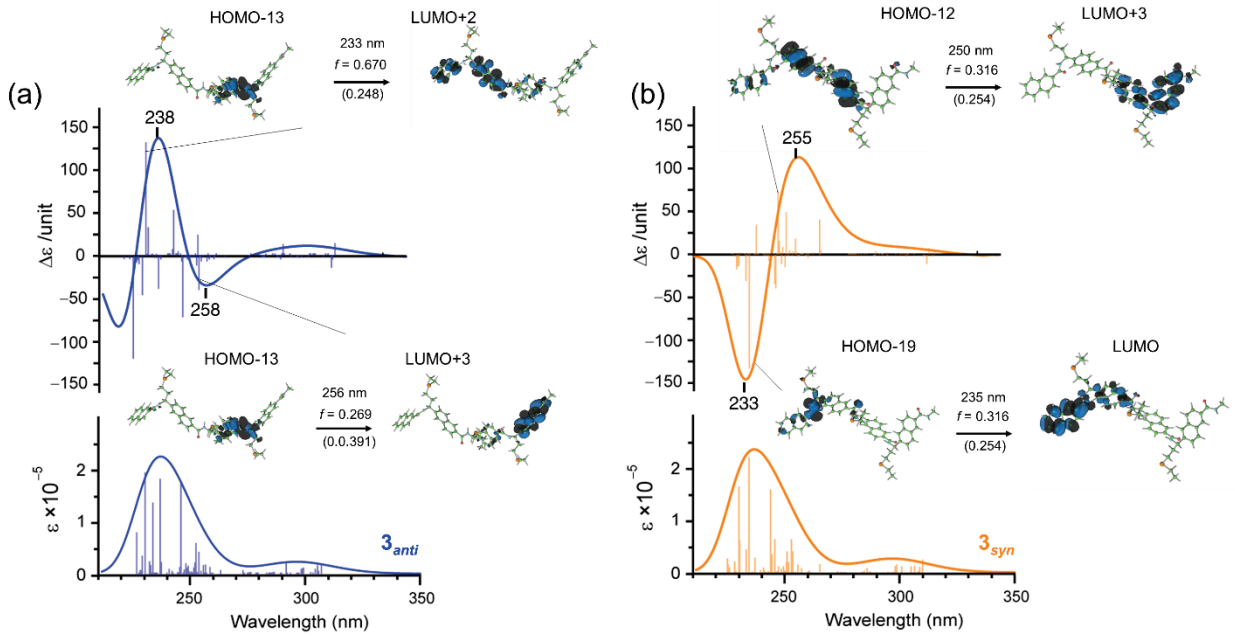

Figure 4-S9. The calculated predominant transitions for the absorption bands (wavelength, nm), oscillator strength (*f*) and the molecular orbitals (MOs) for (A) $\mathbf{3}_{anti}$, and (B) $\mathbf{3}_{syn}$. The coefficients indicating their contributions to the excitation are shown in parentheses under arrows.

Reference

(1) (a) Gellman, S. H. *Acc. Chem. Res.* **1998**, *31*, 173. (b) Hill, D. J.; Mio, M. J.; Prince, R. B.; Hughes, T. S.; Moore, J. S. *Chem. Rev.* **2001**, *101*, 3893.

(2) (a) Nelson, J. C.; Saven, J. G.; Moore, J. S.; Wolynes, P. G. *Science* **1997**, *277*, 1793. (b) Berl, V.; Huc, I.; Khoury, R. G.; Krische, M. J.; Lehn, J. M. *Nature* **2000**, *407*, 720. (c) Cheng, R. P.; Gellman, S. H.; DeGrado, W. F. *Chem. Rev.* **2001**, *101*, 3219.

(3) (a) Nowick, J. S.; Chung, D. M.; Maitra, K.; Maitra, S.; Stigers, K. D.; Sun, Y. *J. Am. Chem. Soc.* **2000**, *122*, 7654. (b) Wyrembak, P. N.; Hamilton, A. D. *J. Am. Chem. Soc.* **2009**, *131*, 4566. (c) Sebaoun, L.; Maurizot, V.; Granier, T.; Kauffmann, B.; Huc, I. *J. Am. Chem. Soc.* **2014**, *136*, 2168.

(4) (a) Stadler, A. M.; Kyritsakas, N.; Lehn, J. M. *Chem. Commun.* **2004**, 2024. (b) Dolain, C.; Jiang, H.; Léger, J. M.; Guionneau, P.; Huc, I. *J. Am. Chem. Soc.* **2005**, *127*, 12943. (c) Stadler, A. M.; Kyritsakas, N.; Graff, R.; Lehn, J. M. *Chem. Eur. J.* **2006**, *12*, 4503.

(5) (a) Gong, B. *Chem. Eur. J.* **2001**, *7*, 4336. (b) Jiang, H.; Léger, J. M.; Huc, I. *J. Am. Chem. Soc.* **2003**, *125*, 3448. (c) Huc, I. *Eur. J. Org. Chem.* **2004**, *2004*, 17. (d) Zhang, D. W.; Zhao, X.; Hou, J. L.; Li, Z. T. *Chem. Rev.* **2012**, *112*, 5271. (e) Ferrand, Y.; Huc, I. *Acc. Chem. Res.* **2018**, *51*, 970.

(6) (a) Dolain, C.; Maurizot, V.; Huc, I. *Angew. Chem., Int. Ed.* **2003**, *42*, 2738. (b) Kolomiets, E.; Berl, V.; Odriozola, I.; Stadler, A. M.; Kyritsakas, N.; Lehn, J. M. *Chem. Commun.* **2003**, 2868.

(7) (a) Green, M. M.; Reidy, M. P.; Johnson, R. D.; Darling, G.; O'Leary, D. J.; Willson, G. *J. Am. Chem. Soc.* **1989**, *111*, 6452. (b) Green, M. M.; Peterson, N. C.; Sato, T.; Teramoto, A.; Cook, R.; Lifson, S. *Science* **1995**, *268*, 1860. (c) Green, M. M.; Park, J. W.; Sato, T.; Teramoto, A.; Lifson, S.; Selinger, R. L. B.; Selinger, J. V. *Angew. Chem., Int. Ed.* **1999**, *38*, 3138.

(8) (a) Cornelissen, J. J. L. M.; Rowan, A. E.; Nolte, R. J. M.; Sommerdijk, N. A. J. M. *Chem. Rev.* **2001**, *101*, 4039. (b) Nakano, T.; Okamoto, Y. *Chem. Rev.* **2001**, *101*, 4013. (c) Yashima, E.; Maeda, K.; Iida, H.; Furusho, Y.; Nagai, K. *Chem. Rev.* **2009**, *109*, 6102. (d) Yashima, E.; Ousaka, N.; Taura, D.; Shimomura, K.; Ikai, T.; Maeda, K. *Chem. Rev.* **2016**, *116*, 13752.

(9) Gu, H.; Nakamura, Y.; Sato, T.; Teramoto, A.; Green, M. M.; Andreola, C.; Peterson, N. C.; Lifson, S. *Macromolecules* **1995**, *28*, 1016.

(10) (a) Yashima, E.; Maeda, K.; Sato, O. *J. Am. Chem. Soc.* **2001**, *123*, 8159. (b) Tang, H. Z.; Novak, B. M.; He, J.; Polavarapu, P. L. *Angew. Chem., Int. Ed.* **2005**, *44*, 7298. (c) Yoshida, Y.; Mawatari, Y.; Motoshige, A.; Motoshige, R.; Hiraoki, T.; Wagner, M.; Müllen, K.; Tabata, M. *J. Am. Chem. Soc.* **2013**, *135*, 4110. (d) Rodríguez, R.; Quiñoá, E.; Riguera, R.; Freire, F. *J. Am. Chem. Soc.* **2016**, *138*, 9620. (e) Kanbayashi, N.; Tokuhara, S.; Sekine, T.; Kataoka, Y.; Okamura, T.; Onitsuka, K. *J. Polym. Sci., Part A: Polym. Chem.* **2018**, *56*, 496. (f) Siriwardane, D. A.; Kulikov, O.; Batchelor, B. L.; Liu, Z.; Cue, J. M.; Nielsen, S. O.; Novak, B. M. *Macromolecules* **2018**, *51*, 3722. (g) Rodríguez, R.; Quiñoá, E.; Riguera, R.; Freire, F. *Small* **2019**, *15*, 1805413.

(11) (a) Okamoto, Y.; Nakano, T.; Ono, E.; Hatada, K. *Chem. Lett.* **1991**, *20*, 525. (b) Green, M. M.; Khatri, C.; Peterson, N. C. *J. Am. Chem. Soc.* **1993**, *115*, 4941. (c) Li, J.; Schuster, G. B.; Cheon, K. S.; Green, M. M.; Selinger, J. V. *J. Am. Chem. Soc.* **2000**, *122*, 2603. (d) Fujiki, M.; Koe, J. R.; Motonaga, M.; Nakashima, H.;

Terao, K.; Teramoto, A. *J. Am. Chem. Soc.* **2001**, *123*, 6253. (e) Sanda, F.; Terada, K.; Masuda, T. *Macromolecules* **2005**, *38*, 8149. (f) Pijper, D.; Feringa, B. L. *Angew. Chem., Int. Ed.* **2007**, *46*, 3693. (g) Yamada, T.; Nagata, Y.; Suginome, M. *Chem. Commun.* **2010**, *46*, 4914. (h) Freire, F.; Seco, J. M.; Quiñoá, E.; Riguera, R. *Angew. Chem., Int. Ed.* **2011**, *50*, 11692. (i) Nagata, Y.; Yamada, T.; Adachi, T.; Akai, Y.; Yamamoto, T.; Suginome, M. *J. Am. Chem. Soc.* **2013**, *135*, 10104. (j) Thodupunuri, P.; Katukuri, S.; Ramakrishna, K. V. S.; Sharma, G. V. M.; Kunwar, A. C.; Sarma, A. V. S.; Hofmann, H. J. *J. Org. Chem.* **2017**, *82*, 2018.

(12) (a) Kanbayashi, N.; Okamura, T.; Onitsuka, K. *Macromolecules* **2014**, *47*, 4178. (b) Kanbayashi, N.; Okamura, T.; Onitsuka, K. *Macromolecules* **2015**, *48*, 8437.

(13) (a) Ishido, Y.; Kanbayashi, N.; Okamura, T.; Onitsuka, K. *Macromolecules* **2017**, *50*, 5301. (b) Kanbayashi, N.; Miyamoto, S.; Ishido, Y.; Okamura, T.; Onitsuka, K. *Polym. Chem.* **2017**, *8*, 985.

(14) Ishido, Y.; Kanbayashi, N.; Okamura, T.-a.; Onitsuka, K. *ACS Macro Lett.* **2019**, *8*, 694.

(15) Frisch, M. J.; Trucks, G. W.; Schlegel, H. B.; Scuseria, G. E.; Robb, M. A.; Cheeseman, J. R.; Scalmani, G.; Barone, V.; Mennucci, B.; Petersson, G. A.; Nakatsuji, H.; Caricato, M.; Li, X.; Hratchian, H. P.; Izmaylov, A. F.; Bloino, J.; Zheng, G.; Sonnenberg, J. L.; Hada, M.; Ehara, M.; Toyota, K.; Fukuda, R.; Hasegawa, J.; Ishida, M.; Nakajima, T.; Honda, Y.; Kitao, O.; Nakai, H.; Vreven, T.; J. A, M.; Peralta, J. E.; Ogliaro, F.; Bearpark, M.; Heyd, J. J.; Brothers, E.; Kudin, K. N.; Staroverov, V. N.; Keith, T.; Kobayashi, R.; Normand, J.; Raghavachari, K.; Rendell, A.; Burant, J. C.; Iyengar, S. S.; Tomasi, J.; Cossi, M.; Rega, N.; Millam, J. M.; Klene, M.; Knox, J. E.; Cross, J. B.; Bakken, V.; Adamo, C.; Jaramillo, J.; Gomperts, R.; Stratmann, R. E.; Yazyev, O.; Austin, A. J.; Cammi, R.; Pomelli, C.; Ochterski, J. W.; Martin, R. L.; Morokuma, K.; Zakrzewski, V. G.; Voth, G. A.; Salvador, P.; Dannenberg, J. J.; Dapprich, S.; Daniels, A. D.; Farkas, O.; Foresman, J. B.; Ortiz, J. V.; Cioslowski, J.; Fox, D. J. *Gaussian 09*, 2010.

(16) Kudo, M.; Maurizot, V.; Kauffmann, B.; Tanatani, A.; Huc, I. *J. Am. Chem. Soc.* **2013**, *135*, 9628.

(17) Habeck, M.; Rieping, W.; Nilges, M. *J. Magn. Reson.* **2005**, *177*, 160.

(18) Nagata, Y.; Nishikawa, T.; Suginome, M.; Sato, S.; Sugiyama, M.; Porcar, L.; Martel, A.; Inoue, R.; Sato, N. *J. Am. Chem. Soc.* **2018**, *140*, 2722.

(19) (a) Dodo, N.; Matsushima, Y.; Uno, M.; Onitsuka, K.; Takahashi, S. *Dalton Trans.* **2000**, 35. (b) Matsushima, Y.; Komatsuzaki, N.; Ajioka, Y.; Yamamoto, M.; Kikuchi, H.; Takata, Y.; Dodo, N.; Onitsuka, K.; Uno, M.; Takahashi, S. *Bull. Chem. Soc. Jpn.* **2001**, *74*, 527. (c) Kanbayashi, N.; Onitsuka, K. *Angew. Chem. Int. Ed.* **2011**, *50*, 5197.

(20) Kanbayashi, N.; Okamura, T.-a.; Onitsuka, K. *Macromolecules* **2014**, *47*, 4178.

(21) Altomare, A.; Burla, M. C.; Camalli, M.; Cascarano, M.; Giacovazzo, C.; Guagliardi, A.; Polidori, G. *J. Appl. Crystallogr.* **1994**, *27*, 435.

(22) Sheldrick, G. M. *Acta Crystallogr., Sect. A: Found. Crystallogr.* **2008**, *64*, 112.

Chapter 5

Relationship Between Backbone, Side Chain and Well-defined Global Conformation of Arylopeptide and Dynamic Switch of the Helix to Helix Transition

5-1: Introduction

Proteins form higher-order structures according to their amino acid sequences and their diverse structures are linked to functions. Although most native structure of proteins turn into random coils depending on various stimuli, some proteins (polypeptide chains) form two well-defined structures, which is greatly related to diseases. For instance, prion protein (PrP^{C}) adopts a helix-rich structure in native and it is converted to sheet-rich structure (PrP^{Sc}) (Figure 5-1). The trigger of this transition is unclear, but it is very important to investigate such a transition that does not obey Amfinsen's dogma.[1]

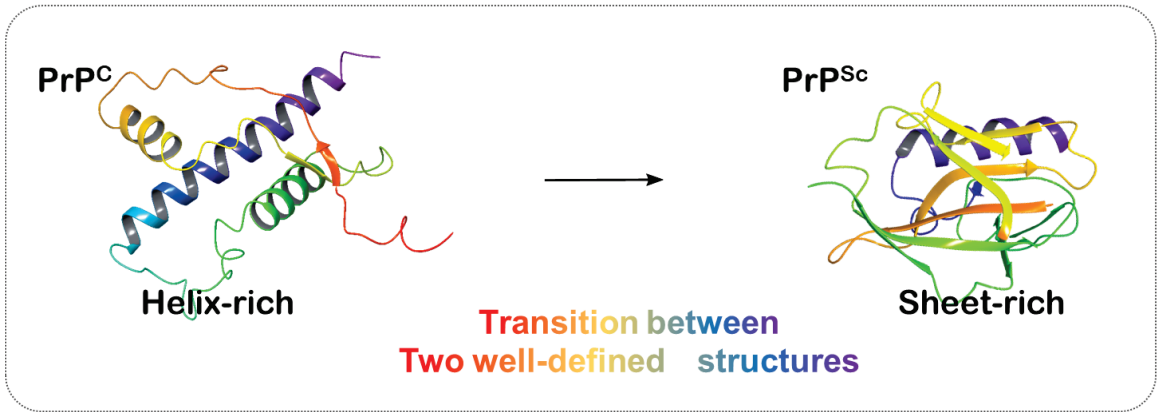

Figure 5-1. Structure of prion protein PrP^{c} and PrP^{Sc}

In Chapter 4, the author described that the arylopeptide containing 2,6-naphthylene spacer forms two well-defined structures—(*P*)-3_1- and (*M*)-4_1-helices—depending on the side chains.[2] However, it is still not possible to predict the folding structure based on the polymer structure and media properties. Therefore, there is great interest in the factor that determines the structure and properties of arylopeptide. Based on the results in Chapter 4, this chapter mainly describes the important factors that determine the dynamics and the folding of the arylopeptide, including main chain, side chain, solvents, and affinity, etc (Figure 5-2). In particular, the

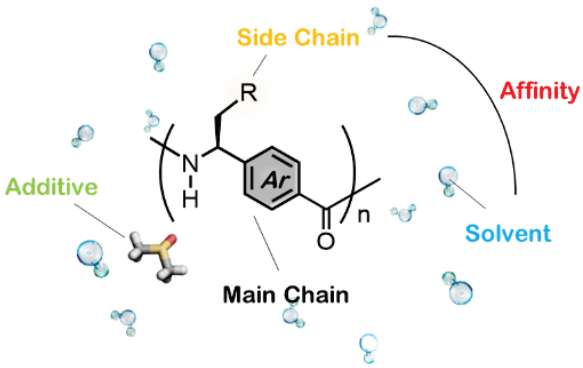

Figure 5-2. A lot of factor of arylopeptide for tuning its structural property.

principle for 4_1- and 3_1-helices of 2,6-naphthylene arylopeptide were revealed. Following the principle, two well-defined structures were formed from the completely the same primary structure using effectively solvents, temperatures, and additives.

5-2: Results and Discussion

Backbone Effects

The results in Chapter 4 suggest that the introduction of an asymmetric spacer into the main chain induces bimodal helix formation. To study the effect of symmetry for helix in detail, arylopeptides having a 1,1′-biphenyl spacer on the main chain were synthesized as a symmetric spacer (**poly-3**). Compared to the CD spectra of **poly-1** (*p*-phenylene spacer) and **poly-2** (2,6-naphthylene spacer) already identified in Chapters 2 and 4 (Figure 5-3a-b), the CD spectra of **poly-3** did not show side chain-dependence (Figure 5-3c).

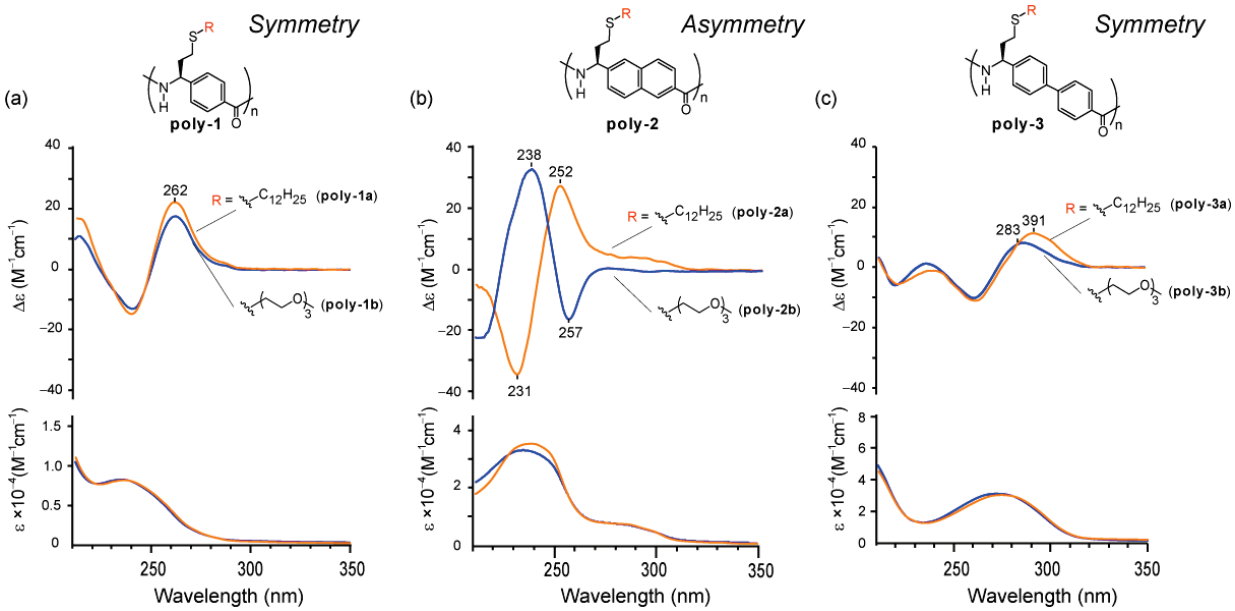

Figure 5-3. CD and UV spectra (in THF, 25 ºC) of (a) **poly-1**, (b) **poly-2** and (c) **poly-3**. Concentration: [**poly-1a**] = 0.32 mM, [**poly-1b**] = 0.30 mM, [**poly-2a**] = 0.40 mM, [**poly-2b**] = 0.39 mM, [**poly-3a**] = 0.38 mM, and [**poly-3b**] = 0.36 mM.

If a symmetric spacer was used (e.g. **poly-1**), there were two folding structures by the successive formation of *zig-zag* and *turn* structure as discussed in Chapter 2. The reason why symmetric substituents form a one-side successive formation of conformer is due to the stability of the whole polymer based on the high molecular-weight. Importantly, the *turn* and the *zig-zag* conformers of **poly-1** have the most stable local conformer is

reflected in the X-ray structure due to the rotation of the symmetric *p*-phenylene spacer affords the local structure equivalent (Figure 5-4). *Turn* conformer is slightly more stable than *zig-zag* conformer (0.21 kJ/mol by DFT), the energy gap will become significant by a typical cooperative effect. In the case of **poly-2**, the local structure containing *anti* is reflected in the crystal structure, but that of *syn*, is the second-most stable local structure (0.33 kJ/mol) supported by DFT (Figure 5b). As a result, the enery gap between *zig-zag* and *turn* structures became very small (0.019 kJ/mol). For this reason, the amplification of energy difference due to polymer does not occur effectively, resulting in a drastic change by some incidental effects.

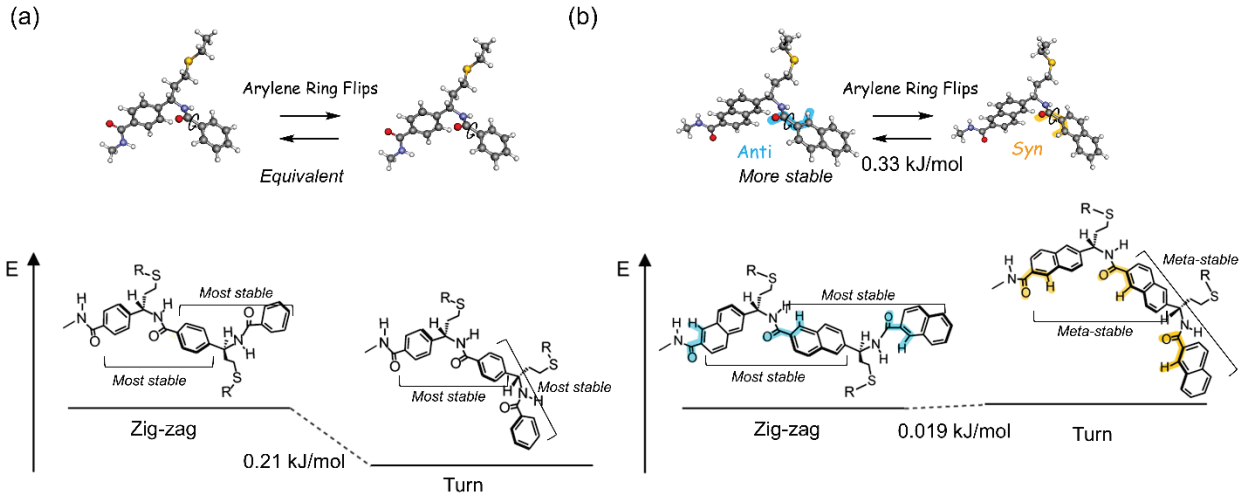

Figure 5-4. Schematic chart of conformational pattern and energy diagram of (a) *p*-phenylene spacer and (b) 2,6-naphthylene spacer. Illustration of pale blue block shows most stable local conformer reflected the crystal structure and orange block shows second-stable local conformer.

Side Chain and Solvent Effects for Folding

As described in Chapter 4, **poly-2** containing dodecyl or oligoether group forms a 4_1- or 3_1-helix respectively. To reveal the folding selectivity of the helices, the relationship between the side chain and the 4_1-helix was first examined. **Poly-2** bearing several type of alkyl chain group were synthesized, and the CD spectra were measured in THF (Figure 5-5). The CD intensity of 4_1-helix decreased obviously depending on the length of alkyl chain, which suspects the importance of hydrophobic alkyl group. In the case of **poly-2c** (R = $–C_6H_{13}$), the CD signal due to 4_1-helix clearly decreased compered to that of **poly-2a**. On the other hand, the CD intensity of **poly-2d** (R = $–CH_2CHC_{12}H_{25}(C_{12}H_{25})$) increased compared to that of **poly-2a**. The results imply that the CD measurements in non-polar solvent will induce more biased formation of 4_1-helix. However, the CD spectra of **poly-2c** in a THF/*n*-hexane mixed solvent exhibited the Cotton effect originated from 3_1-helix even though the intensity is

slightly weaker than that of **poly-2b** in THF (Figure 5-5b). This helix-to-helix transition was reversible. Addition of THF recovered the 4_1-helix again. These results suggest that the affinity between the side chain and solvent is more important than the length of alkyl chain on the side chain to select the 4_1- or 3_1-helix. Alkyl side chain and *n*-hexane as solvent probably have relatively high affinity,and the high affinity in side chain and solvenet will induce 3_1-helix

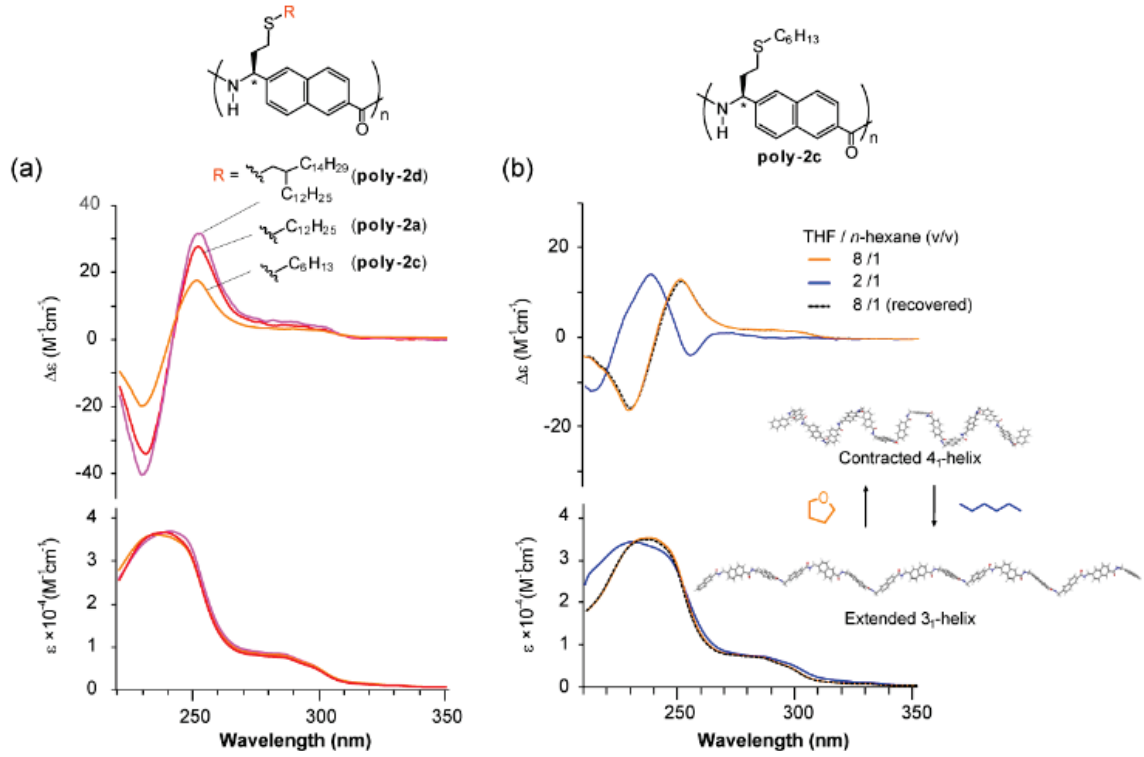

Figure 5-5. CD and UV measurement. (a) **poly-2a** (red curve), **poly-2c** (orange curve) and **poly-2d** (black curve) in THF at 298 K. (b) **poly-2c** in THF/ *n*-hexane = 8/1 (orange curve), 2/1 (blue curve) and re-diluted 8/1 (dash curve) (v/v%) at 298 K. Concentration/unit: (a) [**poly-2a**] = 0.32 mM, [**poly-2c**] = 0.33 mM, [**poly-2d**] = 0.36 mM, and (b) [**poly-2c**] = 0.40 to 0.04 mM.

Arylopeptides with alkyl side chains are soluble in only halogenated solvents and THF, but poly-2b exhibit s a good solubility in various solvents. Therefore, the relationship between the side chains and solvents, and formation selectivity was investigated by **poly-2b**. The Cotton effects of **poly-2b** were drastically changed by the solvents, especially ethanol (Figure 5-6a). The shapes of the Cotton effects can be reproduced by the linear sum of the Cotton effects of **poly-2a** and **poly-2b** in THF, the franctions of **poly-2a**/ **poly-2b** = $4_1/3_1$-helix was estimated to be 55/45 in ethanol (the broken curve in Figure 5-6a). To quantify the affinity between the solvent and side chain, the plot of CD intensity at 238 nm against the Hildebrand parameter δ (SP value) was examined (Figure 5-6b). The Hildebrand parameter (δ) provides a numerical estimation of the affinity between solvents and

solutes.[3] When the δ value of the oligoether group on **poly-2b** was estimated to be that of 1,2-dimethoxyethane (δ = 19.4 $MPa^{1/2}$), the big difference of the δ values between the side chain and solvent caused the increase in the fraction of 4_1-helix. These results support that the high affinity between the side chain and the solvent induce a 3_1-helix as descrived in Figure 5-5. Increasing alkyl groups on the side chain promotes the formation of 4_1-helix because of the low affinity with THF.

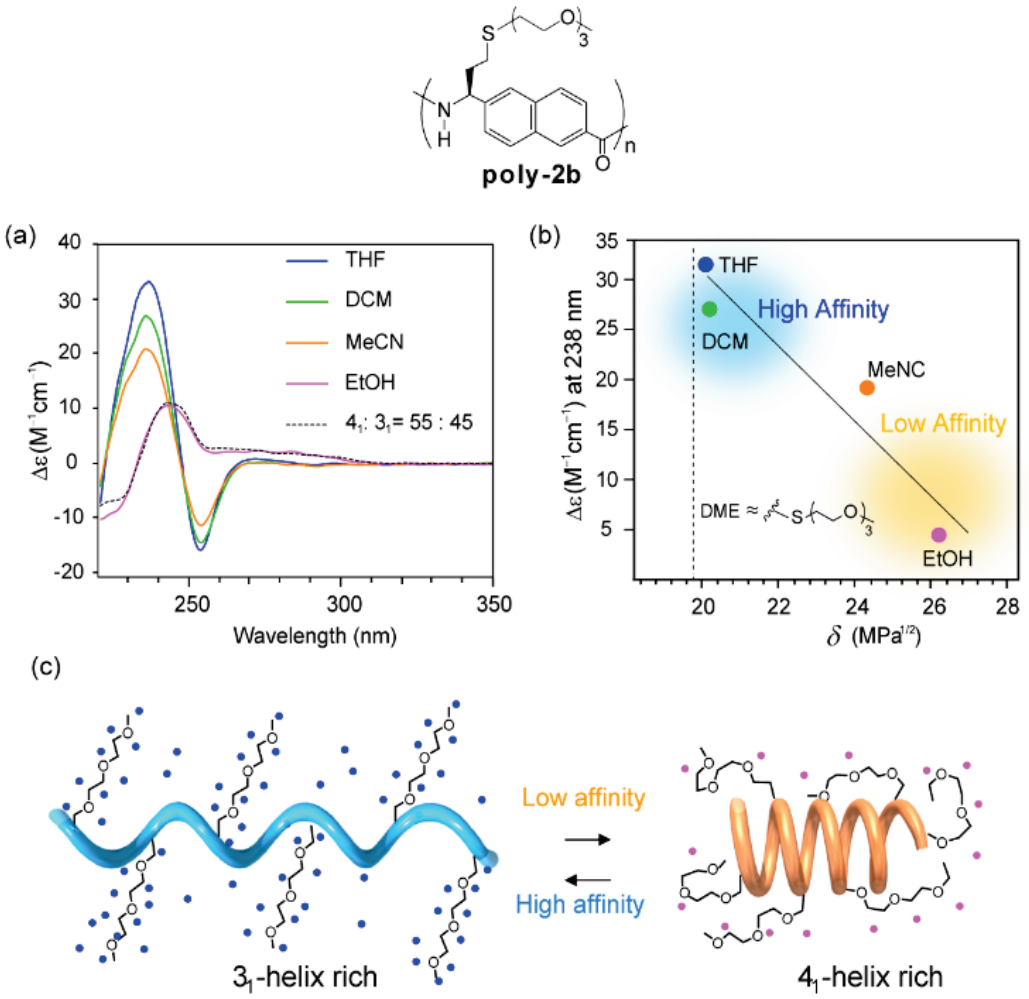

Figure 5-6. (a) CD and UV spectra of **poly-2b** in THF(blue curve), DCM (green curve), acetonitrile (orange curve), ethanol (pink curve) and fitting curve (dash curve) at 298 K. (b) Plot of the CD intensity (**poly-2b**) against SP values in THF(blue dot), DCM (green dot), acetonitrile (orange dot) and ethanol (pink dot) at 298 K. (c) Schematic diagrams of formation selectivity of **poly-2b** against solvents. Concentration/unit: (a) [**poly-2b**] = 0.32 to 0.39 mM.

The CD intensity of **poly-2c** in THF/*n*-hexane is smaller than that of **poly-2b** in THF (Figure 5-5b). Alkyl group and hexane as a solvent has a good affinity, but the force is not enough to give the perfect 3_1-helix. Addition of *n*-hexane to **poly-2a** (R = $C_{12}H_{25}$) and **poly-2d** (R = $CH_2CHC_{12}H_{25}(C_{12}H_{25})$) showed no change in CD signal (Figure 5-7a). This reason is that the long alkyl chains intramolecularly interact each other with polymer chain covering the surface. In the case of **poly-2a**, it is not influenced by *n*-hexane as illustration in interaction Figure 5-7b because of weak alkyl-alkyl interaction not enough to change the structural pathway.[4]

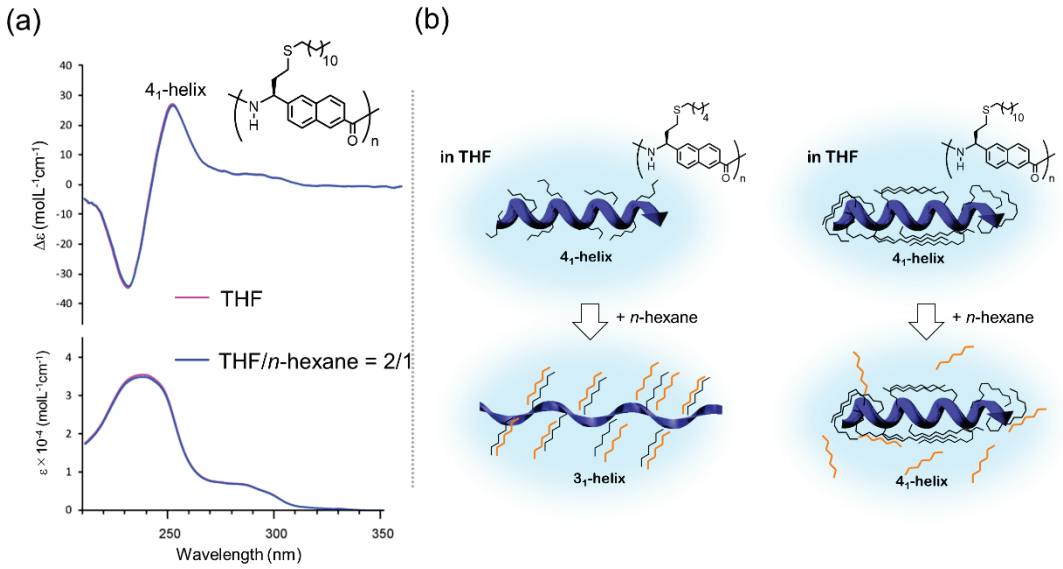

Figure 5-7. (a) CD and UV spectroscopy of **poly-2a** in THF and THF/hexane = 2/1 at 298 K. (b) Schematic diagram of solvation to arylopeptide.

Dynamical Switching of the Helix to Helix Transition for Application

Thermal Stimulation

In the case of artificial polymer, the design of dynamical molecular switches showing bistability in response to an external stimuli, such as solvent,[5] pH,[6] ions,[7] and temperature,[8] has been a growing area of interest. In this section, oligoether (*n* = 9) group as a side chain was introduced to arylopeptide (**poly-2e**, Figure 5-8) and structural transition were attempted. Long-chain oligo(ethylene glycol) group has good affinity for water, but the substituent dehydrates at high temperatures, resulting in a decrease in the affinity for water. Such compounds frequency produce thermo-responsible polymer showing lower critical solution temperature (LCST) behavior.[9] Therefore, the affinity between the side chain and the solvent can be adjusted by the temperature, and the folding behavior would be controllable. **Poly-2e** is solluble in water, and the CD spectrum showed the Cotton effect of

3_1-helix. The CD spectrum in THF was an intermediate feature containing 4_1-helix, caused by low-affinity between the side chain and THF. Upon heating this aqueous solution, the CD intensity decreased, and a new absorption band appeared around 255 nm (Figure 5-8b). The spectra of at high temperature resemble that in THF (Figure 5-8a), indicating the formation of 4_1-helix by dehydration of the oligoether (n = 9) group on the side chain due to a decrement in the affinity of the side chain and the aqueous solvent. When the aqueous solution was heated to about 60 °C, it became turbid showing LCST behavior (Figure 5-9a). In addition, the 3_1-helix-4_1-helix-aggregate transition including LCST was a reversible pathway, it was able to repeat many times (Figure 5-9b). Thus, **poly-2e** is a unique thermoresponsive polymer that can adopt well-defined two structures; 3_1- and 4_1-helices. These results proved the author's hypothesis that the high affinity between the side chain and the solvent is important to induce 3_1-helix.

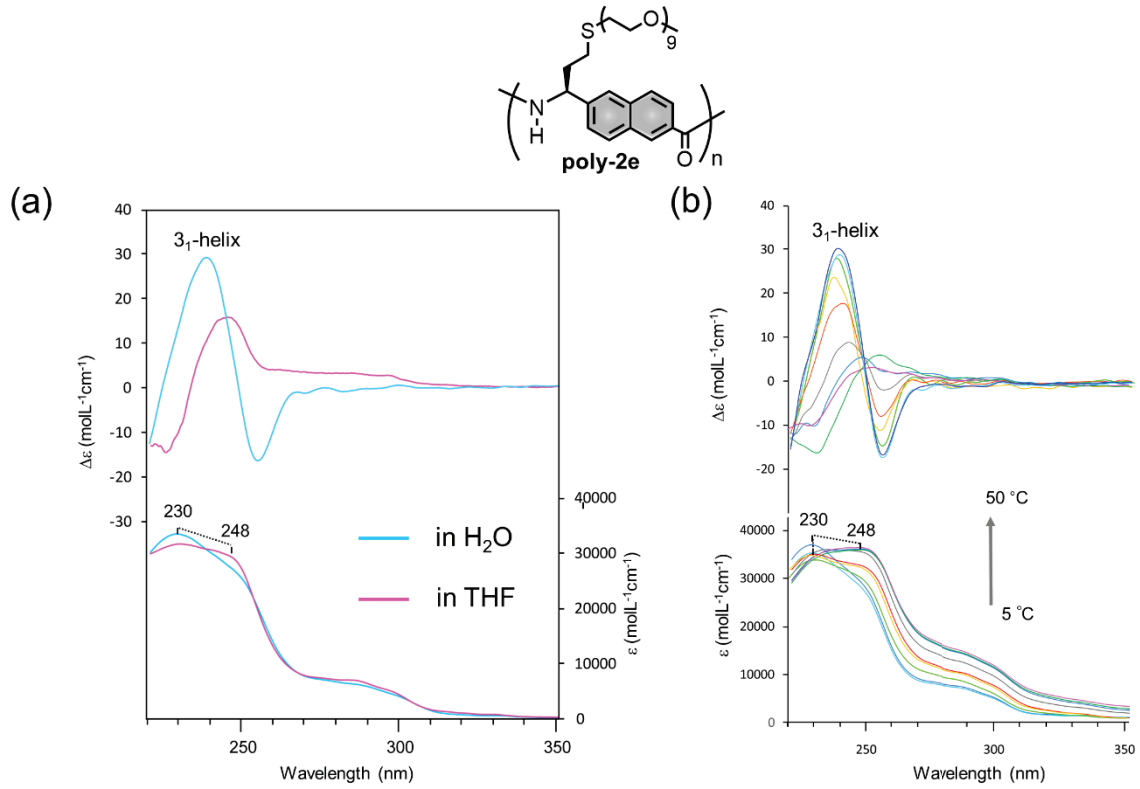

Figure 5-8. (a) CD/UV spectra of **poly-2e** in THF (pink curve) and H_2O (pale blue curve) at 298 K. (b) VT-CD/UV spectra of **poly-2e** in H_2O at various temperature. Concentration: (a) [**poly-3e**] = 0.32 mM.

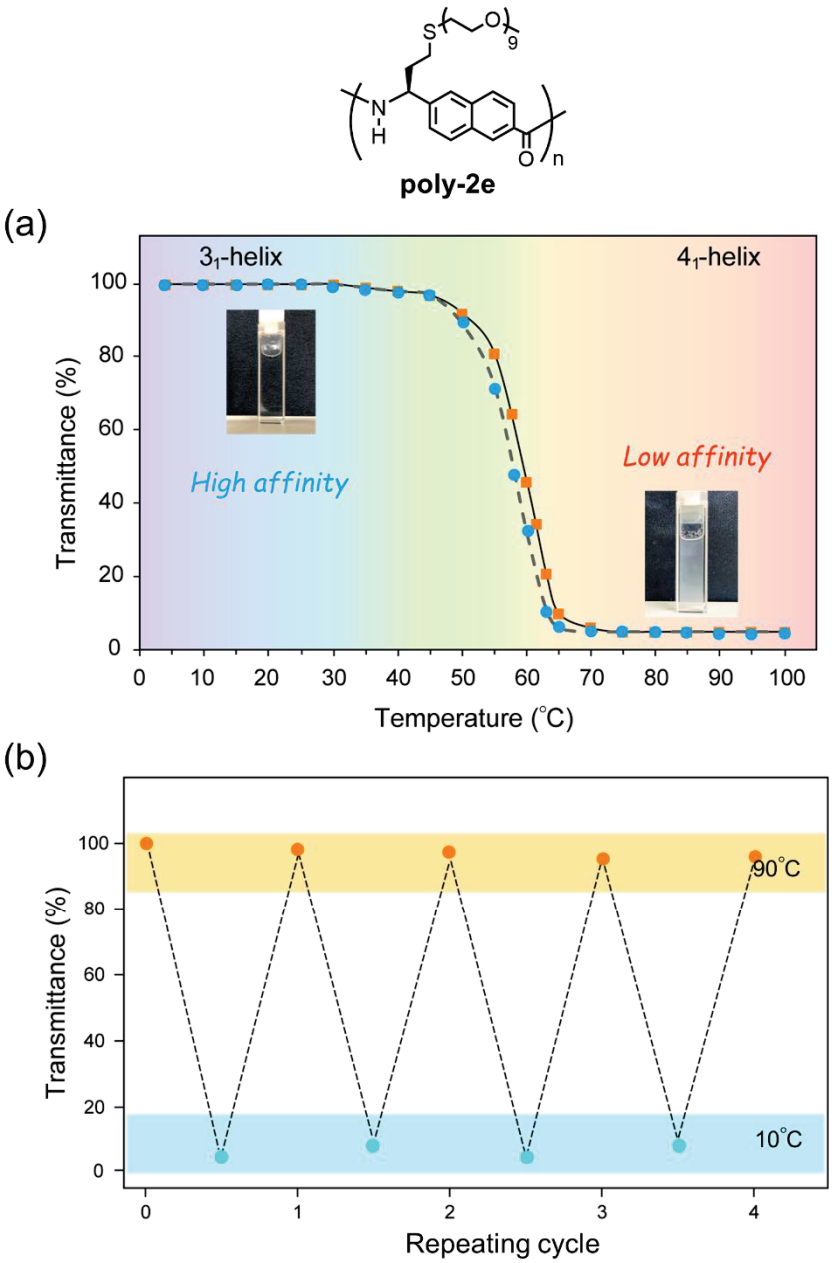

Figure 5-9. (a) Temperature-dependence changes in the transmittance of **poly-2e** [3mg/mL] at 500 nm (black line: heating process, black dash line: cooling process) (b) Reversible change in the transmittance at 10 and 90 °C. (c) Photographs for temperature change.

Two Well-defined Structure from a Primary Structure (Side Chain-Hybrid Arylopeptide)

As described above, dodecyl group strongly supports the formation of 4_1-helix in THF, while oligo(ethylene glycol) group supports the formation of 3_1-helix because of their affinities (Figure 5-10). If a random polymer containing both of these side chains is synthesized, the side chain effects (high and low affinities) may compete with each other.

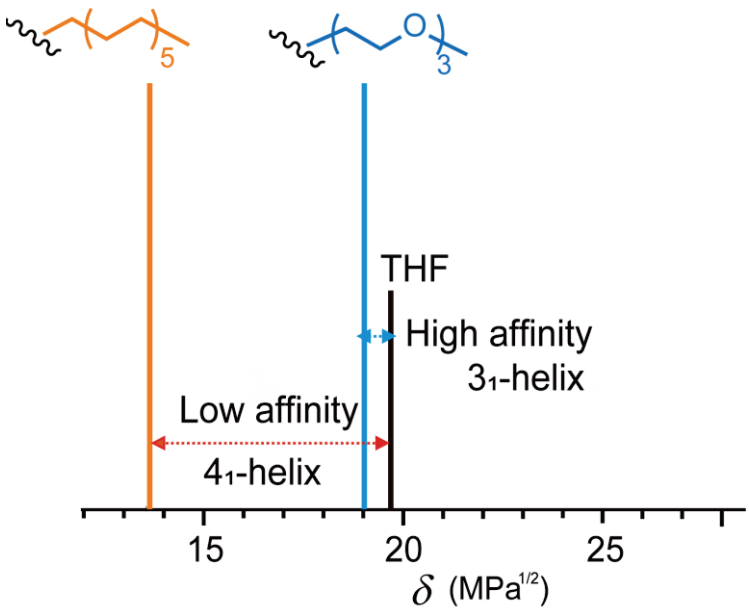

Figure 5-10. Relationship between helical structure and affinities between solvents and side chains. δ ; Hildebrand parameter.

A random copolymer was synthesized according to a similar method to that in Chapter 4. NMR analysis revealed that roughly equal amounts of dodecyl/oligo(ethylene glycol) groups = 53/47 was introduced in polymer (Scheme 5-1).

Scheme 5-1. Synthetic Pathway of Side Chain-Hybrid Arylopeptide

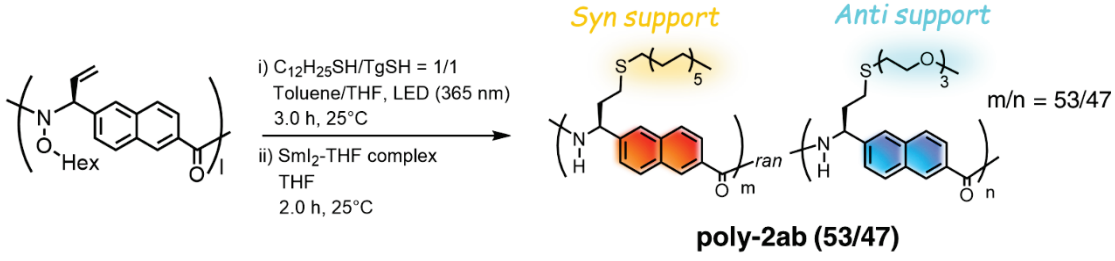

The CD spectrum of **poly-2ab(53/47)** in THF was not consistent with the Cotton effect of 4_1 and 3_1-helices (Figure 5-11b). The shape of Cotton effect can be expressed by the linear combination of the Cotton effects of the 4_1- and 3_1- helices, and the ratio of 4_1 to 3_1-helices was 55/45 (Figure 5-11b, dash line). This result shows that high and low affinities competed each other and resulted in an intermediate state. Therefore, a certain of condition may be used to bias this delicate energy balance to a one-sided structure.

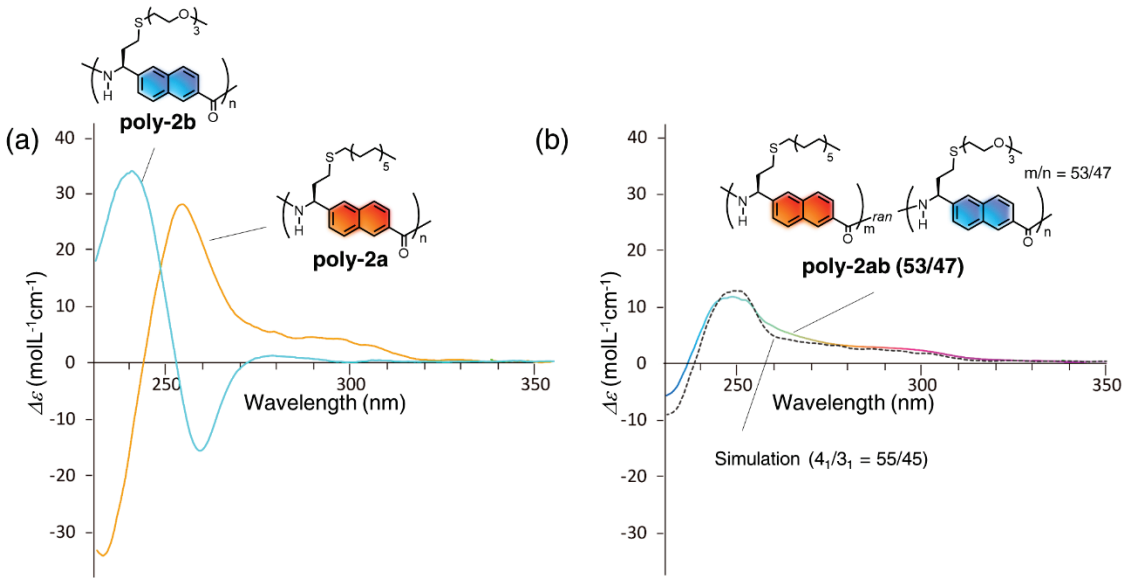

Figure 5-11. CD spectra of (a) **poly-2a**, **poly-2b** and (b) **poly-2ab(53/47)** in THF at 25 °C

The conformational changes by adding solvents were investigated. The value of δ of *n*-hexane is 14.9, which exist in the region between those of side chains (Figure 5-12b). This means that *n*-hexane has a relatively high affinity with both type of side chains. Interestingly, the CD spectrum of **poly-2ab** (53/47) changed dramatically to that of 3_1-helix (Figure 5-12a, blue curve). The CD intensity has reached a level comparable to that of the homopolymer **poly-2b** in THF (Figure 5-11a). Therefore, the oligo (ethylene glycol) side chains in the polymer chain induce the complete 3_1-helical formation because homopolymer **poly-2c** in THF/*n*-hexane did not adopt the sufficient formation of 3_1-helix. Next, when ethanol was added to the intermediate state, the CD spectrum changed to the shape of 4_1-helix (orange curve in Figure 5-12a). The random copolymer **poly-2ab** (53/47) reselect the secondary structure (4_1- and 3_1-helices) in solution responsive to the properties of medium. The value of δ of ethanol is 26.5, which is very different from the value of each side chain (Figure 5-12b), indicative of the low affinity between the side chain and the solvent. When the CD spectrum of homopolymer **poly-2b** was measured in ethanol, the fraction of 3_1-helix decreased and an intermediate state CD spectrum was observed but it was not

biased toward the 4_1-helix (Figure 5-6a). In other words, a complete 4_1-helix was formed by a cooperative effect of the dodecyl groups. The 4_1-helix was able to return to the intermediate state by adding THF.

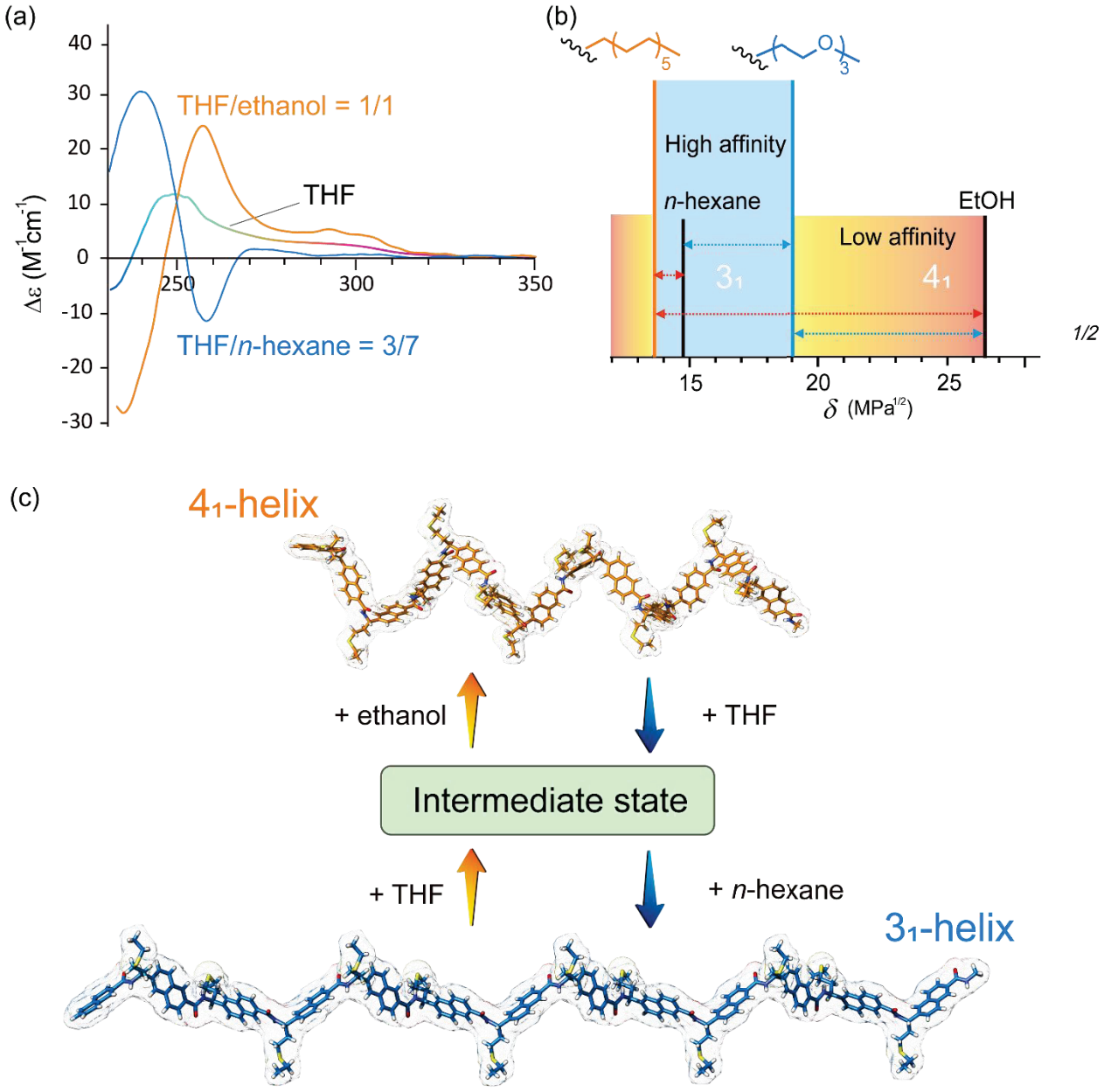

Figure 5-12. (a) Solvent effect of **poly-2ab(53/47)**. (b) The relationship between the side chains and solvents. (c) The Helical transitions with solvents. Side chain are replaced by $–CH_2CH_3$ for clarity.

Irreversible Structural Transitions by Additives

The further development of transition system induced by slight conditions change was aimed. Several experiments revealed that a small amount of dimethylsulfoxide (DMSO) gave a strong impact to the structure of **poly-2**. The results show that addition of DMSO into a solution of **poly-2b** in THFcauses a drastic change in the Cotton effect. Upon increasing DMSO concentration (0 to 700 equiv/unit, where 140 equiv corresponds to 1 vol%), the Cotton effect due to the 3_1-helix changes suddenly to that due to the 4_1-helix (Figure 5-13a). This result suggests an entirely geometrical conversion from the (*anti*, *anti*, *anti*, ...) conformer to the (*syn*, *syn*, *syn*, ...) conformer and the generation of a more contracted helix (Figure 5-13d). This 4_1-helix did not return to 3_1-helix when diluted with a large excess of THF. The CD spectrum shown in Figure 5-13a has a clear isodichroic point and can be represented by a linear combination of the Cotton effect of **poly-2a** and **poly-2b**, which indicates that only two types of chiral architecture exist (4_1- and 3_1 helix). Based on this result, the population of the two geometrical isomers during the titration was estimated (Figure 5-13c). When using DMSO, the population of the *syn* isomer increased nonlinearly as a function of DMSO concentration with a corresponding decrease in

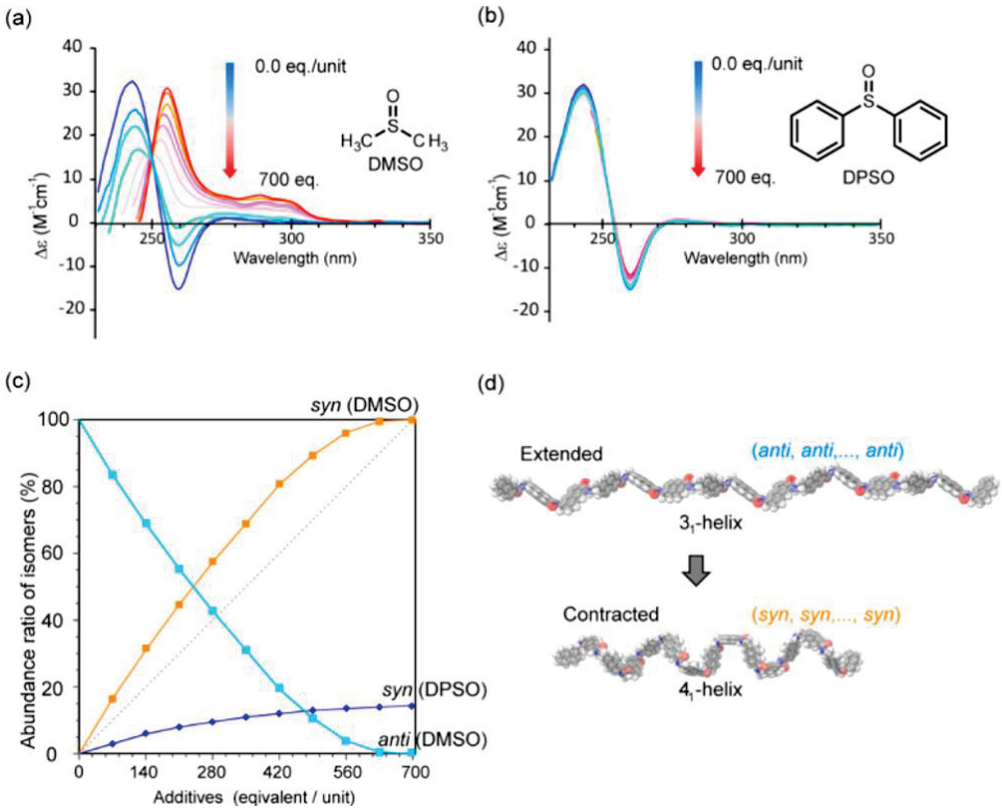

Figure 5-13. Results of CD titration experiment of **poly-2b** in THF at 25 °C in the presence of 0, 70, 140, 210, 280, 350, 420, 490, 560, 630, and 700 equiv of DMSO or DPSO. (a) CD spectra of **poly-2b** with DMSO (b) CD spectra of **poly-2b** with DPSO. Initial concentration/unit: [**poly-2b**] = 0.34 mM. (c) Estimated abundance ratio of isomers in **poly-2b** as a function of additive concentration. (d) Helix-to-helix transition of **poly-2b**. The chain length decreases by about two-thirds (pitch per residue; [4_1-helix] 5.5 Å and [3_1-helix] 8.2 Å). Side chains are omitted for clarity.

the fraction of *anti* isomer. However, adding diphenyl sulfoxide (DPSO) did not induce the helix-to-helix transition (Figure 5-13b). The population of the *syn* isomer as a function of DPSO concentration plateaued at approximately 15% at 560–700 equiv/unit. On the other hand, the addition of dimethylformamide (DMF) also causes a helix transition similar to that of DMSO. Therefore, a small and polarized molecule as an additive is necessary for clear helix-to-helix transitions. It is likely that the polarized molecules interact with amide moieties of the main chain, affecting the thermodynamical stability of the entire peptide (Figure 5-14). The bulkiness of the additive may prevent the effective stabilization of the main chain by the 4_1-helix which is the more compact helix.

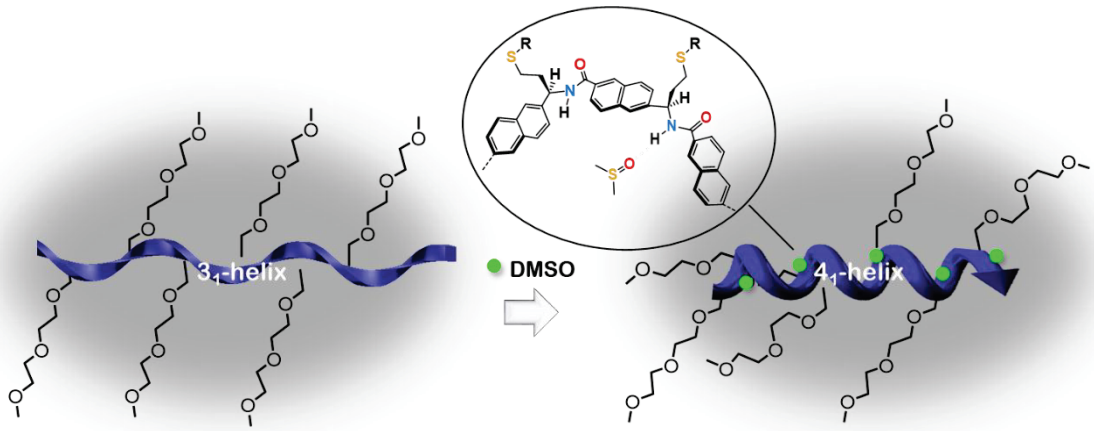

Figure 5-14. Schematic diagram of solvation of DMSO to arylopeptide.

5-3: Conclusions

Chapter 5 focused on the relationship between the main chain, side chain, solvent, and additive. The symmetry of the spacer in the main chain was an important factor that determined whether the helix was static or dynamic. Side chains and solvents need to be considered together, and the author found that the higher affinity induces the dominant of the 3_1-helix due to effective solvation. Using this mechanism, arylopeptide showing LCST behavior with a helix to helix transition has been developed. DMSO and DMF were found to support 4_1-helix formation and the author succeeded in changing the helical structure using polarized small molecules as additives. Random copolymers with mixed side chains potentially have the properties of both side chains, and freely convert from one primary structure to two well-defined structures (4_1- and 3_1-helices).

5-4: Experimental Section

General

Unless otherwise indicated, all reactions were carried out under an Ar atmosphere, whereas the workup was performed in air. ^{1}H NMR spectra were recorded in $CDCl_3$, toluene-d_8, and benzene-d_6 on JEOL JNM-ECS400 or JEOL JNM-ECA500 spectrometers using $SiMe_4$ as an internal standard. IR spectra were recorded on a SHIMADZU IR Prestige-21 spectrometer using KBr tablets. HR-MS and MS/MS (CID) measurements were carried out on a Thermo Fisher Scientific LTQ-Orbitrap XL mass spectrometer. Retention time of polymers were measured by SEC analyses using a SHIMAZU LC-10AS, SPD-10A UV-vis detector, and CTO-10A column oven equipped with two SEC columns TOSOH TSKgel GMH_{HR}-M carried out at 40 °C and a flow rate of 0.7 mL min^{-1} with $CHCl_3$ as the eluent. CD spectra were obtained by a JASCO J-720WO polarimeter with a cryostat thermostated at −75 to 85 °C. UV–vis spectra were obtained by a SHIMAZU UV 3100PC spectrophotometer. Samples for the AFM measurements of **poly-2a** were prepared by drop casting (about 20 μL) of dispersions onto freshly cleaved mica substrates at room temperature (about. 25 °C), and the substrates were then dried under vacuum for 1 h. The AFM images were obtained in air by tapping mode on an Agilent Technology Agilent PicoPlus 5100 microscope.

Materials

All solvents used for reactions were passed through purification columns just before use and tetrahydrofuran was dried by sodium-benzophenone and distilled under argon. Planar-chiral Cp′Ru complexes were prepared as reported previously.[10]

Standard Method of Asymmetric Polymerization

To a mixture of molecular sieve 3A, Na_2CO_3 (1.2 eq), a monomer (1.0 eq) and (*R*) or (*rac*)-**Cp′Ru** (2 mol%) were added THF (0.5 mmol/ 1 mL), which was stirred at 30 °C. After 3days, dichloromethane was added to the reaction mixture. The insoluble part was removed by filtration through Celite. The combined organic layer was washed with water. After drying with anhydrous Na_2SO_4, the solvent was removed under reduced pressure. The product was purified by silica gel column chromatography with CH_2Cl_2 and dried under vacuum to give a pale-yellow solid.

Standard Method of Post-polymerization Modification

To a toluene solution (5 mL) of the polymer (0.15 mmol of C=C groups) and 2,2-dimethoxy-2-phenylacetophenone (DMPA) (38.4 mg, 0.15 mmol) was added a thiol (0.90 mmol), and the reaction mixture was irradiated at 365 nm with an LED lamp (365 nm) for 5 hours. The crude product was purified by SEC using two Shodex KF 2003 columns connected in series at a flow rate of 3.0 mL min^{-1} to give the pale brown solid. To a THF solution (0.10 M) of the resulting polymer, THF solution of SmI_2–THF complex (4.0 equiv) was added at room temperature. After stirring for 2.0 h at room temperature, the reaction was rapidly quenched with a 10% solution of $Na_2S_2O_3 \cdot H_2O$. The mixture was diluted with CH_2Cl_2. The organic layer was separated. the product was extracted from the aqueous layer with CH_2Cl_2 (3 × 20 mL). The combined organic layer were removed under reduced pressure. The product was purified by SEC using two Shodex KF 2003 columns connected in series at a flow rate of 3.0 mL min^{-1} to give the target product.

Characterization of Representative Compounds

Synthesis of poly-2c.

According to the standard method of asymmetric polymerization and post-polymerization modification, **poly-2c** was obtained as a pale brown solid. ^{1}H NMR ($CDCl_3$/trifluoroethanol-d_3 = 2/1, 500 MHz): δ 8.21 (brs, 1H, Ar), 7.89–7.55 (m, 5H, Ar), 5.46 (br, 1H, –C*H*CH_2CH_2S–), 2.56 (br, 4H, –$CHCH_2CH_2$S– and –$CHCH_2CH_2SCH_2$–), 2.33 (br, 2H, –$CHCH_2CH_2$S–), 1.56 (br, 2H, –$CHCH_2CH_2SCH_2CH_2$–), 1.42-1.10 (br, 6H, –CH_2–), 0.83 (br, 3H, CH_3). IR (KBr) 3309, 2922, 2850, 1635, 1538 cm^{-1}.

Synthesis of poly-2d.

According to the standard method of reductive cleavage using the SmI_2-THF complex, **poly-2d** was obtained as a pale brown solid. ^{1}H NMR (DMSO-d_6, 500 MHz): δ 9.10 (brs, 1H, NH), 8.48 (brs, 1H, Ar), 8.18-7.97 (br, 4H, Ar), 7.70 (br, 1H, Ar), 5.38 (br, 1H, –C*H*CH_2CH_2S–), 3.54–3.37 (br, 8H, –OCH_2CH_2O–), 3.16 (br, 3H, OCH_3), 2.67 (br, 2H, –SCH_2CH_2O–), 2.32 (br, 2H, –$CHCH_2CH_2$S). the peak of (–SCH_2CH_2O–) and (–$CHCH_2CH_2$S) overlap with solvent. IR (KBr) 3296, 3040, 2971, 2920, 2868, 1639, 1531, 1260 cm^{-1}.

Synthesis of poly-2e.

According to the standard method of reductive cleavage using the SmI_2-THF complex, **poly-2e** was obtained as a pale brown solid. ^{1}H NMR (DMSO-d_6, 500 MHz): δ 9.09 (brs, 1H, NH), 8.47 (brs, 1H, Ar), 8.18-7.97 (br,

4H, Ar), 7.71 (br, 1H, Ar), 5.37 (br, 1H, –C*H*CH_2CH_2S–), 3.54–3.37 (br, 36H, –OCH_2CH_2O–), 3.14 (br, 3H, OCH_3), 2.65 (br, 2H, –SC$H_2$$CH_2O$–), 2.32 (br, 2H, –CHC$H_2$$CH_2S$). the peak of (–$CHCH_2CH_2$S) overlap with solvent. IR (KBr) 3296, 3040, 2971, 2920, 2868, 1639, 1531, 1260 cm^{-1}.

Synthesis of poly-3a

According to the standard method of asymmetric polymerization and post-polymerization modification, **poly-3a** was obtained as a pale brown solid. ^{1}H NMR ($CDCl_3$, 500 MHz): δ 7.87 (br, 2H, Ar), 7.57–7.41 (br, 6H, Ar), 5.39 (br, 1H, –C*H*CH_2CH_2S–), 2.55 (br, 4H, –$CHCH_2$CH_2S– and –$CHCH_2CH_2$SCH_2–), 2.26 (br, 2H, –CHC$H_2$$CH_2S$–), 1.49-1.10 (br, 20H, –CH_2–), 0.88 (br, 3H, CH_3). IR (KBr) 3319, 2922, 2850, 1633, 1530 cm^{-1}.

Synthesis of poly-3b

According to the standard method of asymmetric polymerization and post-polymerization modification, **poly-2a** was obtained as a pale brown solid (83%). ^{1}H NMR ($CDCl_3$, 500 MHz): δ 7.87 (brs, 2H, Ar), 7.78-7.26 (br, 6H, Ar), 5.38 (br, 1H, –C*H*CH_2CH_2S–), 3.70–3.47 (br, 10H, –OCH_2CH_2O– and –SCH_2CH_2O–), 3.33 (br, 3H, OCH_3), 2.75–2.60 (br, 4H, –SC$H_2$$CH_2O$– and –$CHCH_2CH_2$S), 2.32 (br, 2H, –CHC$H_2$$CH_2S$). IR (KBr) 3319, 1637, 1535, 1261 cm^{-1}.

Synthesis of poly-2ab(53/47)

According to the standard method of asymmetric polymerization and post-polymerization modification, **poly-2a** was obtained as a pale brown solid. ^{1}H NMR ($CDCl_3$/trifluoroethanol-d_3 = 2/1, 500 MHz): δ 8.20 (brs, 1H, Ar), 7.89–7.55 (m, 5H, Ar), 5.47 (br, 1H, –C*H*CH_2CH_2S–), 2.55 (br, 4H, –$CHCH_2$CH_2S– and –$CHCH_2CH_2$SCH_2–), 2.33 (br, 2H, –CHC$H_2$$CH_2S$–), 1.56 (br, 2H, –$CHCH_2CH_2SCH_2CH_2$–), 1.42-1.10 (br, 18H, –CH_2–), 0.84 (br, 3H, CH_3). IR (KBr) 3309, 2922, 2850, 1635, 1538 cm^{-1}.

References

(1) Anfinsen, C. B.; Haber, E.; Sela, M.; White Jr, F. *Proc. Natl. Acad. Sci. USA* **1961**, *47*, 1309.

(2) Ishido, Y.; Kanbayashi, N.; Okamura, T.-a.; Onitsuka, K. *ACS Macro Lett.* **2019**, *8*, 694.

(3) (a) Hansen, C. M. *Hansen solubility parameters: a user's handbook*; CRC press, 2002. (b) Barton, A. F. *CRC handbook of solubility parameters and other cohesion parameters*; Routledge, 2017.

(4) Nagata, Y.; Nishikawa, T.; Suginome, M.; Sato, S.; Sugiyama, M.; Porcar, L.; Martel, A.; Inoue, R.; Sato, N. *J. Am. Chem. Soc.* **2018**, *140*, 2722.

(5) Kennemur, J. G.; Kilgore, C. A.; Novak, B. M. *J. Polym. Sci., Part A: Polym. Chem.* **2011**, *49*, 719.

(6) Zarzar, L. D.; Sresht, V.; Sletten, E. M.; Kalow, J. A.; Blankschtein, D.; Swager, T. M. *Nature* **2015**, *518*, 520.

(7) Dinçalp, H.; Yavuz, S.; Haklı, Ö.; Zafer, C.; Özsoy, C.; Durucasu, İ.; İçli, S. *J. Photochem. Photobiol., A* **2010**, *210*, 8.

(8) Ge, F.; Zhao, Y. *Chem. Sci.* **2017**, *8*, 6307.

(9) (a) Koda, Y.; Terashima, T.; Sawamoto, M. *ACS Macro Lett.* **2015**, *4*, 1366. (b) Saeki, S.; Kuwahara, N.; Nakata, M.; Kaneko, M. *Polymer* **1976**, *17*, 685.

(10) (a) Dodo, N.; Matsushima, Y.; Uno, M.; Onitsuka, K.; Takahashi, S. *Dalton Trans.* **2000**, 35. (b) Matsushima, Y.; Komatsuzaki, N.; Ajioka, Y.; Yamamoto, M.; Kikuchi, H.; Takata, Y.; Dodo, N.; Onitsuka, K.; Uno, M.; Takahashi, S. *Bull. Chem. Soc. Jpn.* **2001**, *74*, 527. (c) Kanbayashi, N.; Onitsuka, K. *Angew. Chem. Int. Ed.* **2011**, *50*, 5197.

Summary

In this thesis, the author described the novel type of non-natural polypeptide is called “arylopeptide”. The peptide structure has advantages such as that the rigidity of amide and asymmetric carbons in the main chain to provide chiral structures. On the other hand, aromatic units show good rigidness, high designability, and so on. However, a peptide molecule, which has achieved both of these two advantages, has never existed because if you try to introduce an asymmetric carbon in the main chain, chiral source depends on the natural product, but no chiral amino acid having an aromatic ring on the backbone exists in nature.

In Chapter 2, an innovative synthetic strategy to arylopeptides was demonstrated, which involved the use of asymmetric polymerization and reduction of N–O bonds. The reaction proceeds smoothly regardless of the substituents on the side chains to afford an arylopeptide that contains a *p*-phenylene unit in the main chain, which is a new type of polypeptide. The resulting polymer exhibits a one-handed helical conformation. This method does not require enantiomerically pure amino acids and its condensation on stepwise synthetic chemistry and affords a long peptidic chain, whose asymmetric centers were controlled. The precursor polymer (**poly-2**) containing various arylene spacers (R) on the main chain and bearing a wide range of substituents in the side chain can be synthesized.

In Chapter 3, we succeeded in development of saccharides directive system of helical structure and helicity of glycoarylopeptide. The glycoarylopeptide distinguished the length of sugar chain and even the configuration of a single stereo-genic center in epimers D-glucose and D-mannnose, perfectly glucose-selective phenomenon. This is the first example in which the epimer induced different helical structure of artificial polymer. Their result indicates that even the properties of the arylopeptides which are completely artificial polypeptide molecules is dominated by the type of saccharides same as nature.

In Chapter 4, the author showed unique dual structural systems of poly arylopeptide by using the energy difference between geometrical *anti* and *syn* conformations of the 2,6-naphthalene spacer. Although the formations of the *syn* and *anti* conformers of the 2,6-naphthalene ring cannot be controlled within the oligomers, longer polymeric chains adopt either the contracted 4_1-helix or the expanded 3_1-helix in response to the conditions and without specific interactions. This geometrical control of the local structure is due to the relative thermodynamic stability of the polymers. The 4_1- and 3_1-helices can be selectively formed by the appropriate side chain, and polypeptide reselects the geometrical isomers. The presented results utilize a small energy

difference of the monomer units to create stable particular secondary structures in polymer by polymer effects, which are expected to be a new guideline for designing the primary structure of synthetic polymers. Polypeptide chain would create branching point and allow to control conformers by various condition

In Chapter 5 focused on the relationship between the main chain, side chain, solvent, additive, and the fraction of side chain. The symmetry of the spacer on the main chain was an important factor that determines whether the helix is static or dynamic. Side chains and solvents need to be considered together, and I found that the higher affinity induces the dominant of the 3_1-helix side due to effective solvation. Using this mechanism, arylopeptides that exhibit LCST behavior with helix to helix transition have been developed. DMSO and DMF were found to exhibit a very strong 4_1-helix formation effects even in small amounts, and succeeded in changing the helical structure with irreversible. Random copolymers with mixed side chains potentially have the properties of two side chains, and freely converted from one primary structure to two well-defined structures (4_1- and 3_1-helices). Each helix was formed with strong cooperativity depending on ratio of the two side chains.

In conclusion, the authors created a new field of “arylopeptide” and the field was pioneered from various viewpoint. The synthetic method based on polycondensation and post-polymerization modifications allow to produce endless new molecular designs. There must be a lot of hidden properties of arylopeptide. Arylopeptide is closely related to polypeptides, aromatic polymers, and helical polymer chemistry, and the author believes that “arylopeptide” must contribute to the development of their respective fields in a cooperative manner.

List of Publications

Chapter 2

Yuki Ishido, Naoya Kanbayashi, Taka-aki Okamura, Kiyotaka Onitsuka
"Synthesis of Non-natural Helical Polypeptide via Asymmetric Polymerization and Reductive Cleavage of N–O Bond" *Macromolecules*, **2017**, *50*, 5301-5307.

Chapter 3

Yuki Ishido, Naoya Kanbayashi, Naoka Fujii, Taka-aki Okamura, Takeharu Haino, Kiyotaka Onitsuka
"Folding Control of Non-natural Glycopeptide Using Saccharide-coded Structural Information for Polypeptide" *Chem. Commun*., **2020**, *in press*.

Chapter 4

Yuki Ishido, Naoya Kanbayashi, Taka-aki Okamura, Kiyotaka Onitsuka
"Side-Chain-Driven Dual Structural System of Poly-Arylopeptide: Selective Helical Formation Derived from Aromatic Ring Flips on the Backbone" *ACS Macro Lett*. **2019**, *8*, 694-699.

Chapter 5

Yuki Ishido, Naoya Kanbayashi, Naoka Fujii, Taka-aki Okamura, Takeharu Haino, Kiyotaka Onitsuka
"Dynamically Reselectable Bistable Helix Arylopeptide via Temperature and Solvents" to be submitted

Related Publication

Naoya Kanbayashi, Sou Miyamoto, Yuki Ishido, Taka-aki Okamura, Kiyotaka Onitsuka
"Post-Polymerization Modification of the Side Chain in Optically Active Polymer by Thiol-Ene Reaction" *Polym. Chem.,* **2017**, *8*, 985-994.